5-7-2012 12:00 AM

Mechanical Instability of Thin Solid Film Structures

Masoud Noroozi
The University of Western Ontario

Supervisor
Dr. Liying Y. Jiang
The University of Western Ontario

Graduate Program in Mechanical and Materials Engineering
A thesis submitted in partial fulfillment of the requirements for the degree in Doctor of Philosophy

MECHANICAL INSTABILITY OF THIN SOLID FILM STRUCTURES

(Spine title: Mechanical Instability of Thin Solid Film Structures)

(Thesis format: Integrated Article)

by

Masoud Noroozi

Faculty of Engineering
Department of Mechanical and Materials Engineering

A thesis submitted in partial fulfillment
of the requirements for the degree of
Doctor of Philosophy

The School of Graduate and Postdoctoral Studies
The University of Western Ontario
London, Ontario, Canada

THE UNIVERSITY OF WESTERN ONTARIO
School of Graduate and Postdoctoral Studies

CERTIFICATE OF EXAMINATION

Supervisor

Dr. Liying Jiang

Advisory Committee

Dr. John R. Dryden

Dr. Jun Yang

Examiners

Dr. John R. Dryden

Dr. Xueliang Sun

Dr. Xianbin Wang

Dr. Jinjun Shan

The thesis by

Masoud Noroozi

Entitled:

Mechanical Instability of Thin Solid Film Structures

is accepted in partial fulfillment of the
requirements for the degree of
Doctor of Philosophy

Date

Chair of the Thesis Examination Board

Abstract

Instability of thin film structures as buckling and wrinkling are important issues in various fields such as skin aging, mechanics of scars, metrology of the material properties of thin layers, coating of surfaces and etc. Similar to buckling, highly ordered patterns of wrinkles may be developed on the film–substrate due to compressive stresses. They may cause a failure of the system as structural damage or inappropriate operation, however once they are well understood, it is possible to control and even use them properly in various systems such as the gossamer structures in the space, stretchable electronics, eyelike digital cameras and wound healing in surgery.

In this thesis, the mechanical instability of thin film is considered analytically and numerically by solving the eigenvalue problem for the governing equation of the system, and the effects of the different factors on the instability parameters such as load, amplitude, wave number and length of the wrinkles are studied. Different problems such as wrinkling within an area on the film, and buckling and wrinkling of the non–uniform systems with variable geometry and material properties for both of the film and substrate and also wrinkling–folding transition are investigated. It is shown that the effects of the non–uniformity of the system are very significant in localization of the wrinkles on the film; however, such a factor has been ignored by many researchers to simplify the problems. In fact, for the non–uniform systems, the wrinkles accumulate around the weakest locations of the system with lower stiffness and the wrinkling parameters are highly affected by the non–uniformity effects. Such effects are important especially in thin film technology where the thickness of the film is in the order of Micro/Nano scale and the uniformity of the system is unrealizable.

The results of this dissertation are useful in the design and applications of thin solid films in science, technology and industry. They consider the relation of the loading and structural stiffness with the wrinkling parameters and provide more insight into the physics of the localization of the wrinkling on the thin structures, how and why wrinkles are accumulated at some positions. Therefore, deliberate application of these results provides appropriate tools to control and use the buckling and wrinkling of thin films effectively in different fields.

Keywords

Thin Solid Film, Mechanical Instability, Buckling, Wrinkling, Variable Thickness Beam, Functionally Graded Material (FGM), Substrate, Winkler Foundation, Localized Wrinkling, Eigenvalue Problem, Finite Difference Method, Energy Methods.

Acknowledgments

Various parts of this project would not have been accomplished without the inspiring supervision of Dr. Liying Jiang. I am grateful to her for all of her supports, motivations, enthusiasm and guidance towards me during my Ph.D. program. Her guidance helped me through the research and writing of my thesis. I also would like to thank my advisor committee, Dr. John Dryden and Dr. Jun Yang for their supports and their advice. I appreciate the support provided by faculty and stuff of the Department of Mechanical and Materials Engineering at UWO. Besides my advisors, I would like to thank the rest of my thesis committee for their encouragement, insightful comments, and hard questions.

I would like to thank the many people who have taught me: my primary school and my high school teachers, my undergraduate and my graduate teachers at Sharif University of Technology.

I wish to thank my best friends for helping me get through the difficult times, and for all the emotional support, camaraderie, entertainment and caring they provided.

Lastly, and most importantly, I also give my special thanks and appreciation to my lovely family members, my father Mohammad–Ali, my mother Zahra and my sisters Narges and Nasrin for all of their kindness, their support and their patience for me. My parents gave birth to me, raised me, taught me and my family supported me and loved me. To them I dedicate this thesis.

Table of Contents

List of Tables

List of Figures

Chapter 1

1 Introduction

Buckling and wrinkling of thin solid film structures are considered as one of the important instability issues in the film applications for example in sandwich panels, aviation, solar sails and stitching of the skin in medical operations. Investigations on the buckling and wrinkling of thin films have been pursued by researchers experimentally and theoretically.

1.1 Thin Film Structures, Their Applications and Properties

Thin solid films are thin layers of materials ranging from nanometer to hundreds of microns in thickness that behave like solid structures. The first application of thin films originated from ancient Egypt in 3000 B.C. when thin fold of gold with thickness about six microns were used to cover the statues, wooden and metallic objects, and jewelry technology by skilled workers [James, 1972]. They used layers of thin gold with a composite system of leather under excessive pressure to make leaves of gold with the thickness of microns and attached them on the objects skillfully.

Thin films have many applications in Micro/Nano Electro–Mechanical Systems (*MEMS/NEMS)*, electronic devices especially semiconductors and IC technology, solar cells, computer memories, optical coatings including mirrors, anti–reflective coatings, solar sails and astronavigation, coatings in tribological applications, wear and corrosion–oxidation resistant of the mechanical components, tooling, biomedical implants, magnetic devices and etc. In fact, thin layers on the surface of a substrate lead to completely different characteristics of the surface and therefore result in versatile and useful applications of thin films in various fields [Freund and Suresh, 2003; Riad and Barlow, 1998]. For example, the relatively high hardness of ceramic materials makes ceramic thin coating interesting and applicable for protection of the substrate materials against corrosion, oxidation and wear. In particular, the use of such coatings on cutting tools can extend the life of these parts by several orders of magnitude due to delay in fatigue crack growth and propagation. Also, the performance of the optical coatings and

anti–reflectiveness typically increases when the thin film coating consists of multiple layers with different thickness and refractive indices. Deposition of the films with desirable electrical, mechanical and optical properties on the substrate changes the surface properties of the foundation drastically which brings more ability for the engineers to design more effective systems with less cost.

The act of producing a thin film on a surface is called deposition of the film. There are various techniques for depositing a thin film of material onto a substrate or previously deposited layers which generally fall into two categories, depending on the chemical or physical nature of the process. In chemical vapor deposition (CVD), the process of the deposition is carried out during a chemical reaction so that the atoms of film and the substrate materials chemically react in a reaction chamber. In contrast with the CVD, physical vapor deposition (PVD) uses mechanical, electromechanical or thermodynamic methods to deposit a thin film of solid on the substrate similar to the formation of frost. For example, in thermodynamic method of PVD the material to be deposited is placed in a highly energetic entropic environment, so that particles of material are detached from the source surface and when they arrive to the cooler surface of target, they lose their energy and solidifies on the surface to form a layer. The deposition chamber is vacuumed to allow the particles to travel as freely as possible [Ohring, 2002].

The thickness of thin film is another issue considered by the researchers. Films with a thickness comparable to one or a few atomic layers are categorized as atomically thin films. When the thickness of the film is in the order of characteristic micro–structural size scale of the material such as grain size or dislocation cell size, the film is considered to be micro–structurally thin film. A mechanically thin film has a thickness much larger than the characteristic micro–structural length scales. Such structures have tens or hundreds of microns in thickness and the continuum mechanics approach for analyzing the stress, strain and other mechanical issues are applicable for them [Freund and Suresh, 2003, pp. 5]. Mechanical properties of these systems and the stresses developed in the films affect the behavior and the durability of the systems.

The material properties of the free standing film or film–substrate system are considered under different conditions. Many experimental works have been directed to characterize the material properties of the films. Due to the miniature structure of thin

films along the thickness, traditional methods usually are not applicable or produce inaccurate results. As an example, the effect of the substrate is dominated on the structural stiffness of the system that overwhelms the stiffness of the film. Therefore, the necessity of developing new methods was augmented by the researchers. For example, by considering the wrinkling of rigid films on elastomeric substrates, Stafford and coworkers (2004) introduced an experimental method for measuring the stiffness of the polymeric thin films called "strain–induced elastic buckling instability for mechanical measurements method" in which the relation of the wavelength of the wrinkles with other characteristics of the system such as thickness and stiffness of the film and substrate are developed. Therefore, for a deposited film with unknown modulus on the elastomeric foundation with known modulus, by measuring the wrinkle wavelength beyond the critical strain, the unknown modulus of the film can be determined.

In order to predict the mechanical behavior of the system, the material properties of the film such as hardness and Young's modulus, and also the residual stresses of the film must be known [Ohring, 2002; Freund and Suresh, 2003; Bachmann *et al*., 2006]. Figure 1-1 [Freund and Suresh, 2003] shows two traditional tests: Bulge test and Stoney test which work based on the force–deflection monitoring method. In bulge test, by monitoring the deformation of the thin film as a function of the applied pressure p on the film, the parameters of the size and the material properties of the film are determined. By using the Stoney test, one may find the residual stress developed in the thin film–substrate system [Stoney, 1909]. According to the Stoney formula, the residual stress of the film depends on the material properties of the film–substrate and the deflection curvature of the system. These stresses develop in the system due to different sources such as mismatch of the film and substrate during the deposition process or dissimilar material properties of the film and substrate during the application. The existence of the residual stresses in films deposited on the substrate, and the effects of such stresses on delamination and mechanical behavior of the system are important [Fu *et al*., 2004; Jeon *et al*., 2005].

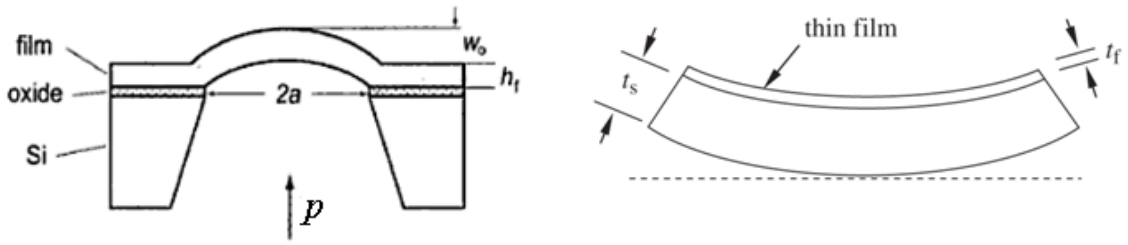

Figure 1-1: Different experimental methods for mechanical characterization of thin films: Bulge test (left–hand side) and Stoney test (right–hand side) [Freund and Suresh, 2003]

1.2 Wrinkling of Thin Film Structures

Wrinkles are defined in the dictionary as small furrows, ridges, or creases on a smooth surface, caused by crumpling, folding, or shrinking. In thin solid films, wrinkling causes a highly ordered wavy pattern on the film due to local compressive stresses. Similar to the buckling of a beam under compressive loading introduced by Leonard Euler in 1757, the wrinkling problem is categorized as the instability of the mechanical system. The wrinkling of the beam/film supported by an elastic foundation was introduced by Allen (1969) for sandwich panels in airplanes and Ker (1974) for welded rail roads under thermal expansion. Wrinkling of the thin films has been investigated especially in recent years in different fields. Genzer and Groenewold (2006) reviewed different aspects of the wrinkling of thin film structures comprehensively. They described various examples from everyday life to demonstrate the versatile and useful applications of wrinkling which can help in developing new structures and methods beyond its frustrating features on human skin studied by Lavker *et al*. (1989) as the morphology of aged skin. As an example, by considering the wrinkling localization around a scar, Cerda (2005) determined the effect of background tension of the skin on the formation of the wrinkles around the scar as the application of the wrinkling in medical science. In addition to skin aging and wound healing, thin film wrinkling can be found in many other fields such as carbon nanotubes [Lourie *et al*. 1998], stretchable connectors [Lacour *et al*., 2003 and 2004; Sun *et al*., 2006; Khang *et al*., 2009], semiconductor technology [Chen and Hutchinson, 2004; Huang *et al*., 2007], electronics and polymer actuators [Watanabe, 2005; Liu *et al*., 2010;

Zhao *et al*., 2011; Jia *et al*., 2012], optical devices [Harrison *et al*., 2004], Microfluidic sieves [Efimenko *et al*., 2005], Topographic matrices for cell alignment [Teixeira *et al*., 2003] in bioengineering, metrology of the material properties [Cerda and Mahadevan, 2003; Chung *et al*., 2011; Li *et al.*, 2012], stretched thin sheets [Bouzid and Lecieux, 2010; Nayyar *et al.*, 2011; Puntel *et al.*, 2011; Kim *et al.*, 2012; Jillella and Peddieson, 2012], coating of the surfaces [Basu *et al*., 2005], gossamer structures [Wang *et al.*, 2009], solar sails and aeronautical structures in aerospace science [Heald and Potvin, 2006; Kumar and Pellegrino, 2000; Orszulik *et al*., 2011], sheet metal forming [Kawka *et al*. 2001; Wang and Cao, 2000; Cao and Boyce, 1997; Yu and Stronge, 1985; Music *et al.*, 2010], failure of sandwich structures as face wrinkling [McCormack *et al*., 2001; Cote *et al*., 2007], patterning and topographical structuring of surfaces [Schweikart and Fery, 2009; Kang and Huang, 2011; Lackner *et al.*, 2012] and so on. In these areas, wrinkling is either regarded as nuisance to be avoided or an interesting pattern to be exploited. Similar to the method proposed by Stafford *et al*. (2004) to predict the film material properties, other researchers have also studied on characterization of the material properties of thin film–substrate system in material science. Wilder *et al*. (2006) used the method proposed by Stafford (2004) to determine the properties of the substrate when the properties of the film are known. Cerda *et al*. (2002) considered the wrinkling of a free standing stretched film and derived the scaling law for the wavelength and amplitude of the wrinkling in polyethylene sheets, so that by analyzing the pattern of the wrinkles, the tension on the film and the material properties of the sheet can be determined. Bernal *et al*. (2007) used a capillary–type technique to estimate the elastic modulus of the films by wrinkle pattern produced by crawling of cells onto elastic membrane due to the locomotion of living cells.

Wrinkles can be developed on the film by various methods. By depositing a film on the elastomeric substrate and cooling/heating the entire structure, the developed compressive stresses in the film are relieved by wrinkling with a uniform wavelength [Bowden *et al*., 1998 and 1999]. You *et al.* (2002) applied thermal expansion mismatch method to create wrinkling pattern on the film substrate system. Some researchers also used other methods to produce wrinkling on the film instead of heating/cooling the system [Gilat, 2010]. For example, exposing UV radiation on the surface of some

elastomers which changes the stiffness of the substrate locally can create ordered wrinkle pattern [Huck *et al*., 2000]. Volynskii *et al.* (2000), Lacour *et al.* (2004) and Watanabe (2005) applied mechanical strain to produce uniaxial wrinkling pattern on the deposited film on the substrate. For this purpose, the film is usually chosen as a metal such as gold or platinum, while the substrate is a polymer such as PDMS, polyethylene and so on. By depositing the film on a pre–stretched substrate and releasing the entire system, an ordered wrinkle patterns develop on the system.

Different buckling and wrinkling patterns of thin films have been reported by researchers in literature. Wang *et al.* (2008) considered the specific ratios of thickness and length of the film–substrate and critical loading on the system under which the global buckling or local wrinkling appears on the system. They introduced some relations for critical loading of the system analytically, and proposed specific ratios which discretize the global buckling and local wrinkling. For wrinkling of a deposited film on the substrate, different wrinkling pattern are represented as one dimensional or two dimensional patterns. The one–dimensional uniaxial wrinkling pattern is one of the common patterns in which the wrinkles propagate along the film span in one direction. In this pattern, the wrinkles are represented by a periodic function with a wave number parameter along the film length span [Huang *et al*., 2005; Hu *et al.*, 2009]. Huang and Im (2006) studied the evolution of the wrinkling from initial growth at the onset of instability followed by coarsening till final equilibrium. They showed that during coarsening of the troughs and crests, the wrinkling amplitude grows exponentially over time with a power–law scaling under uniaxial compression and finally, a uniaxial pattern is obtained, while chaotic labyrinth pattern appears under equibiaxial loading at equilibrium. Both of the patterns under the loading of the same magnitude have the same average wavelength, but different amplitudes. Other two dimensional patterns are also observed for films under in–plane biaxial loading. If the wavelengths of the wrinkling in two directions are equal to each other, the pattern is called checkerboard pattern. Other complex patterns such as herringbone zigzag patterns were observed due to highly nonlinear nature of the system [Chen and Hutchinson, 2004] as shown in figure 1-2. As another example, Yoo and Lee (2003) reported a spinodal wrinkling pattern on the system due to nonlinear properties of the viscoelastic substrate.

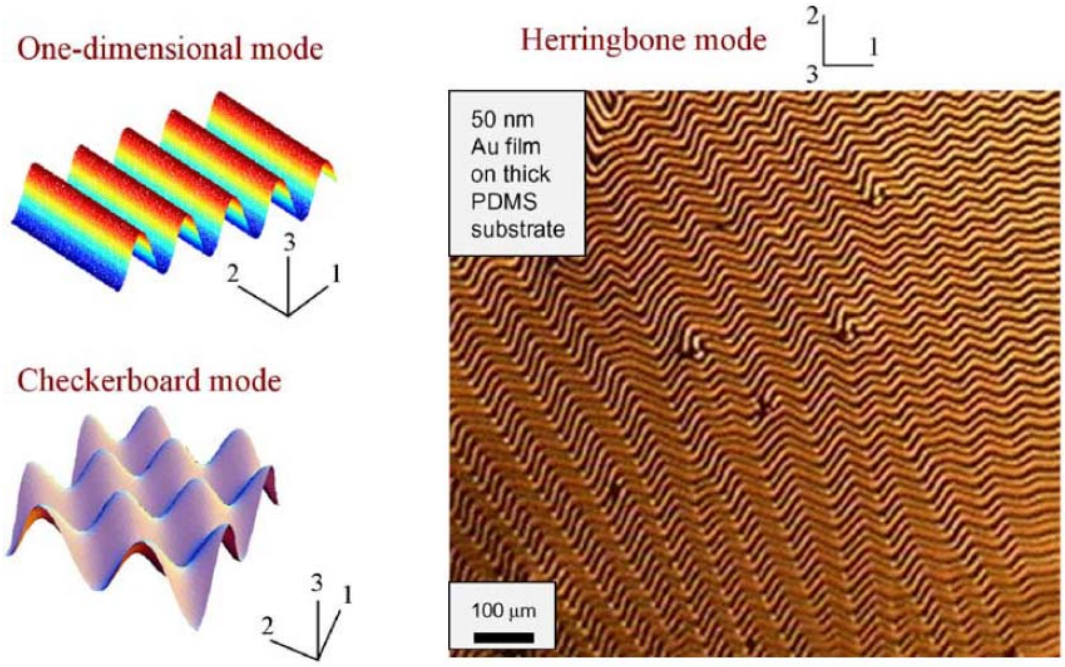

Figure 1-2: Various patterns of the wrinkling [Chen and Hutchinson, 2004]

By using the linear perturbation analysis, Allen (1969) showed that for sandwich panels with a soft core between two hard panels subjected to a compressive loading, the critical force for wrinkling depends on the stiffness of the substrate. Niu and Talreja (1999) proposed a relation for the buckling stress versus thickness and stiffness of the core and panels from long to short wavelengths by using Allen's linear perturbation analysis. By using the classical plate theory and minimization of the potential energy, Groenewold (2001) proposed relations for wavelength and amplitude of the wrinkling of a thin solid film deposited on a soft substrate. Subsequently, Cerda and Mahadevan (2003) suggested a set of scaling laws for the wavelength (λ) and amplitude (A) of the wrinkles in the film–substrate system as

$$\lambda \sim \left(\frac{B}{K}\right)^{\frac{1}{4}} \tag{1-1}$$

$$A \sim \lambda \left(\frac{\Delta}{W}\right)^{\frac{1}{2}} \tag{1-2}$$

where B is the bending stiffness of the film, K is the modulus of the substrate and (Δ/W) is the applied compressive strain on the system. The above results provide clear explanation for wrinkling parameters and form the basis of quantitative wrinkling assay for mechanical characterization of thin solid films on the substrate. Pocivavsek *et al.*

(2008) clearly demonstrated the effect of the stiffness of the substrate and floating thin film on the wrinkling experimentally. Their results show that for gold film which is much thinner than a polymer film floated on the same substrate (e.g. water), the wavelength of the wrinkling is several order smaller. On the other hand, for the same polymer film on different substrates (e.g. water versus gel), the wavelength of the wrinkling on the softer substrate is bigger as predicted by relation (1-1). Some other effects such as the finite width of the system on the wrinkling problem were investigated by modifying the substrate stiffness. For example, Tarasovs and Anderson (2008) proposed a model for substrate with finite width and considered the wrinkling parameters. They showed that for small wavelength of the wrinkles with respect to the width of the system, the uniform assumption for the substrate stiffness remains valid.

Recently, some researchers also considered the wrinkling of thin film by using plate theory and the minimization of the potential energy to characterize the effective parameters of the wrinkling. Chen and Hutchinson (2004) and Song *et al*. (2008) developed analytical approaches to predict one–dimensional, checkerboard, and ordered herringbone patterns for a film under bi–axial in–plane loading by introducing wavelength and amplitude in terms of the stiffness modulus and the thickness of the film and substrate and the applied loading. The results of their analysis showed that for a biaxial in–plane loading on the film, the herringbone pattern has the lowest energy with respect to other modes and therefore it was frequently observed in experiments. They proposed those classes of materials for high performance electronics with two–dimensional stretchability. Many other researchers used the above methodology to investigate different problems in various fields with practical applications. For example, Friedl *et al*. (2000) and Jacques *et al*. (2005 and 2007) considered the wrinkling of stretched strips by using finite element analyses and analytical solution methods. The results of their works predict uniaxial wrinkling pattern developed on the thin film strip which plays an important role during strip conveying in processing lines. For free standing films under tension, the wrinkles appear on the film according to tension filed theory discussed in chapter 2. In fact, the effect of tension on the film is introduced as an equivalent substrate under the film which leads to wrinkling as studied by Coman (2010) analytically and Lecieux and Bouzidi (2010) experimentally and numerically. Wong and

Pellegrino (2005) also considered the wrinkling of square membranes subjected to corner forces which can be used in controlling the flatness of solar sails, solar collectors, and sunshields. They showed that two wrinkling regimes develop diagonally or around the corners of the square membrane according to the ratio of applied loading at the corners.

On the other hand, many analytical results based on the bifurcation theory and the instability of the thin plate were provided by the researchers. For example, wrinkling around a point in circular free standing film was considered by Adams (1993) and Geminard *et al*. (2004) by solving equilibrium equations of the film. Coman *et al*. considered the effects of the various torsional and stretching loadings on the wrinkling of the film with annular geometry in some successive works from 2006 till 2008.

Using numerical methods such as finite element technique is another powerful method to predict wrinkling patterns of thin films. Many researchers such as Kang and Im (1997) and Lu *et al*. (2001) implemented finite element method in analyzing wrinkling problem of membrane under various loading pattern and geometries. They developed a continuum theory combined with finite element formulation which resulted in explicit expressions for internal forces and stiffness matrix. Wang and Cao (2000) and Kawka *et al*. (2001) simulated the wrinkling of conical cups in sheet metal forming using finite element commercial software for both dynamic and static analysis. Lee and Youn (2006) developed a finite element code to analyze the large deformation of wrinkled membrane. Based on a tensile strain energy concept, the wrinkling directions are determined such that the wrinkles alignment maximizes the tensile strain energy. By using this method, they considered the torsion of a membrane in a circular disk, Inflation of a square airbag and the inflatable reflector of a large lightweight space antenna without involving the complexity of analytical solution.

All of the existing theoretical works on the wrinkling of the substrate–bonded films discussed here used the homogenous assumption for the film material properties with uniform thickness all over the domain. The film is usually considered like an infinite matter while the wrinkles propagate with uniform amplitude all over the domain. However, there is no evidence for these simplifications especially in thin film technology. For thin film structure deposited on the substrate by using various deposition techniques, the assumption of homogeneity of the film is very flabby due to importance of the

microstructure of the small scale system. Here, some concerns may arise about the importance of the change of the material properties of the film and the effect of these variations on the instability parameters. On the other hand, in thin film technology the thickness of the film is tiny and even small variation of the thickness violates the assumption of the uniformity of the thickness in classical theory and all the conclusions resulted from the analyses. Besides, in real application of thin film system the thickness of the film cannot be controlled to be perfectly uniform all over the substrate; hence it is necessary to consider the effect of the variations of the film thickness on the critical load and pattern (i.e. amplitude and wave number) of the wrinkling to see whether these variations in thickness and material properties have any effect on the wrinkling patterns.

1.3 Objectives of the Thesis

This dissertation considers the mechanical instability of thin solid films, such as buckling of a free standing film and wrinkling of a substrate–bonded film. The main objective of the thesis is to predict the buckling and wrinkling parameters such as load and patterns of the deformation on the onset of instability and afterwards. The following problems are considered to achieve these main objectives:

1) Considering the wrinkling of the film locally loaded
2) Studying the wrinkling of the film with finite length in comparison with an infinite one
3) Investigating the effect of the non–uniformity of the material properties and thickness of the film on the buckling/wrinkling load and patterns
4) Predicting the post-buckling/wrinkling behavior of the film–substrate system after the instability onset and studying the effective parameters on it
5) Investigating the wrinkling–folding transition of the film–substrate system and studying the effective parameters on the transition phase
6) Considering the effect of the non–uniformity of the substrate on the wrinkling of the film
7) Studying the effect of the surface elasticity and residual stress on the wrinkling of Micro/Nanoscale thin films

In this study, by ignoring the assumptions such as uniformity of the system and deformation used by other researchers in wrinkling analysis of thin film structures, an interesting behavior of the system is introduced in which wrinkles accumulate around a particular area of the film due to the effect of the non–uniformity. The results of this work increase the insight in physics and mechanics of instability of thin film structures and open new windows in potential applications of thin film technology in various fields.

1.4 Organization of the Thesis

By using the classical theories of plate and beam, the film substrate system is modeled and the instability of the system including buckling and wrinkling are analyzed. A brief description of the chapters of the dissertation is presented as follow.

In chapter 2, some basic materials on the required concepts and theories are described. These materials mainly include stability of a system, bifurcation theory, beam and plate theory and finite difference method which are used for numerical analysis in other chapters.

In chapter 3, the wrinkling around an inclusion on a thin solid film is investigated using the instability analysis. The film is modeled by using the classical plate theory with orthotropic properties and the effect of the inclusion is imposed on the film as a compressive loading along the inclusion line. For a decaying function representing the wrinkling pattern along the film, the potential energy of the film is minimized and parameters of the wrinkling (i.e. load and pattern) are determined. The results are useful in characterizing the wrinkling around an inclusion on free standing or deposited films on the substrate such as wrinkles due to suturing of the skin in surgical operation in mechanics of scars.

Chapter 4 considers the instability of a functionally graded material (FGM) beam/strip as a free standing film or substrate–bonded film. The stiffness modulus of the film is assumed to change exponentially along the length span which leads to the softening or stiffening of the film. The buckling of a free standing FGM film is investigated analytically. For substrate–bonded film, the wrinkling load and wrinkling pattern are determined numerically. Unlike the homogenous film in which the wrinkles

propagated along the entire domain, it is shown that for the FGM film wrinkles accumulate around the location with minimum stiffness.

In chapter 5, the instability of a beam/strip with variable thickness is investigated for a free standing film and a deposited film on a substrate. The thickness pattern is assumed with a quadratic profile with its minimum at the middle of the length span. For the free standing film, the buckling loads and mode shapes are studied analytically by using a closed form solution. For substrate–bonded film, the substrate is modeled by using the Winkler foundation and the effects of the non–uniform thickness and the substrate stiffness on the wrinkling parameters are investigated. For the non–uniform film, it is shown that the wrinkles accumulate around the location with minimum thickness along the span.

The effect of the fluctuation of the thickness on the instability parameters of a thin film with variable thickness is considered by using a finite difference method in chapter 6. The thickness profile is modeled with a wavy function and the buckling and wrinkling behavior of the system are investigated. The results show that the fluctuations of the thickness strongly influence on the buckling and wrinkling parameters.

Chapter 7 considers the behavior of a beam/strip with uniaxial deformation after instability by solving the nonlinear equation of the large deflection theory. For free standing film the buckling and postbuckling is considered, while for the deposited film on the substrate the fine wavy pattern of wrinkling and post–wrinkling behavior is investigated by using numerical solution of finite difference method for various systems such as non–homogenous material properties and non–uniform thickness of the film.

The effects of the surface elasticity and the residual surface stress on the wrinkling of the film are investigated in chapter 8. Also, a non–uniform model for the substrate is proposed and the wrinkling of the film on the non–uniform substrate is investigated.

Finally, chapter 9 represents an overall review of all the materials presented in the previous chapters and discusses the general results and conclusions.

1.5 References

[1] G. G. Adams, “Elastic wrinkling of a tensioned circular plate using von Karman plate theory”, *Journal of Applied Mechanics*, Vol. 60, 1993, pp. 520–525.

[2] H. G. Allen, *Analysis and Design of Structural Sandwich Panels*, 1969, Pergamon, NewYork.

[3] D. Bachmann, B. Schoberle, S. Kuhne, Y. Leiner, C. Hierold, “Fabrication and characterization of folded SU–8 suspensions for MEMS applications", *Sensors and Actuators A: Physical*, Vol. 130–131, 2006, pp. 379–386.

[4] S. K. Basu, L.E. Scriven, L.F. Francis, A.V. McCormick, “Mechanism of wrinkle formation in curing coatings”, *Progress in Organic Coatings*, Vol. 53, 2005, pp. 1–16.

[5] R. Bernal, C. Tassius, F. Melo, “Mechanical characterization of elastic membranes: Cell mechanics applications”, *Applied Physics Letters*, Vol. 90, 2007, pp. 063903.

[6] R. Bouzidi, Y. Lecieux, “Experimental analysis on membrane wrinkling under biaxial load – Comparison with bifurcation analysis”, *International Journal of Solids and Structures*, Vol. 47 (18–19), 2010, pp. 2459–2475.

[7] N. Bowden, S. Brittain, A. G. Evans, J. W. Hutchinson, G. M. Whitesides, “Spontaneous formation of ordered structures in thin films of metals supported on an elastomeric polymer”, *Nature*, Vol. 393, 1998, pp. 146–149.

[8] N. Bowden, W. T. S. Huck, K. E. Paul, G. M. Whitesides, “The controlled formation of ordered, sinusoidal structures by plasma oxidation of an elastomeric polymer”, *Applied Physics Letters*, Vol. 75 (17), 1999, pp. 2557–2559.

[9] J. Cao, M.C. Boyce, “Wrinkling behavior of rectangular plates under lateral constraint”, *International Journal of Solids and Structures*, Vol. 34 (2), 1997, pp. 153–176.

[10] E. Cerda, K. Ravi–Chandar, L. Mahadevan, “Thin films: Wrinkling of an elastic sheet under tension”, *Nature*, Vol. 419, 2002, pp. 579–580.

[11] E. Cerda, L. Mahadevan, “Geometry and physics of wrinkling”, *Physical Review Letters*, Vol. 90 (7), 2003, pp. 074302/1–4.

[12] E. Cerda, “Mechanics of scars”, *Journal of Biomechanics*, Vol. 38, 2005, pp. 1598–1603.

[13] X. Chen, J. W. Hutchinson, "A family of herringbone patterns in thin films", *Scripta Materialia*, Vol. 50, 2004, pp. 797–801.

[14] J.Y. Chung, A.J. Nolte, C.M. Stafford, "Surface wrinkling: A versatile platform for measuring thin–film properties", *Advanced Materials*, Vol. 23 (3), 2011, pp. 349–368.

[15] C. D. Coman, D. M. Haughton, "Localized wrinkling instabilities in radially stretched annular thin films", *Acta Mechanica*, Vol. 185, 2006, pp. 179–200.

[16] C. D. Coman, A. P. Bassom, "On the wrinkling of a pre–stressed annular thin film in tension", *Journal of the Mechanics and Physics of Solids*, Vol. 55, 2007, pp. 1601–1617.

[17] C. D. Coman, "On the applicability of tension field theory to a wrinkling instability problem", *Acta Mechanica*, Vol. 190, 2007, pp. 57–72.

[18] C. D. Coman, A. P. Bassom, "Wrinkling of pre–stressed annular thin films under azimuthal shearing", *Mathematics and Mechanics of Solids*, Vol. 13, 2008, pp.513–531.

[19] C.D. Coman, "Global asymptotic approximations for wrinkling of polar orthotropic annular plates in tension", *International Journal of Solids and Structures*, Vol. 47 (11–12), 2010, pp. 1572–1579.

[20] F. Cote, R. Biagi, H. Bart–Smith, V.S. Deshpande, "Structural response of pyramidal core sandwich columns", *International Journal of Solids and Structure*, Vol. 44 (10), 2007, pp. 3533–3556.

[21] K. Efimenko, M. Rackaitis, E. Manias, A. Vaziri, L. Mahadevan, J. Genzer, "Nested self–similar wrinkling patterns in skins", *Nature Materials*, Vol. 4(4), 2005, pp. 293–297.

[22] L.B. Freund, S. Suresh, *Thin Film Materials: Stress, Defect Formation, and Surface Evolution*, 2003, Cambridge University Press.

[23] N. Friedl, F.G. Rammerstorfer, F.D. Fisher, "Buckling of stretched strips", *Computers & Structures*, Vol. 78, 2000, pp.185–190.

[24] Y. Fu, H. Du, W. Huang, S. Zhang, M.Hu, "TiNi–based thin films in MEMS applications: A review", *Sensors and Actuators A: Physical*, Vol 112 (2–3), 2004, pp. 395–408.

[25] J.C. Geminard, R. Bernal, F. Melo, "Wrinkle formations in axi–symmetrically stretched membranes", *The European Physical Journal E*, Vol. 15, 2004, pp. 117–126.

[26] J.Genzer, J.Groenewold, "Soft matter with hard skin: From skin wrinkles to templating and material characterization", *Soft Matter*, Vol. 2 (4), 2006, pp. 310–323.

[27] J. Groenewold, “Wrinkling of plates coupled with soft elastic media”, *Physica A Statistical Mechanics and its Applications*, Vol. 298 (1), 2001, pp.32–45.

[28] R. Gilat, “A 3–D thermoelastic analysis of the buckling of a layer bonded to a compliant substrate and related problems”, *International Journal of Solids and Structures*, Vol. 47 (18–19), 2010, pp.2533–2542.

[29] C. Harrison, C. M. Stafford, W. Xhang, A. Karim, “Sinusoidal phase grating created by a tunably buckled surface”, *Applied Physics Letters*, Vol. 85 (18), 2004, pp. 4016–4018.

[30] J. C. Heald, M. J. Potvin, “Experimental mechanics of a wrinkled multi–layer deployable membrane space antenna”, *Collection of Technical Papers – AIAA/ASME/ASCE/AHS/ASC, Structures, Structural Dynamics and Materials Conference*, Vol. 1, 2006, pp. 74–84.

[31] H. Hu, S. Belouettar, M. Potier–Ferry, A. Makradi, “A novel finite element for global and local buckling analysis of sandwich beams”, *Composite Structures*, Vol. 90 (3), 2009, pp. 270–278.

[32] Z. Y. Huang, W. Hong, Z. Suo, “Nonlinear analyses of wrinkles in a film bonded to a compliant substrates”, *Journal of the Mechanics and Physics of Solids*, Vol. 53, 2005, pp. 2101–2118

[33] R. Huang, S. H. Im, “Dynamics of wrinkle growth and coarsening in stressed thin films”, *Physical Review E*, Vol. 74 (2), 2006, Article No. 026214.

[34] J. Huang, M. Juszkiewicz, W.H. De Jeu, E. Cerda,T. Emrick, N. Menon, T.P. Russell, “Capillary wrinkling of floating thin polymer films”, *Science*, Vol. 317, No. 5838, 2007, pp. 650–653.

[35] W. T. S. Huck, N. Bowden, P. Onck, T. Pardoen, J. W. Hutchinson, G. M. Whitesides, “Ordering of spontaneously formed buckles on planar surfaces”, *Langmuir*, Vol. 16, 2000, pp. 3497–3501.

[36] N. Jacques, M. Potier–Ferry, “On mode localisation in tensile plate buckling”, *Compter Rendus Mecanique*, Vol. 333, 2005, pp. 804–809.

[37] N. Jacques, A. Elias, M. Potier–Ferry, H. Zahrouni, “Buckling and wrinkling during strip conveying in processing lines”, *Journal of Materials Processing Technology*, Vol. 190, 2007, pp. 33–40.

[38] T.G.H. James, “Gold technology in ancient Egypt– Mastery of metal working methods”, *Gold Bulletin*, Vol. 5 (2), 1972, pp. 38–42.
[39] Y. B. Jeon, R. Sood, J.H. Jeong, S.G. Kim, “MEMS power generator with transverse mode thin film PZT”, *Sensors and Actuators A: Physical*, Vol 122 (1), 2005, pp. 16–22.
[40] F. Jia, Y.P. Cao, T.S. Liu, Y. Jiang, X.Q. Feng, S.W. Yu, “Wrinkling of a bilayer resting on a soft substrate under in–plane compression”, *Philosophical Magazine*, Vol. 92 (12), 2012, pp. 1554–1568.
[41] N. Jillella, J. Peddieson, “Modeling of wrinkling of thin circular sheets”, *International Journal of Non–Linear Mechanics*, Vol. 47 (1), 2012, pp. 85–91.
[42] S. Kang, S. Im, “Finite element analysis of wrinkling membranes”, *Journal of Applied Mechanics*, Vol. 64, 1997, pp. 263–269.
[43] M. Kawka, L. Olejnik, A. Rosochowski, H. Sunaga, A. Makinouchi, “Simulation of wrinkling in sheet metal forming”, *Journal of Materials Processing Technology*, Vol. 109 (3), 2001, pp. 283–289.
[44] A.D. Kerr, “The stress and stability analyses of railroad tracks”, *ASME Journal of Applied Mechanics*, Vol. 41, 1974, pp. 841–848.
[45] D.Y. Khang, J.A. Rogers, H.H. Lee, “Mechanical buckling: mechanics, metrology, and stretchable electronics”, *Advanced Functional Materials*, Vol. 19, 2009, pp. 1526–1536.
[46] M.K. Kang, R. Huang, “Swelling–induced instability of substrate–attached hydrogel lines”, *International Journal of Applied Mechanics*, Vol. 3 (2), 2011, pp. 219–233.
[47] T.Y. Kim, E. Puntel, E. Fried, “Numerical study of the wrinkling of a stretched thin sheet”, *International Journal of Solids and Structures*, Vol. 49 (5), 2012, pp. 771–782.
[48] P. Kumar, S. Pellegrino, “Computation of kinematic paths and bifurcation points”, *International Journal of Solids and Structures*, Vol. 37 (46), 2000, pp. 7003–7027.
[49] J.M. Lackner, W. Waldhauser, P. Hartmann, O. Miskovics, F. Schmied, C. Teichert, T. Schoberl, “Self–assembling (nano) wrinkling topography formation in low–temperature vacuum deposition on soft polymer surfaces”, *Thin Solid Films*, Vol. 520 (7) , 2012, pp. 2833–2840.

[50] S.P. Lacour, S. Wagner, Z. Huang, Z. Suo, “Stretchable gold conductors on elastomeric substrates”, *Applied Physics Letters*, Vol. 82 (15), 2003, pp. 2404–2406.
[51] S. P. Lacour, J. Jones, Z. Suo, S.Wagner, “Design and performance of thin metal film interconnects for skin–like electronic circuits”, *IEEE Electron Device Letters*, Vol. 25(4), 2004, pp.179–181.
[52] R.M. Lavker, P. Zheng, G. Dong, “Morphology of aged skin”, *Clinics in Geriatric Medicine*, Vol. 5(1), 1989, pp. 53–67.
[53] E.S. Lee, S.K. Youn, “Finite element analysis of wrinkling membrane structures with large deformations”, *Finite Element in Analysis and Design*, Vol. 42, 2006, pp. 780–791.
[54] Y. Lecieux, R. Bouzidi, “Experimental analysis on membrane wrinkling under biaxial load – Comparison with bifurcation analysis”, *International Journal of Solids and Structures*, Vol. 47(18–19), 2010, pp. 2459–2475.
[55] Y.L. Li, M.Y. Lu, H.F. Tan, Y.Q. Tan, “A study on wrinkling characteristics and dynamic mechanical behavior of membrane”, *Acta Mechanica Sinica*, Vol. 28 (1) , 2012, pp. 201–210.
[56] Z.S. Liu, S. Swaddiwudhipong, F.S. Cui, W. Hong, Z. Suo, Y.W. Zhang, “Analytical olutions of polymeric gel structures under buckling and wrinkle”**,** *International Journal of Applied Mechanics*, Vol. 3(2), 2011, pp. 235–257.
[57] O. Lourie, D. M. Cox, H. D. Wagner, “Buckling and collapse of embedded carbon nanotubes”, *Physical Review Letters*, Vol. 81(8), 1998, pp.1638–1641.
[58] K. Lu, M. Accorsi, J. Leonard, “Finite element analysis of membrane wrinkling”, *International Journal for Numerical Methods in Engineering*, Vol. 50, 2001, pp.1017–1038.
[59] T.M. McCormack, R. Miller, O. Kesler, L.J. Gibson, “Failure of sandwich beams with metallic foam cores”, *International Journal of Solids and Structures*, Vol. 38 (28–29), 2001, pp. 4901–4920.
[60] O. Music, J.M. Allwood, K. Kawai, “A review of the mechanics of metal spinning”, *Journal of Materials Processing Technology*, Vol. 210 (1), 2010, pp. 3–23.

[61] V. Nayyar, K. Ravi–Chandar, R. Huang, "Stretch–induced stress patterns and wrinkles in hyperelastic thin sheets", *International Journal of Solids and Structures*, Vol. 48 (25–26), 2011, pp. 3471–3483.

[62] K. Niu, R. Talreja, "Modeling of wrinkling in sandwich panels under compression", *Journal of Engineering Mechanics,* Vol. 125(8), 1999, pp. 875–883.

[63] M. Ohring, *Materials Science of Thin Films: Deposition and Structure*, 2nd. Ed., 2002, Elsevier, Inc.

[64] R. Orszulik, J. Shan, M. Stachowsky, "Membrane structure active flatness control using genetic algorithm with online objective reweighting", *Acta Astronautica*, Vol. 68 (11–12), 2011, pp. 2012–2024.

[65] L. Pocivavsek, R. Dellsy, A. Kern, S. Johnson, B. Lin, K. C. Lee, E. Cerda, "Stress and fold localization in thin elastic membranes", *Science*, Vol. 320 , 2008, pp. 912–916.

[66] E. Puntel, L. Deseri, E. Fried, "Wrinkling of a stretched thin sheet", *Journal of Elasticity*, Vol. 105(1–2), 2011, pp. 137–170.

[67] A. E. Riad, F. D. Barlow, *Thin Film Technology Handbook*, 1998, McGraw–Hill.

[68] A. Schweikart, A. Fery, "Controlled wrinkling as a novel method for the fabrication of patterned surfaces", *Microchimica Acta*, Vol. 165 (3–4), 2009, pp. 249–263.

[69] J. Song, H. Jiang, W. M. Choi, D. Y. Khang, Y. Huang, J. A. Rogers, An analytical study of two–dimensional buckling of thin films on compliant substrates", *Journal of Applied Physics*, Vol. 103, 2008, Article No. 014303.

[70] C. M. Stafford, C. Harrison, K. L. Beers, A. Karim, E. J. Amis, M.R. Vanlandingham, H. Kim, W. Volksen, R. D. Miller, E. E. Simonyi, "A buckling–based metrology for measuring the elastic moduli of polymeric thin films", *Nature Materials*, Vol. 3, 2004, pp. 545–550.

[71] G.G. Stoney, "The tension of metallic films deposited by electrolysis", *Proceedings of the Royal Society of London*, Series A, Vol. 82, 1909, pp. 172–175.

[72] Y. Sun, W.M. Choi, H. Jiang, Y. Huang, J.A. Rogers, "Controlled buckling of semiconductor nanoribbons for stretchable electronics", *Nature Nanotechnology*, Vol. 1, 2006, pp. 201–207.

[73] A. I. Teixeira, G. A. Abrams, P. J. Bertics, C. J. Murphy, P. F. Nealey, “Epithelial contact guidance on well–defined micro– and nanostructured substrates”, *Journal of Cell Science*, Vol. 116, 2003, pp.1881–1892.

[74] S. Tarasovs, J. Andersons, “Buckling of a coating strip of finite width bonded to elastic half–space”, *International Journal of Solids and Structures*, Vol. 45 (2), 2008, pp. 593–600.

[75] A. L. Volynskii, S. Bazhenov, O. V. Lebedeva, N. F. Bakeev, “Mechanical buckling instability of thin coatings deposited on soft polymer substrates”, *Journal of Materials Science*, Vol. 35(3), 2000, pp. 547–554.

[76] X. Wang, J. Cao, “On the prediction of side–wall wrinkling in sheet metal forming processes”, *International Journal of Mechanical Sciences*, Vol. 42(12), 2000, pp. 2369–2394.

[77] S. Wang, J. Song, D. Kim, Y. Huang, J. A. Rogers, “Local versus global buckling of thin films on elastomeric substrates”, *Applied Physics Letters*, Vol. 93, 2008, Article No. 023126.

[78] C.G. Wang, X.W. Du, H.F. Tan, X.D. He, “A new computational method for wrinkling analysis of gossamer space structures”, *International Journal of Solids and Structures*, Vol. 46 (6), 2009, pp. 1516–1526.

[79] M. Watanabe, “Striped–pattern formation of a thin gold film deposited onto a stretched elastic silicone substrate”, *Journal of Polymer Science Part B: Polymer Physics*, Vol. 43, 2005, pp. 1532–1537.

[80] E. A. Wilder, S. Guo, S. Lin–Gibson, M. J. Fasolka, C. M. Stafford, “Measuring the modulus of soft polymer networks via a buckling–based metrology”, *Macromolecules*, Vol. 39(12), 2006, pp. 4138–4143.

[81] Y.W. Wong & S. Pellegrino, “Wrinkles in square membranes”, *Computational Methods in Applied Sciences: Textile Composites and Inflatable Structures*, Vol. 3, 2005, pp. 109–122.

[82] P. J. Yoo, H. H. Lee, “Evolution of a stress–driven pattern in thin bilayer films: Spinodal wrinkling”, *Physical Review Letters*, Vol. 91(15), 2003, pp. 154502/1–4.

[83] P. J. You, K. Y. Suh, S. Y. Park, H. H. Lee, “Physical self–assembly of microstructures by anisotropic buckling”, *Advanced Materials*, Vol. 14 (19), 2002, pp. 1383–1387.

[84] T.X. Yu, W.J. Stronge, “Wrinkling of a circular elastic plate stamped by a spherical punch”, *International Journal of Solids and Structures*, Vol. 21(10), 1985, pp. 995–1003.

[85] Y. Zhao, W.M. Huang, Y.Q. Fu, “Formation of micro/nano–scale wrinkling patterns atop shape memory polymers”, *Journal of Micromechanics and Microengineering*, Vol. 21 (6), 2011, pp. 067007/1–8.

Chapter 2

2 Fundamental Theories and Formulations

In this chapter, some fundamental concepts and theories required for the thesis are described. These materials mainly include stability of a system, bifurcation theory, beam and plate theory and finite difference method.

2.1 Structural Stability of a System

Stability is defined as the state or quality of being stable as the resistance to change, deterioration or displacement. Stability theory mathematically considers the stability of solutions of differential equations under small perturbations. In other words, a theorem is stable if small changes in the hypothesis result in small variations in the conclusion. This concept can be extended to various fields such as numerical stability in numerical analysis, probability stability in probability theory, chemical stability, thermal stability, ecological stability and so on. For a dynamical system, the Lyapunov stability and the structural stability are two main classes categorized in the literature. The Lyapunov stability occurs when the system remains stable under perturbations of initial conditions such that for all of the points sufficiently near an equilibrium point, the solutions of the system stay near the solution of the equilibrium point. Unlike the Lyapunov stability, the structural stability considers the perturbations of the system itself, so that the qualitative behavior of the structure is unaffected by small perturbations. A. Andronov and L. Pontryagin in 1937 introduced the structurally stable systems under the name "systemes grossieres" or rough systems and proposed a characterization of rough systems coined as Andronov–Pontryagin criterion [Kuznetsov, 2004].

For a mechanical system modeled by using a set of differential equations mathematically, all the solutions that satisfy the governing differential equation represent an admissible domain of the solution and satisfy static or dynamic equilibrium condition. The admissible domain is represented by equilibrium paths and the configurations of the equilibrium of the system represent the points of these paths. The system is stable at some points and at the others it is unstable. “According to the dynamic criterion for loss of

stability, an equilibrium configuration is stable if and only if a small perturbation of the configuration results in configurations that are confined to the immediate vicinity of the equilibrium configuration" [Brush and Almroth, 1975, pp. 15].

Leonhard Euler (1707–1783) is known as the founder of the elastic stability, who considered the equilibrium equation and buckling load of a compressed elastic column by using the theory of calculus of variations, published in 1744 as the appendix "*De curvis elastics*" of his book entitled as "*Methodus inveniendi lineas curvas maximi minimive proprietate gaudentes*". By developing an energy approach, Joseph–Louis Lagrange (1736–1813) studied the mechanical problems and established the fundamental energy theorem of minimum total potential energy to be sufficient for the stability analysis. Jules H. Poincare (1854–1912) introduced the bifurcation theory and classified the singularities. Aleksandr M. Lyapunov (1857–1918) presented the definitions of the stability by energy functions and Lev S. Pontryagin (1908–1988) and Aleksandr A. Andronov (1901–1952) introduced the topological concept of the structural stability. Theodore von Karman (1881–1963) worked on inelastic buckling of columns and proposed a model to explain hysteresis loops and plastic deformation of beams. Warner T. Koiter (1914–1997) developed the classical nonlinear bifurcation theory followed by John W. Hutchinson to propose the nonlinear branching theory of structures in plastic range [Wang *et al*. 2005, pp. 5].

Stability of a static system can be investigated by considering its potential energy. Based on the principle of minimum potential energy, "the system takes a configuration of stable equilibrium if and only if the change of the total potential energy corresponding to any sufficiently small kinematically admissible displacement is positive. A displacement is kinematically admissible if it satisfies certain continuity and boundary conditions" [Brush and Almroth, 1975, pp. 15].

Therefore, if the change in the potential energy I of the system is represented by ΔI, then by using Taylor expansion

$$\Delta I = I - I_0 = \delta I + \frac{1}{2!}\delta^2 I + \frac{1}{3!}\delta^3 I + \cdots \qquad (2\text{-}1)$$

in which the first term on the right hand side is the first variation of the potential energy, the second term is the second variation of the potential energy and so forth. On the other hand, for an infinitesimally small variational displacement, terms on the right hand side

are linear, quadratic, etc., respectively. Based on the principle of minimum potential energy, the potential energy of the system in the equilibrium configuration is stationary which leads to $\delta I = 0$. Therefore the sign of ΔI which determines the stability mode (stable, neutral or unstable equilibrium) is determined by the sign of the second variation. For the positive values of the second variation, the system is in stable mode; while for the negative values of the second variation, it is in unstable mode. The vanishing of the second variation is defined as the criterion of the loosing stability of the stable systems known as Trefftz criterion [Brush and Almroth, 1975, pp. 365]. Adjacent equilibrium criterion also leads to the same results of the minimum potential energy criterion for the stability of the static conservative structural systems.

By solving the governing differential equations of the system, an equilibrium configuration is established as the primary equilibrium path. The linear equation can be used to determine whether an adjacent equilibrium configuration exists at some points of the primary path. Existence of such a configuration introduces the points on the equilibrium path that multiple configurations are allowed for the system which are called bifurcation points.

2.2 Bifurcation, Buckling and Wrinkling

The bifurcation points or branch points are attributed to the points of the solution domain for which multiple equilibrium configurations emerge [Bloom and Coffin, 2001, pp. 7]. When the boundary value problem of a static conservative structural system is represented in the form of

$$G(\lambda, u) = 0 \tag{2-2}$$

where λ is a real number corresponding with the loading on the system, u is an element of a real Banach space (i.e. a complete vector space with defined norm) corresponding with the displacement field and G is a nonlinear mapping representing the governing equation of the system, then ordered pair (λ^*,u^*) which satisfies the equation (2-2) is the solution of the governing equation of the system or the primary path which determines the behavior of the system. In order to find the nontrivial solution of the system (λ^*,u^*) $\neq$ (λ^*,0) so that when λ approaches λ^* then norm of u^* goes to a nonzero small value, the

bifurcation theory is used. In other words, $\lambda = \lambda^*$ is a bifurcation point (equivalently a branch point) of the equation (2-2) if every neighborhood of $(\lambda^*,0)$ consists a solution (λ^*,u^*) with nonzero norm of u^* [Bloom and Coffin, 2001, pp. 8].

The bifurcation theory determines the location of the branch points and the relation of them with the eigenvalue problem of the differential equation of the system. Also it determines how many distinct branches originate from a bifurcation point. According to the bifurcation theory, for the nonlinear differential equation (2-2) with an equilibrium solution pair (λ^*,u^*) satisfying the equation, if the linearized mapping $G_{Linear}(\lambda,u)$ has an inverse at (λ^*,u^*) which is bounded, then (λ^*,u^*) is unique so that for λ sufficiently near to λ^*, the pair (λ^*,u^*) is the only solution of the equation [Bloom and Coffin, 2001].

Since for the nonlinear mapping $G(\lambda,u)$ with a bounded invertible $G_{Linear}(\lambda,u)$ at the equilibrium solution (λ^*,u^*), the solution of the system is unique, one may conclude that no branching or bifurcation of the solutions can occur. Consequently, it is concluded that bifurcation or branching of the solution can only occur if the linear mapping $G_{Linear}(\lambda,u)$ is singular at (λ^*,u^*).

The nonlinear mapping $G(\lambda,u)$ is usually assumed in a particular form of nonlinear differential operator L as

$$G(\lambda,u) = L[u] - \lambda u = 0 \qquad (2\text{-}3)$$

For linear mapping, the parameters λ and u are the eigenvalue and eigenfunction of the eigenvalue problem for the differential equation, which are corresponding with the bifurcation point of the system. At a bifurcation point the equilibrium equations of the system have multiple solutions and for each solution a new equilibrium path appears on the stability diagram which can be followed by the system. Small disturbances at the bifurcation point leads that system follows a new stable path or remains on the previous one [Bloom and Coffin, 2001].

Structural instability of the mechanical systems can be categorized in two main groups as buckling and wrinkling. The global instability refers to the overall buckling of the system under applied loading, while local instability is corresponding with the local wrinkling of the system with a fine wavy pattern. In contrast with the global buckling with large wavelength, in wrinkling the flexures have tiny wavelength. Therefore, in order to investigate the buckling/wrinkling phenomenon, the instability of the system

should be considered. The same procedure for analyzing the global buckling of the mechanical systems is also used in considering the wrinkling of the system; while for the later the number of flexures is increased to create a fine wavy pattern with tiny wavelength.

For a mechanical system, the bifurcation points are related with the vanishing of the change of the potential energy of the system in equation (2-1). In fact, at the branch point the second variation of the potential energy vanishes for small perturbation around the equilibrium position and the critical instability load is attributed to the minimum load in which the instability occurs [Jones, 2006].

2.3 Tension Field Theory

Other than the instability theory based on the minimum potential energy principle, a number of theories have been developed by the researchers over the years. Among these theories, one is known as tension field theory which mainly focuses on the shape of the wrinkled regions geometrically, while other factors such as amplitude and wavelength of the wrinkles remain undetermined.

Tension field theory, first developed by Wanger in 1929 on airplane wing assumes that the structure is too thin to bear any in–plane compression. By using the concept of plane stress field, a state with only tensile stress components is sought and concludes that for the membrane with negligible resistance against the compression, the principal stress along a wrinkle is tensile [Reissner, 1938]. By introducing a geometrical ray analysis, Kondo *et al*. (1955) and Mansfield (1968, 1970) contributed to the theory by replacing the strain energy used in the tension field theory by a suitable relaxed energy density. Pipkin (1986) and Steigmann and Pipkin (1989) developed the relaxation strain energy of the isotropic elastic membranes with wrinkling deformation which represents the average energy per unit initial area over a region containing many wrinkles. Wu (1978) found the strains of wrinkled and taut parts separately, and by using the continuity of stresses and displacements at the wrinkled/taut transition locations analyzed partly wrinkled structures.

A membrane can take one of the following states; it can be taut under tensile loading, it can be slack or free of stress; or it can be wrinkled when there is a uniaxial state of tensile stress [Hornig and Schoop, 2003]. The Stein–Hedgepeth theory (1961) represents that in the wrinkled membranes, all the compressive stresses are eliminated completely while the minor principal stress is non–negative everywhere on the membrane. The wrinkles along the directions of the troughs and crests carry the entire tensile load in the wrinkled regions and the minor principal stress perpendicular to the load paths are zero. The theory based on the principal stresses σ_1 and $\sigma_2 \leq \sigma_1$ of the film is represented as [Ding and Yang, 2003]

A. $\sigma_2 > 0$: Taut membrane
B. $\sigma_1 > 0$ and $\sigma_2 \leq 0$: Wrinkled membrane
C. $\sigma_1 \leq 0$: Slack membrane

Similar criteria can be defined based on the principal strains or a combination of the principal stress/strain of the membrane. As mentioned before, such theories only provide some information for the shape of the wrinkling region based on the geometrical ray analysis in which wrinkles propagate along the ray in the direction of the uniaxial tensile loading on the film. While, the bifurcation theory determines both the applied load on the mechanical system upon instability and the pattern of the wrinkles (i.e. wavelength, amplitude).

2.4 Beam and Plate Theory

Beams and plates are structural elements used commonly in mechanics of deformable bodies to describe the relation of the displacement and loading on the system. For these elements, by using the simplifying assumptions, the necessity of solving the elasticity differential equations of the equilibrium of the structure in the general form is cancelled out and the solution is obtained easier. By using the linear and nonlinear theories of beam/plate, the small and large deflection of the structures are considered.

For a beam element in which one dimension is much longer than two other dimensions, the basic equations of the system are derived by using kinematic assumptions. Based on the zero shear strain assumption for thin structures with small

deformation, plane sections remain planar and perpendicular to the neutral axis during deformation and hence the moment displacement relation is given by [Timoshenko, 1940]

$$M = EI\ \frac{d^2w}{dx^2} \tag{2-4}$$

where EI is the flexural rigidity, w is the deflection, x is the longitudinal coordinate and M is the bending moment. It is shown that the equilibrium equations of the beam are given by

$$Q = \frac{dM}{dx} \tag{2-5-A}$$

$$\frac{dQ}{dx} = -N\frac{d^2w}{dx^2} - p \tag{2-5-B}$$

while Q is the transverse shear force on the section of the beam subjected to an axial compressive force N and a distributed lateral load with intensity p along the beam. Substituting (2-4) and (2-5-A) into (2-5-B) leads to the Euler beam equation as

$$\frac{d^2}{dx^2}\left[EI\frac{d^2w}{dx^2}\right] + N\frac{d^2w}{dx^2} + p = 0 \tag{2-6}$$

Plates are described as flat structural elements in the mechanical systems in which one dimension (i.e. thickness) is much smaller than two other dimensions. In contrast with the membrane elements which can support only in–plane loadings, plates hold the moment components too. The displacement components of each point of the plate are represented versus displacement field of the mid–plane of the plate by a kinematic assumption. Therefore, a complicated three dimensional system is reduced to a more simplified system. For thin plate structures, small and large deflection theories are introduced in the literature. Kirchhoff plate theory which holds for small deflection of thin plates considers only the effect of the bending and by using plane stress and plane strain assumptions, its governing equation is derived for the static isotropic plate by [Timoshenko, 1940]

$$D\nabla^4 w = p \tag{2-7}$$

where w is out of plane displacement of the plate (i.e. deflection), D is the bending stiffness of the plate and p is the lateral distributed loading on the plate.

For large deflection of thin plate, von Karman plate theory is represented in which the effect of the in–plane loading is considered on the mid–plane of the plate. The differential equations governing on a von Karman rectangular isotropic plate under the

effect of in–plane forces N_x, N_y and N_{xy} and lateral distributed loading p are represented by [Bloom and Coffin, 2001]

$$\frac{\partial N_x}{\partial x} + \frac{\partial N_{xy}}{\partial y} = 0 \quad \text{(2-8-A)}$$

$$\frac{\partial N_{xy}}{\partial x} + \frac{\partial N_y}{\partial y} = 0 \quad \text{(2-8-B)}$$

$$D\nabla^4 w - N_x \frac{\partial^2 w}{\partial x^2} - N_y \frac{\partial^2 w}{\partial y^2} - 2N_{xy} \frac{\partial^2 w}{\partial x\, \partial y} = p \quad \text{(2-8-C)}$$

Also the potential energy of the plate is represented by considering bending strain energy, stretching strain energy and external work on the plate [Bloom and Coffin, 2001] described in the next chapters whenever is needed. There are other theories for plate structures developed by other researchers and are found in the literature comprehensively.

2.5 Different Models for the Foundation

In order to consider the effect of the elastic foundation (i.e. the substrate of the film) on the mechanical behavior of the beam/plate, various models have been introduced by the researchers reviewed by Wang *et al.* (2005). Models represent the elastic, viscoelastic and plastic behavior of the materials and cover different loading patterns such as transverse loading or in–plane loading on the beam/plate, described as follow.

2.5.1 Linear Pressure Model

For short beams on an elastic foundation, the contact pressure is assumed to be uniform under symmetric loading. The profile of the contact pressure can also be assumed linear for other types of loading. For a plate resting on the foundation, a two dimensional linear profile is assumed for the plate–foundation interaction [Selvadurai, 1979; Wang *et al.*, 2005].

2.5.2 Winkler Model

In Winkler model, the interaction of the foundation–beam/plate is modeled with a spring system which applies distributed external transverse load on the beam/plate. In other words, the contact pressure at any point on the beam/plate is assumed to be proportional to the deflection of the system at that position and independent of the deflection at other

locations. Therefore, according to the spring model of the Winkler foundation, the elements of the film with bigger deflection endure bigger interaction from the foundation. The Winkler model can be formulated mathematically as [Winkler, 1867],

$$q(x,y) = K\, w(x,y) \tag{8-1}$$

where the parameter $q(x, y)$ is the imposed contact pressure from the foundation on the beam/plate, $w(x, y)$ is the deflection of the beam/plate at the coordinate (x, y) and K is the spring stiffness of the Winkler foundation called as the modulus of the foundation. The modulus of the Winkler foundation is proportional to the elastic modulus E_f and finite depth of the foundation H_f proposed by Allen (1969) as,

$$K \sim \frac{E_f}{H_f} \tag{8-2}$$

Niu (1998) modified the classical definition of Winkler modulus in (8-2) for plane stress and plane strain foundations respectively by,

$$K = \frac{E_f}{(1-v_f{}^2)H_f} \tag{8-3-A}$$

and

$$K = \frac{(1-v_f)E_f}{(1-2v_f)(1+v_f)H_f} \tag{8-3-B}$$

where E_f, v_f and H_f are Young's modulus, Poisson's ratio and thickness of the foundation. For thick foundation in wrinkling problem, H_f is replaced by an equivalent thickness according to the wrinkling wavelength [Niu and Talreja, 1999].

In the above mentioned studies, the Winkler modulus was assumed as a constant parameter along the domain for a uniform foundation. While for a non–uniform foundation [Soldrttos and Selvadurau, 1985; Mofid and Noroozi, 2009; Teodoru and Musat, 2008], a variable modulus $K(x,y)$ is assumed as a function of x and y.

Besides the linear interaction between the film and the substrate in equation (8-1), a nonlinear interaction between the substrate and the beam/plate can be proposed as

$$q(x,y) = K_1\, w + K_3\, w^3 \tag{8-4}$$

where K_1 and K_3 are linear and nonlinear (cubic) foundation modulus, respectively [Raju and Rao, 1993, Shih and Blotter, 1993; Coskun, 2000; Wasti and Senkaya, 2008].

2.5.3 Two–Parameters Model

Two–parameter foundation models can be considered as the Filonenko–Borodich, Pasternak, Hetenyi and Vlasov models [Wang *et. al*, 2005]. In these models, the in–plane interaction of the foundation and the film is also taken into account so that the load–displacement relation of the interaction is given by [Wang *et. al*, 2005; Naidu and Rao, 1996; Shen, 2000]

$$q(x,y) = K_f\, w(x,y) - G_f\, \nabla^2 w(x,y) \qquad (8\text{-}5)$$

where $q(x, y)$ is the imposed contact pressure from the foundation on the beam/plate, K_f is the Winkler foundation stiffness and G_f is a constant showing the effect of the in–plane interactions on the film, and ∇^2 is the Laplace operator in x and y. The parameter G_f can be represented by tension action on the film in Filonenko–Borodich model or substrate shear parameter in Pasternak model.

In addition, other models have been proposed by Kerr (1964), Reissner (1958) and Vlasov & Leontev (1966) which commonly have other parameters in addition to the in–plane interaction parameter G_f. However, the additional parameters improve the accuracy of the modeling, but determining those parameters is considered as a difficult process [Wang *et. al*, 2005]. More detailed information about these models can be found in the related literatures [Winkler, 1867; Zimmermann, 1930; Hetenyi, 1946; Pasternak, 1954].

2.6 Finite Difference Method

Among various methods to solve the differential equations numerically, finite difference method is one of the most important techniques commonly used by the researchers. It is simple, versatile and suitable for computer programs with high accuracy in solving differential equations. In this method, the differential equation is replaced by difference equations and the solution of the problem reduces to the simultaneous solution of a set of algebraic equations.

The finite difference is the discrete analog of the derivative as discussed by Hildebrand (1968). In this method, the domain is desctitized by introducing some nodes of stencil configuration. A stencil is a geometric arrangement of a nodal group related to

the point of interest by using a numerical approximation routine. For example, for a five–point stencil configuration in one dimension, four nodes are located on the neighborhood of the central node x_0 at the locations $\{x_0–2h,\ x_0–h,\ x_0+h,\ x_0+2h\}$. The relation of the finite difference is applied on the nodes of a N–point stencil configuration and the derivatives of the field variable are approximated by the finite differences of the values of the field variable at the nodes by using the difference quotient formula [Abramowitz and Stegun, 1972]. For a continuous function of x as $y=f(x)$, the first forward difference of y at point x_n denoted by Δy_n is given by [Hildebrand, 1968]

$$\Delta y_n = y_{n+1} - y_n \cong h\frac{dy}{dx} \tag{2-9}$$

where $h= x_{n+1} - x_n$ is the step size between neighborhood nodes. Similarly, the first backward difference of y at point x_n denoted by ∇y_n is

$$\nabla y_n = y_n - y_{n-1} \cong h\frac{dy}{dx} \tag{2-10}$$

The central difference method deals with the nodes symmetrically located with respect to x_n and often results in more accurate approximation than forward and backward differences. The first central difference δy_n is given by

$$\delta y_n = \frac{1}{2}(y_{n+1} - y_{n-1}) \cong h\frac{dy}{dx} \tag{2-11-A}$$

The corresponding central differences of higher order are defined by iteration as

$$\delta^2 y_n = y_{n+1} - 2y_n + y_{n-1} \cong h^2\frac{d^2y}{dx^2} \tag{2-11-B}$$

$$\delta^3 y_n = \frac{1}{2}y_{n+2} - y_{n+1} + y_{n-1} - \frac{1}{2}y_{n-2} \cong h^3\frac{d^3y}{dx^3} \tag{2-11-C}$$

$$\delta^4 y_n = y_{n+2} - 4y_{n+1} + 6y_n - 4y_{n-1} + y_{n-2} \cong h^4\frac{d^4y}{dx^4} \tag{2-11-D}$$

In order to determine the finite difference coefficients of a k order derivative with an arbitrary order of accuracy, two different methods are introduced. The first method uses the Taylor expansion formula of the continuous function $y=f(x)$ at x_n+h in the neighborhood of x_n as

$$f(x_n + h) = f(x_n) + \frac{h}{1!}\frac{df(x_n)}{dx} + \frac{h^2}{2!}\frac{d^2f(x_n)}{dx^2} + \cdots + \frac{h^k}{k!}\frac{d^kf(x_n)}{dx^k} + R_{k+1}(x) \tag{2-12}$$

where R_{k+1} is the remaining term denoting the difference between Taylor expansion of degree k and the exact value of the function $f(x)$. For example, for the first order approximation of Taylor expansion one may find

$$f(x_n + h) = f(x_n) + \frac{df(x_n)}{dx} h + R_2(x) \tag{2-13}$$

From (2-13) with some algebraic manipulation, the first forward difference in (2-9) is derived and the first derivative is approximated by

$$\frac{df(x_n)}{dx} = \frac{f(x_n+h)-f(x_n)}{h} - \frac{R_2(x)}{h} \tag{2-14}$$

The error in approximating the first derivative of function $f(x)$ by using forward finite difference in (2-14) is

$$\frac{R_2(x)}{h} = \frac{1}{h}\sum_{k=2}^{\infty} \frac{h^k}{k!} \frac{d^k f(x_n)}{dx^k} \cong O(h) \tag{2-15}$$

which is in the order of the step size h. Similar procedure for central method shows that the error of the first derivative is in the order of $O(h^2)$, so the central method has a higher convergence rate than forward and backward methods.

The second method used to derive the difference formula is based on the differentiating the Lagrange polynomials [Abramowitz and Stegun, 1972]. The Lagrange polynomials are defined as

$$L_j(x) = \prod_{\substack{0\le m\le k \\ m\neq j}} \frac{x-x_m}{x_j-x_m} = \frac{x-x_0}{x_j-x_0} \dots \frac{x-x_{j-1}}{x_j-x_{j-1}} \frac{x-x_{j+1}}{x_j-x_{j+1}} \dots \frac{x-x_k}{x_j-x_k} \tag{2-16}$$

and the function $f(x)$ is approximated as

$$f(x) = \sum_{j=-M}^{j=M} L_j(x)\, f(x_j) \tag{2-17}$$

where the domain is meshed by an N–point stencil configuration with N=2M+1 nodes (along each direction for multi–dimensional case). Therefore, the k^{th} order derivative of function $f(x)$ is approximated by a weighted linear sum of the function values at 2M+1 nodes as [Zhao and Wei, 2009]

$$\frac{d^k}{dx^k} f(x) = \sum_{j=-M}^{M} \frac{d^k L_j(x)}{dx^k} f(x_j) \tag{2-18}$$

The differentiation of the Lagrange polynomials is carried out analytically. For example, for first, second, third and forth order derivatives, one may find

$$\frac{d}{dx} L_j(x) = \sum_{\substack{k=-M \\ k\neq j}}^{M} \frac{1}{x_j-x_k} \prod_{\substack{i=-M \\ i\neq k,j}}^{M} \frac{x-x_i}{x_j-x_i} \tag{2-19-A}$$

$$\frac{d^2}{dx^2} L_j(x) = \sum_{\substack{k,m=-M \\ k\neq j\neq m}}^{M} \frac{1}{x_j-x_k} \frac{1}{x_j-x_m} \prod_{\substack{i=-M \\ i\neq k,j,m}}^{M} \frac{x-x_i}{x_j-x_i} \tag{2-19-B}$$

$$\frac{d^3}{dx^3} L_j(x) = \sum_{\substack{k,m,p=-M \\ k\neq j\neq m\neq p}}^{M} \frac{1}{x_j-x_k} \frac{1}{x_j-x_m} \frac{1}{x_j-x_p} \prod_{\substack{i=-M \\ i\neq k,j,m,p}}^{M} \frac{x-x_i}{x_j-x_i} \tag{2-19-C}$$

$$\frac{d^4}{dx^4}L_j(x) = \sum_{\substack{k,m,p,q=-M \\ k\neq j\neq m\neq p\neq q}}^{M} \frac{1}{x_j-x_k}\frac{1}{x_j-x_m}\frac{1}{x_j-x_p}\frac{1}{x_j-x_q}\prod_{\substack{i=-M \\ i\neq k,j,m,p,q}}^{M}\frac{x-x_i}{x_j-x_i} \qquad (2\text{-}19\text{-}D)$$

and by substituting the coordinate of each node of the stencil configuration in (2-19-A-D), the corresponding coefficients of the finite difference approach are obtained [Zhao and Wei, 2009].

There are two sources of error in finite difference method. The first one is the loss of precision due to computer rounding of decimal numbers which is called round–off error. The second source is truncation error or discretization error, which is the difference between the solution of the finite difference equation and the exact solution of the problem. The truncation error deals with the finite difference formulation used to approximate the problem which is controlled by handling the number of nodes attributed to the system. As mentioned before, the truncation of Taylor expansion leads to the remaining term of R_{k+1} in (2-12) as [Hildebrand, 1968]

$$R_{k+1}(x+h) = \frac{1}{(k+1)!}\frac{d^{k+1}f(x_n)}{dx^{k+1}}h^{k+1} \qquad (2\text{-}20)$$

which is in the order of h^{k+1} denoted by $O(h^{k+1})$ and indicates a quantity that approaches zero proportional to h^{k+1} as $h\rightarrow 0$. Clearly, for finite difference formulation with higher order of $O(h^{k+1})$, the rate of convergence increases as the number of mesh of the system increases too. More nodes in the stencil configuration lead to higher order approximation of the finite difference formulation. For example, a central difference formula for a stencil configuration with three, five and seven nodes provides an approximation with second, fourth, and sixth order of accuracy (i.e. $O(h^2)$, $O(h^4)$ and $O(h^6)$), respectively.

The finite difference formulation substitutes the differential equation of the system with a set of the algebraic equations system. The values of field variable at the nodes of the discretized system are unknowns of the algebraic equations system. On the other hand, in order to complete the system of algebraic equations and remove the singularity of the system, the boundary conditions are applied. The Dirichlet condition is the simplest type of boundary conditions which constrains the field variable on the boundaries known as the first type boundary condition. In this case, the values corresponding with the variable field are introduced on the boundaries such as fixed ends of a solid body. The second type boundary condition known as Neumann condition is applied on the derivatives of the filed variable along the boundaries. For the boundary

conditions that the derivatives of the function are given (i.e. Neumann or mixed boundary condition), imposing the finite difference technique for the problems seems to be difficult or inapplicable, because the derivatives of the field variable are represented by using the values of the function at the neighbor nodes of the boundaries which include some nodes outside the domain. In these cases, by introducing some virtual nodes outside the domain, the derivatives of the function are approximated by using the finite difference formulation. The values of the field variable on the virtual nodes are defined by using some assumptions. For example, symmetric and antisymmetric extensions of the field variable on the boundaries provide the values of the field variable at the virtual nodes. Such a fictitious domain boundary treatment has successfully handled many boundary conditions such as the simply supported, clamped and transversely supported edges in structural analysis [Wei, 1999; Zhao and Wei, 2009]. For example, at a clamped edge the boundary conditions are given as zero deflection and slop which is represented by using a symmetric extension [Wei *et al.*, 2002]. At a simply supported edge, the boundary conditions are given as zero deflection and moment and hence, the anti–symmetric extension [Wei *et al.*, 2002] is used. However, for more complex boundary conditions, such as Robin condition or the free edge condition, the proposed method cannot maintain high–order accuracy at the boundaries.

2.7 Summary

In this chapter, essential theories for analyzing the instability of thin solid films are introduced. The stability of the mechanical systems is considered by using the potential energy of the system. According to the bifurcation theory, the instability of the system corresponds with the eigenvalue problem for the differential equation of the system. On the other hand, tension field theory proposes a criterion for the onset of wrinkling of the films. Other materials such as structural elements of beam and plate used to model the film are introduced. Finally, solution techniques for solving the differential equations according to finite difference method are reviewed.

2.8 References

[1] M. Abramowitz, I.A. Stegun, *Handbook of Mathematical Functions*, 1972, Dover Publications, New York.

[2] H.G. Allen, *Analysis and Design of Structural Sandwich Panels*, 1969, Pergamon Press, Oxford.

[3] A.A. Andronov, L. S. Pontryagin, "*Грубые системы* [Coarse systems]". *Doklady Akademii Nauk SSSR*, Vol. 14 (5), 1937, pp. 247–250.

[4] F. Bloom, D. Coffin, *Handbook of Thin Plate Buckling and Postbuckling*, 2001, Chapman & Hall CRC.

[5] D.O. Brush, B.O. Almroth, *Buckling of Bars, Plates and Shells*, 1975, McGraw–Hill, Inc.

[6] I. Coskun, "Non–linear vibrations of a beam resting on a tensionless Winkler foundation", *Journal of Sound and Vibration*, Vol. 236 (3), 2000, pp. 401–411.

[7] H. Ding, B. Yang, "The modeling and numerical analysis of wrinkled membranes", *International Journal for Numerical Methods in Engineering*, vol. 58, 2003, pp.1785–1801.

[8] M. Hetenyi, *Beams on Elastic Foundation; Theory with Applications in the Fields of Civil and Mechanical Engineering*, 1946, The University of Michigan press, Ann Arbor.

[9] F.B. Hildebrand, *Finite Difference Equations and Simulations*, 1968, Prentice Hall, Inc.

[10] J. Hornig, H. Schoop, "Closed form analysis of wrinkled membranes with linear stress–strain relation", *Computational Mechanics*, Vol. 30, 2003, pp. 259–263.

[11] R. M. Jones, *Buckling of Bars, Plates and Shells*, 2006, Bull Ridge Publishing.

[12] A.D. Kerr, "Elastic and viscoelastic foundation models", *Journal of Applied Mechanics* (*ASME*), Vol. 31, 1964, pp. 491–498.

[13] K. Kondo, T. Iai, S. Moriguri, T. Murasaki, "Tension field theory", *Memoirs of the Unifying Study of the Basic Problems in Engineering, Science by Means of Geometry*, Vol. 1, 1955, pp. 417–441.

[14] Y. A. Kuznetsov, *Elements of Applied Bifurcation Theory*, 2004, Springer.

[15] E. H. Mansfield, "Tension field theory", *Proceeding XII International Congress of Applied Mechanics*, 1968, pp. 305–329.

[16] E. H. Mansfield, “Load transfer via a wrinkled membrane”, *Proceeding of Royal Society of London A*, Vol. 316, 1970, pp. 269–289.

[17] M. Mofid, M. Noroozi, "A plate on Winkler foundation with variable coefficient", *Scientia Iranica, Transaction A: Civil Engineering*, Vol. 16 (3), 2009, pp. 249–255.

[18] N. R. Naidu, G. V. Rao, “Free vibration and stability behaviour of uniform beams and columns on nonlinear elastic foundation”, *Computers & Structures*, Vol. 58 (6), 1996, pp. 1213–1215.

[19] K. Niu, *Compressive Behavior of Sandwich Panels and Laminates with Damage*, PhD Dissertation, 1998, Georgia Institute of Technology, Atlanta.

[20] K. Niu, R. Talreja, “Modeling of wrinkling in sandwich panels under compression”, *Journal of Engineering Mechanics*, Vol. 125 (8), 1999, pp. 875–883.

[21] K. Niu, R. Talreja, “Buckling of a thin face layer on Winkler foundation with debonds”, *Journal of Sandwich Structures and Materials*, Vol. 1, 1999, pp. 259–278.

[22] P.L. Pasternak, “New method of calculation for flexible substructures on two–parameter elastic foundation”, *Gosudarstvennoe Izdatelstoo,* 1954, Literaturi po Stroitelstvu Arkhitekture, Moskau, pp. 1–56.

[23] A.C. Pipkin, “The relaxed energy density for isotropic elastic membranes”, *Archive for Rational Mechanics and Analysis*, Vol. 95, 1986, pp. 93–115.

[24] K.K. Raju, G.V. Rao, “Effect of a non–linear elastic foundation on the mode shapes in stability and vibration problems of uniform columns/beams”, *Journal of Sound and Vibration*, Vol. 160, 1993, pp. 369–371.

[25] E. Reissner, “On tension field theory”, *Proceeding of 5th International Congress on Applied Mechanics*, Vol. 5, 1938, pp. 88–92.

[26] E. Reissner, “Deflection of plates on viscoelastic foundation”, *Journal of Applied Mechanics* (*ASME*), Vol. 80, 1958, pp. 144–145.

[27] A.P.S. Selvadurai, *Elastic Analysis of Soil–Foundation Interaction*, 1979, Elsevier Scientific Publication, Amsterdam.

[28] H.S. Shen, “Nonlinear analysis of simply supported Reissner–Mindlin plates subjected to lateral pressure and thermal loading and resting on two–parameter elastic foundations”, *Engineering Structures*, Vol. 23, 2000, pp. 1481–1493.

[29] Y. S. Shih, B. T. Blotter," Non–linear vibration analysis of arbitrarily laminated thin rectangular plates on elastic foundations", *Journal of Sound and Vibration*, Vol. 167, 1993, pp. 433–459.

[30] K.P. Soldrttos, A.P.S. Selvadurau, "Flexure of beams on hyperbolic elastic foundations", *International Journal of Solids and Structures*, Vol. 21(4), 1985, pp. 373–388.

[31] M. Stein, J. M. Hedgepeth, "Analysis of partly wrinkled membranes", *NASA Technical Note D-813*, 1961.

[32] D.J. Steigmann, A.C. Pipkin, "Wrinkling of pressurized membranes", *ASME Journal of Applied Mechanics*, Vol. 56, 1989, pp. 624–628.

[33] I.B. Teodoru, V. Musat, "Beam elements on linear variable two–parameter elastic foundation", *Bulletin of the Polytechnic Institute of Jassy: Constructions, Architechture Section*, Vol. 54–58 (2), 2008, pp. 69–78.

[34] S.P. Timoshenko, *Theory of Plates and Shells*, 1940, McGraw–Hill Book Company, Inc.

[35] V.Z. Vlazov, U.N. Leontev, *Beams, Plates and Shells on Elastic Foundations*, 1966, Israel Program for Scientific Translations, Jerusalem.

[36] C.M. Wang, C.Y. Wang, J.N. Reddy, *Exact Solutions for Buckling of Structural Members*, 2005, CRC Press LLC.

[37] Y.H. Wang, L. G. Tham, Y. K. Cheung, "Beams and plates on elastic foundations: A review", *Progress in Structural Engineering and Materials*, Vol. 7 (4), 2005, pp. 174–182.

[38] H. Wagner, "Flat sheet metal girders with a very thin metal web", *Zeitschrift Flugtechne Motor*, Vol. 20, 1929, pp. 8–12.

[39] S. Wasti, E. Senkaya, "A simple finite element for beams on elastic foundations", *Strain*, Vol. 31 (4), 2008, pp. 135–142.

[40] G.W. Wei, "Discrete singular convolution for the solution of the Fokker–Planck equations", *Journal of Chemical Physics*, Vol. 110, 1999, pp. 8930 –8942.

[41] G.W. Wei, Y.B. Zhao, Y. Xiang, "Discrete singular convolution and its application to the analysis of plates with internal supports. Part I: Theory and algorithm",

International Journal for Numerical Methods in Engineering, Vol. 55, 2002, pp. 913–946.

[42] E. Winkler, *Die Lehre von der Elastizitat und Festigkeit*, 1867, Dominicius, Prague.

[43] C. H. Wu, "Nonlinear wrinkling of nonlinear membranes of revolution", *ASME Journal of Applied Mechanics*, Vol. 45, 1978, pp. 533–538.

[44] H. Zimmermann, *Die Berechnung des Eisenbahnoberbaues*, 2nd Ed., 1930, Ernst & Sohn, Berlin.

[45] S. Zhao, G. W. Wei, "Matched interface and boundary (MIB) for the implementation of boundary conditions in high–order central finite differences", *International Journal for Numerical Methods in Engineering*, Vol. 77, 2009, pp. 1690–1730.

Chapter 3

3 Wrinkling Within a Local Region on Thin Film[1]

The wrinkling around an inclusion on a thin solid film is investigated using the instability analysis. The film is modeled by using the classical plate theory with isotropic/orthotropic properties and the effect of the inclusion is imposed on the film as a compressive loading along the inclusion line. For a decaying function representing the wrinkling pattern along the film, the potential energy of the film is minimized and the parameters of the wrinkling (i.e. load and pattern) are determined. The results are useful in characterizing the wrinkling around an inclusion on free standing film or deposited film on the substrate such as wrinkling due to suturing of the skin in surgical operation in mechanics of scars.

3.1 Introduction

Local compressive stresses result in highly ordered patterns on thin film structures called wrinkling [Genzer and Groenewold, 2006]. In thin film structures, the occurrence of the wrinkling is a common phenomenon due to tiny thickness of the film. In these systems, the resistance of the film against bending is very low. As a result, the flat film undergoes an out–of–plane deformation even under small in–plane compressive loading, and the system experiences the mechanical instability as buckling and wrinkling. Wrinkles have various sources to initiate and propagate on the films. For example stretching of the film in one direction leads to wrinkling in other directions [Jacques *et al.*, 2005]. Applying a concentrated force [Adams, 1993], imposing a constraint on the system [Wong and Pellegrino, 2005], applying a crumpling mechanical load on the system [Watanabe, 2005] or thermal condensation of the film–substrate system [Bowden *et al.*, 1998] develop an in–plane compressive stress in the film which leads to the instability of the film as buckling and wrinkling [Wang *et al.*, 2008].

---

[1] The results of this chapter were published as "Wrinkling around an inclusion line on thin film structures" in *Proceedings of the 23rd Canadian Congress of Applied Mechanics*, Vol. 1, 2011, pp. 674–677.

On the other hand, studying the formation of the wrinkles around the stitched skin, fabrics, and thin layers is a very interesting and challenging topic. Stitching and its related issues have attracted great attention of many researchers in different fields. For example, in sandwich panels the effect of through the thickness stitching is considered on the stiffness and failure strength of the structure [Ma *et al.*, 2011], delamination [Whitman *et al.*, 2005], energy absorption and buckling and wrinkling parameters [Raju *et al.*, 1999; Sharma *et al.*, 2004; Ghate *et al.*, 2004]. Furthermore, the sewing pattern and its effect on fabric and garment products being stitched by professional embroiderers and sewing machines [Momsen, 2011] is one of the most important issues for apparel manufacturers [Moore, 1995]. Especially, many investigations have been accomplished on the wrinkling of the fabric during production and packaging, and some methods have been proposed to produce wrinkle–free materials [Robers, 2000] and to avoid wrinkled stitches [Seizova, 2004]. Also, stitching of the skin in surgical operations and avoiding/controlling the wrinkling of the skin after treatment is another important issue that needs extensive investigations [Yamamoto *et al.*, 2001; Cerda, 2005; Bezon *et al.*, 2006; Genzer and Groenewold, 2006]. Figure 3-1 shows the stitching pattern of the skin in surgical operation schematically. The objective of this chapter is to propose a model to consider the effective parameters on the localized wrinkling of thin films around the regions with locally crumpling load (i.e. inclusion).

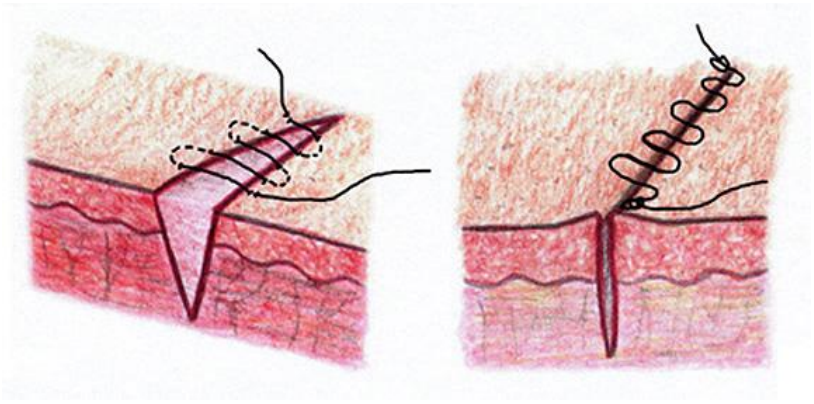

Figure 3-1: Stitching of the wound in surgery
[http://emedicine.medscape.com/article/1824895–overview #a15]

An inclusion is defined as a subdomain Ω in a general domain *D* where eigenstrain ε^* given in the subdomain Ω is different with the strain in the domain *D*–Ω (Figure 3-2). It is supposed that the material properties of both the subdomain Ω and the domain *D*–Ω are same [Qu and Cherkaoui, 2006]. Therefore, the only difference between these domains is related to the eigenstrain in the subdomain Ω. Eigenstrain ε^* is introduced to represent inelastic strains such as thermal strains, initial strains, residual strains, plastic strains, mismatch strains and the likes. This parameter is defined as the difference between total strain and mechanical strain [Korsunsky, 2009].

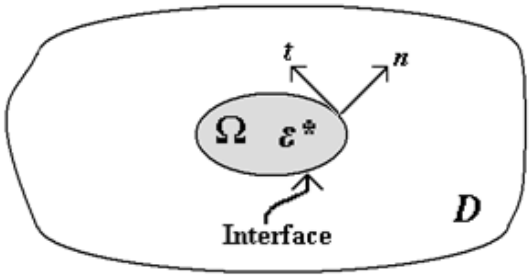

Figure 3-2: An inclusion with eigenstrain ε^* in general domain

On the interface of the inclusion region, for perfect attachment of the interfaces in which there is no gap and no slip between the domains, the displacement field should be continuous and also the tractions on the interface which are accounted for holding the equilibrium conditions should be same. The continuity of displacement field results that the tangential strain components on the interface are equal (i.e. $\varepsilon_{tt}^{in} = \varepsilon_{tt}^{out}$), however the normal strain component on the interface (i.e. ε_{nn}) has a jump due to the eigenstrain ε^* inside the inclusion as [Qu and Cherkaoui, 2006],

$$\varepsilon_{nn}^{in} - \varepsilon_{nn}^{out} = q\varepsilon^* \tag{3-1}$$

and the balance of tractions concludes that the traction on the interface for both sides, inside and outside of the inclusion should be equal as $\sigma_{nn}^{in} = \sigma_{nn}^{out}$ and $\sigma_{nt}^{in} = \sigma_{nt}^{out}$, where σ_{nn} and σ_{nt} are components of stress tensor. The condition on the third component of the stress tensor σ_{tt} is derived by using the constitutive equation of the system as

$$\sigma_{tt}^{out} - \sigma_{tt}^{in} = Q\varepsilon^* \tag{3-2}$$

where $Q = \frac{Q_{11}Q_{22} - Q_{12}Q_{21}}{Q_{11}}$ and $q = 1 + \frac{Q_{12}}{Q_{11}}$ are determined versus the components of the stiffness matrix of the film Q_{ij} (i,j=1,2). Therefore, the effect of the inclusion on the

system is simulated by considering the traction on the interface of the inclusion which is created due to eigenstrain ε^*.

An inclusion with shrinking eigenstrain in thin film system leads to the wrinkling of the film in the region around the inclusion. The film under compressive loading of the inclusion cannot support the deformation in its initial plane; hence based on the bifurcation theory, it undergoes new modes of deformation out of its initial plane and small size fluctuations (i.e. wrinkles) appear on the film. The stitching pattern in surgical operation of the patient's skin shown in figure 3-1 is modeled by using the concept of the inclusion described here.

3.2 Formulation

The wrinkling of a thin rectangular film around an inclusion is considered for the film with thickness h, width b and length L as shown in figure 3-3. The film can be supported by a substrate or it can be considered as free standing film. The inclusion is assumed as a narrow line on the film illustrated in figure 3-4. This model is similar to the stitching pattern in surgical operation of the patient's skin in figure 3-1. It also models a constraining line on a thin film which is similar to the case of point glue on the balloon in polar coordinate presented by Cerda (2005).

The Cartesian coordinate system $x_0 - y_0$ in figure 3-4 shows the longitudinal and transverse directions of the rectangular plate. Axis x_1 is perpendicular to the inclusion line while axis y_1 is along the inclusion line. On the other hand, $x_2 - y_2$ is a coordinate system with unknown direction in which wrinkles propagate on the film such that they lay along the x_2 direction with a periodicity along the y_2 direction. The inclusion line is considered far from the edges of the film so that the boundary conditions of the edges do not influence on the wrinkling region.

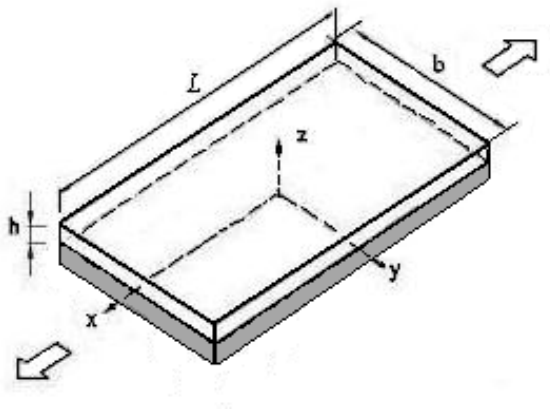

Figure 3-3: The film on the substrate, dimensions and loading parameters

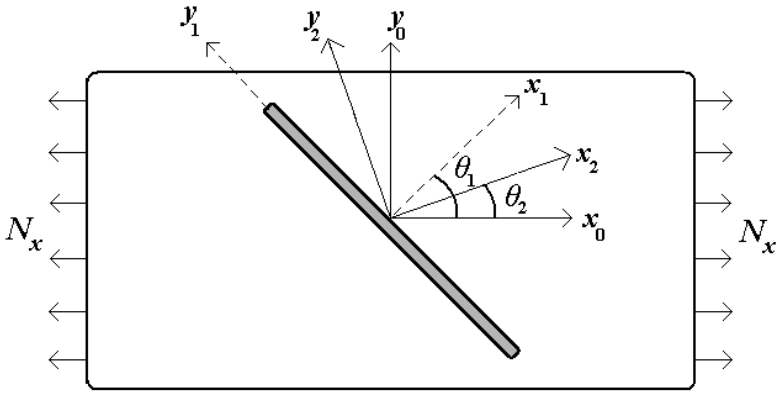

Figure 3-4: The inclusion line on the film and different coordinate systems

The film is modeled as a rectangular plate with orthotropic material properties. The main axis of the plate is considered to be in an arbitrary direction (i.e. $x_3 - y_3$) not necessarily on the abovementioned coordinate axes. The bending stiffness matrix of the orthotropic plate for off–axis formulation is obtained by using transformation law of the different coordinate systems as

$$[D] = \begin{bmatrix} D_1 & D_2 & D_3 \\ D_2 & D_4 & D_5 \\ D_3 & D_5 & D_6 \end{bmatrix} \tag{3-3}$$

in which D_i's (i=1…6) are functions of the off–axis direction (called θ_3) and main axis material properties presented in literature [Ugural, 1999].

The bending strain energy of the plate is represented versus curvature κ and internal bending moment resultant M of the plate as

$$U_b = \frac{1}{2}\int_A \{M\}^T\{\kappa\}\ dA = \frac{1}{2}\int_A \{\kappa\}^T[D]\{\kappa\}\ dA \tag{3-4}$$

According to the classical plate theory, the curvature is a function of the deflection of the plate (i.e. w) as

$$\{\kappa\} = \begin{Bmatrix} \kappa_x \\ \kappa_y \\ \kappa_{xy} \end{Bmatrix} = \begin{Bmatrix} \frac{\partial^2 w}{\partial x^2} \\ \frac{\partial^2 w}{\partial y^2} \\ 2\frac{\partial^2 w}{\partial x\, \partial y} \end{Bmatrix} \tag{3-5}$$

The stress field of the plate is represented by considering the effects of the longitudinal tension of the film and compression along the inclusion line. The longitudinal tension imposes a stress resultant component N_0 in $x_0 - y_0$ coordinate system as

$$[N]_{x_0-y_0} = \begin{bmatrix} N_{x_0} & N_{x_0y_0} \\ N_{x_0y_0} & N_{y_0} \end{bmatrix} = \begin{bmatrix} N_0 & 0 \\ 0 & 0 \end{bmatrix} \tag{3-6}$$

and the inclusion line is assumed to impose a compressive in–plane stress resultant on the film with the pattern $T(x_1)$ and the magnitude N_1, which can be represented in $x_1 - y_1$ coordinate system as

$$[N]_{x_1-y_1} = \begin{bmatrix} 0 & 0 \\ 0 & -N_1 T(x_1) \end{bmatrix} \tag{3-7}$$

while the dimensionless function $T(x)$ is represented by a descending function as

$$T(x) = \exp\left(-\frac{|x|}{l_\sigma}\right) = \begin{cases} \exp\left(-\frac{x}{l_\sigma}\right) & x > 0 \\ \exp\left(\frac{x}{l_\sigma}\right) & x < 0 \end{cases} \tag{3-8}$$

in which l_σ is the effective length of the stress distribution around the inclusion line. Various magnitudes of l_σ simulate different distributions around the inclusion. For tiny values of l_σ, the function $T(x)$ represents a concentrated stress distribution around the inclusion line similar to a Dirac function which vanishes all over the domain except on the inclusion line. Also N_1 is the stress resultant imposed from the inclusion on the film just along the inclusion line. This parameter is represented versus eigenstrain ε^* of the inclusion as

$$N_1 = h\, Q\, \varepsilon^* \tag{3-9}$$

which shows that applied force on the film due to inclusion is proportional to the eigenstrain of the inclusion according to equation (3-2) [Ugural, 1999].

The abovementioned loading pattern can be represented in any arbitrary coordinate system based on the transformation law. For example in $x_2 - y_2$ coordinate system in the figure 3-4, the components of the in–plane stress resultant are represented as

$$[N]_{x_2-y_2} = R_{\theta_2}[N]_{x_0-y_0}R_{\theta_2}^T + R_{\theta_2-\theta_1}[N]_{x_1-y_1}R_{\theta_2-\theta_1}^T \quad (3\text{-}10)$$

in which the first part is corresponding to the longitudinal loading rotated with angle θ_2 and the second part is corresponding to the inclusion loading rotated with angle $\theta_2 - \theta_1$ to transform the components of the loading in $x_2 - y_2$ coordinate system. And R_α is the rotation matrix around the out of plane axis (here z).

Therefore the total potential energy of the system is represented by

$$I = \frac{1}{2}\int_A \left\{\{\kappa\}^T[D]\{\kappa\} + N_x\left(\frac{\partial w}{\partial x}\right)^2 + N_y\left(\frac{\partial w}{\partial y}\right)^2 + 2N_{xy}\frac{\partial w}{\partial x}\frac{\partial w}{\partial y} + K_{sub}w^2\right\} dA \quad (3\text{-}11)$$

where x and y are any arbitrary Cartesian coordinate system and K_{sub} is the stiffness of the Winkler substrate. The configuration of the system in its equilibrium state minimizes the total potential energy. The crumpling load of the inclusion leads to the wrinkling of the film along the $x_2 - y_2$ coordinate system. The wrinkles propagate around the inclusion by a sinusoidal pattern in y_2 direction, while they decay by getting far from the inclusion as x_2 increases. The proposed wrinkling pattern is assumed to have the following form

$$w = \bar{w}_0\, F(x_2)\cos(\beta y_2) \quad (3\text{-}12)$$

in which $\bar{w}_0$ is the amplitude of the wrinkles, β is the wave number of the wrinkling and $F(x_2)$ is a decaying function shown in figure 3-5 as

$$F(x_2) = \exp\left(-\frac{|x_2|}{l}\right) = \begin{cases} \exp\left(-\frac{x_2}{l}\right) & x > 0 \\ \exp\left(\frac{x_2}{l}\right) & x < 0 \end{cases} \quad (3\text{-}13)$$

where l stands for the length of the wrinkles in the system along the x_2 direction and it is supposed that for slender wrinkles $l >> l_\sigma$ in equation (3-8). Also the slenderness of the wrinkles is defined by the ratio of the length of the wrinkles (i.e. l) to the transverse wavelength of the wrinkles (i.e. λ_y) as

$$\xi = l\beta = 2\pi\frac{l}{\lambda_y} \quad (3\text{-}14)$$

The total potential energy of the film–inclusion system for small values of l_σ is derived consequently by integrating in x_2–y_2 coordinate system, and by considering the

stationary condition of the potential energy of the system in the equilibrium state, the expressions for wrinkling parameters are then derived.

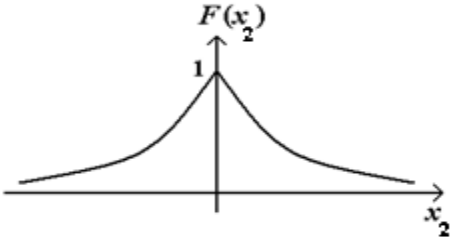

Figure 3-5: Decaying function of the wrinkling pattern

3.3 Results and Discussions

The results of the wrinkling analysis for thin solid film are presented here. It is shown that for slender wrinkles the dominant angle of the wrinkling is perpendicular to the inclusion line. The relations are simplified for isotropic films and the effect of the substrate on the wave number and length of the wrinkling is considered.

3.3.1 Wrinkling Perpendicular to the Inclusion Line

For slender wrinkles by using the principle of minimum potential energy, one can find the wave number of the wrinkling of the film as

$$\beta^4 = \frac{N_0}{D_4 l^2} \cos^2(\theta_2) + \frac{K_{sub}}{D_4} \tag{3-15}$$

which is the well known relation for wave number of wrinkling in the literature [Cerda and Mahadevan, 2003; Birman and Bert, 2004; Jacques and Potier–Ferry, 2005]. Also the crumpling load of the inclusion in general form is derived versus angles θ_1 and θ_2, material properties, loading and wrinkling parameters. Among the entire solution domain, the solution set which minimizes the crumpling load of the inclusion is sought. Equivalently, minimizing the potential energy with respect to the wrinkling direction (i.e. angle θ_2) represents the expression of the wrinkling direction. Figure 3-6 shows the diagram of the potential energy of an isotropic film versus angle of the wrinkling (i.e. θ_2) which takes its minimum at two main directions for the wrinkles, one of them in the longitudinal direction with θ_2=0 and the other one is perpendicular to the inclusion line (i.e. $\theta_2 = \theta_1$). For an orthotropic film, a similar diagram as figure 3-6 is obtained.

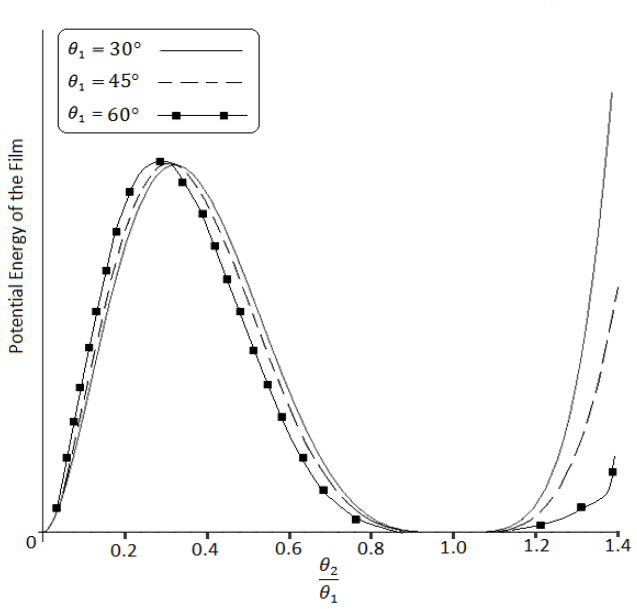

Figure 3-6: Total potential energy versus various wrinkling angles for isotropic materials with Poisson's ratio v=1/3

For the case in which wrinkles are perpendicular to the inclusion line (i.e. $\theta_1 = \theta_2 = \theta$), the x_2–y_2 coordinate system in figure 3-4 coincides on the x_1–y_1 coordinate system, and the crumpling load of the inclusion is derived as

$$2\Lambda l_\sigma N_1 = \frac{\beta}{\xi}\left\{\left(D_4 + \frac{N_0 \sin^2(\theta)}{\beta^2} + \frac{K_{sub}}{\beta^4}\right)\xi^2 + 4D_6 - 2D_2 + \frac{N_0 \cos^2(\theta)}{\beta^2}\right\} \tag{3-16}$$

in which

$$\Lambda = \frac{1}{l_\sigma}\int_{x=0}^{l} T(x)\ \left(F(x)\right)^2\, dx \tag{3-17}$$

and Λ determines the distribution coefficient of the loading model of the film. Substituting $T(x)$ and $F(x)$ in (3-17) leads to the analytical expression of Λ as

$$\Lambda = \frac{1}{1+2\frac{l_\sigma}{l}} \tag{3-18}$$

which is shown in figure 3-7. For concentrated loading with $\frac{l_\sigma}{l} \longrightarrow 0$, the parameter Λ=1, while for a uniform distributed of stress resultant $T(x)$=1, then Λ takes its lower bound as $\frac{1}{2}$.

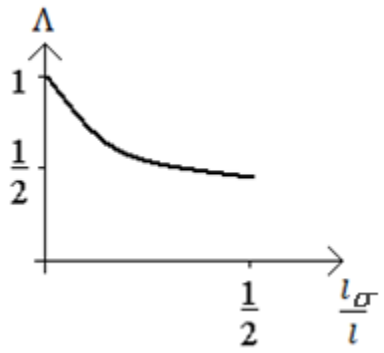

Figure 3-7: Distribution coefficient for various loading patterns

Finally, the wave number β, the length l and the slenderness ratio $\xi = \beta l$ are determined from simultaneous solution of equations (3-15) and (3-16) versus loading on the film and material properties of the system.

3.3.2 Free Standing Film

For a free standing film, by ignoring the substrate effect the abovementioned relations are simplified analytically. The wave number of the wrinkling is given by

$$\beta^4 = \frac{N_0}{D_4 l^2}\cos^2(\theta) \tag{3-19}$$

and the slenderness ratio ξ is introduced as

$$\xi = \beta l = \frac{1}{\tan(\theta)}\sqrt{2(\Gamma - 1)} \tag{3-20}$$

where Γ is the loading parameter of the inclusion on the free standing film defined by

$$\Gamma = \frac{l_\sigma N_1}{\sqrt{N_0 D_4}}\frac{1}{\cos(\theta)} \tag{3-21}$$

For a free standing isotropic film in which the material properties are independent of the direction, the bending stiffness matrix of the isotropic film is given by

$$[D] = D\begin{bmatrix} 1 & v & 0 \\ v & 1 & 0 \\ 0 & 0 & \frac{1-v}{2} \end{bmatrix} \tag{3-22}$$

where D is the bending stiffness modulus of the film with thickness h, Young's modulus E and Poisson's ratio v given by $D = \frac{Eh^3}{12(1-v^2)}$. Therefore, the wave number β and the loading parameter Γ are represented by replacing D_4 with D in equations (3-19) and (3-21).

For loading parameter Γ bigger than the threshold value (Γ=1), wrinkles propagate in the system. In other words, for thick and stiff films with high stiffness bending D under small crumpling load when Γ<1, wrinkles do not appear in the system (as expected). In this case, the effective compressive loading on the film cannot overcome the bending resistance of the film to form the wrinkles.

Figure 3-8 shows the slenderness ratio of the wrinkles versus loading parameter of the inclusion (i.e. Γ) in equation (3-21) for a free standing isotropic film. Obviously, for higher magnitudes of the loading parameter Γ (i.e. by increasing the crumpling loading or decreasing bending rigidity D of the film) the length of the wrinkles increases. Also for bigger values of parameter θ, the slenderness ratio of the wrinkles decreases because the effective crumpling load on the film decreases. For $\theta = 0^o$ the wrinkles propagate over the entire length span. In this case, the inclusion line is along the transverse direction of the rectangular film, and the length of the wrinkles on the free standing film approaches to infinity mathematically from equation (3-20), and physically the length of the wrinkles is restricted by the length of the film. By increasing θ the length of the wrinkles decreases so that for $\theta = 90^o$ where the inclusion line is along the longitudinal direction, the length of the wrinkles approaches to its minimum value (almost zero according to equation 3-20) as expected.

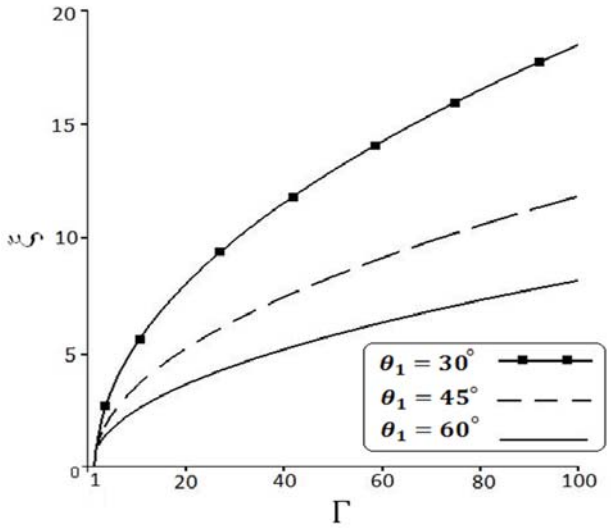

Figure 3-8: Slenderness ratio of the wrinkles versus various loading for isotropic materials with Poisson's ratio ν=1/3

Similar to the isotropic films, for orthotropic films with transversely isotropic plane in which the stiffness parameters are functions of θ_2 and main axis angle θ_3, the wrinkles propagate almost perpendicular to the inclusion line independent of the loading direction (Figure 3-6); however, some negligible deviations are seen due to the change of the principal axis orientation of the orthotropic film (Figure 3-9). In fact, the change in the orientation of the material principle direction is effective on the length and wave number of the wrinkles which both of them correspond to $\frac{1}{\sqrt{D_4}}$ according to equations (3-19) and (3-21). Hence, by decreasing the bending stiffness D_4 of the film, the wave number and the length of the wrinkles increase (as expected).

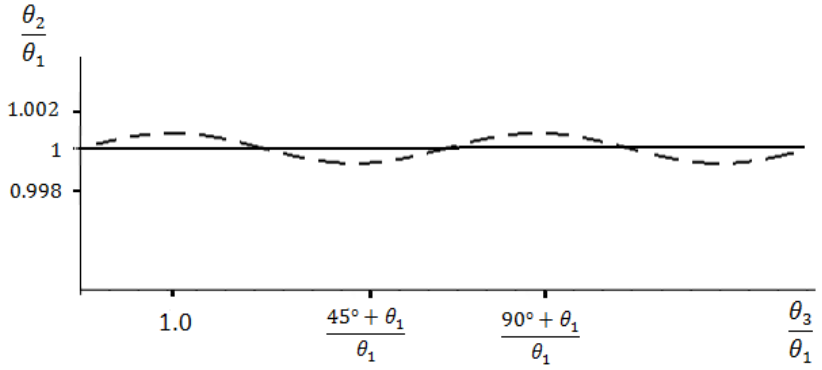

Figure 3-9: Variation of the wrinkling direction versus change in the principal direction of a typical orthotropic film

3.3.3 Film Deposited on the Substrate

For taut substrates, when the effect of the substrate stiffness is more important than stretching loads, the relations are simplified by ignoring the first term of (3-15) as

$$\beta^4 = \frac{K_{sub}}{D_4} \tag{3-23}$$

And

$$\Lambda l_\sigma N_1 = \frac{\beta}{\xi}\left\{\left(D_4 + \frac{N_0 \sin^2(\theta)}{2\beta^2}\right)\xi^2 + 2D_6 - D_2 + \frac{N_0 \cos^2(\theta)}{2\beta^2}\right\} \tag{3-24}$$

The quadratic equation (3-24) directly leads to the relation of the slenderness ratio ξ to the loading and stiffness parameters as

$$\xi = p\left\{1 + \sqrt{1 - q}\right\} \cong 2p \tag{3-25}$$

where

$$p = \frac{\Lambda l_\sigma N_1}{2\beta D_4} \tag{3-26}$$

$$q = \frac{1}{pD_4}\left\{2D_6 - D_2 + \frac{N_0 cos^2(\theta)}{2\beta^2}\right\} \tag{3-27}$$

According to equations (3-23, 3-26), increasing the substrate stiffness K_{sub} increases the wave number of the wrinkles and decreases the slenderness ratio and the length of the wrinkles as $\xi \propto \frac{1}{\sqrt[4]{K_{sub}}}$ and $l \propto \frac{1}{\sqrt{K_{sub}}}$, respectively. Therefore, by increasing the substrate stiffness, the number of the wrinkles increases while their length decreases (as expected). The results provide adequate insights in physics of the wrinkling and develop appropriate tools for controlling of the wrinkling around an inclusion.

3.4 Summary

The wrinkling of thin film structures is an important area with a lot of applications in various fields in everyday life, fabric industry, health science and surgical operation, thin film science and technology and so on. The wrinkles appear on the film due to compressive stresses from various sources such as inclusion. The wrinkles around the inclusion are affected by the inclusion eigenstrain and film properties. By modeling the solid film with thin plate theory and minimizing the total potential energy of the system, the effect of the inclusion on the instability behavior of the film was investigated. The wrinkling parameters including wave number and length of the wrinkles are derived for the isotropic/ orthotropic film as free standing/deposited film on the substrate and it is shown that the wrinkles propagate almost perpendicular to the inclusion line. The results of the work provide adequate insights to understand the wrinkling phenomenon and to control the wrinkles effectively in the design and operation of thin film structures.

3.5 References

[1] G. G. Adams, “Elastic wrinkling of a tensioned circular plate using von Karman plate theory”, *Journal of Applied Mechanics*, Vol. 60, 1993, pp. 520–525.

[2] R.K. Annabattula, P.R. Onck, “Micron–scale pattern formation in prestressed polygonal films”, *Journal of Applied Physics*, Vol. 109(3), 2011, Article No. 033517.

[3] E. Bezon, A.I.A.A. Khalifa, J.N. Choplain, J.A. Barra,” Homemade expanded–polytetrafluoroethylene flexible mitral annuloplasty ring”, *European Journal of Cardio–thoracic Surgery*, Vol. 29(2), 2006, pp. 251–252.

[4] V. Birman, C.W. Bert, “Wrinkling of composite–facing sandwich panels under biaxial loading”, *Journal of Sandwich Structures and Materials*, Vol. 6 (3), 2004, pp. 217–237.

[5] N. Bowden, S. Brittain, A. G. Evans, J. W. Hutchinson, G. M. Whitesides, “Spontaneous formation of ordered structures in thin films of metals supported on an elastomeric polymer”, *Nature*, Vol. 393, 1998, pp. 146–149.

[6] E. Cerda, L. Mahadevan, “Geometry and physics of wrinkling”, *Physical Review Letters*, Vol. 90–7, 2003, pp. 074302/1–4.

[7] E. Cerda, “Mechanics of scars”, *Journal of Biomechanics*, Vol. 38, 2005, pp. 1598–1603.

[8] J. Genzer, J. Groenewold, “Soft matter with hard skin: From skin wrinkles to templating and material characterization”, *Soft Matter*, Vol. 2, No. 4, 2006, pp. 310–323.

[9] V. Ghate, V. La Saponara, P. Singh, Z. Whitman, “Buckling and face wrinkling of stitched sandwich panels”, *Proceedings of International SAMPE Symposium and Exhibition*, Vol. 49, Long Beach, Canada, May 16– 20, 2004, pp. 3578–3590.

[10] J. Huang, M. Juszkiewicz, W.H. De Jeu, E. Cerda,T. Emrick, N. Menon, T.P. Russell, “Capillary wrinkling of floating thin polymer films”, *Science*, Vol. 317(5838), 2007, pp. 650–653.

[11] N. Jacques, M. Potier–Ferry, “On mode localisation in tensile plate buckling”, *Compter Rendus Mecanique*, Vol. 333, 2005, pp. 804–809.

[12] A.M. Korsunsky, “Eigenstrain analysis of residual strains and stresses”, *Journal of Strain Analysis for Engineering Design*, Vol. 44(1), 2009, pp. 29–43.

[13] Y. Ma, H. Han, Z. Lu, W. Lu, T. Qiu, J. Guo, "Theoretical prediction of the stiffness and failure strength of stitched foam–core sandwich composites", *Polymers and Polymer Composites*, Vol. 19(4–5), 2011, pp. 303–312.

[14] H.H. Momsen, "Charting stitching success", *Printwear*, Vol. 24(6), 2011, pp. 32–35.

[15] L. Moore, "Time and money", *Apparel Industry Magazine*, Vol. 56(3), 1995, pp. QR 17–18.

[16] J. Qu, M. Cherkaoui, *Fundamentals of Micromechanics of Solids*, 2006, John Wiley and Sons Inc.

[17] K.S. Raju, J.S. Tomblin, "Energy absorption characteristics of stitched composite sandwich panels", *Journal of Composite Materials*, Vol. 33(8),1999, pp. 712–728.

[18] F. Robers, "Wrinkle–free technology for shirting materials", *New Cloth Market*, Vol. 14(4), 2000, pp. 19–22.

[19] N. Seizova, "Wrinkled stitches? How to avoid them", *Textilat*, Vol. 6, 2004, pp. 34–37.

[20] S.C. Sharma, M. Krishna, H.N. Narasimha Murthy, "Buckling response of stitched polyurethane foam composite sandwich structures", *Journal of Reinforced Plastics and Composites*, Vol. 23(12), 2004, pp. 1267–1277.

[21] A.C. Ugural, *Stresses in Plates and Shells*, 1999, McGraw–Hill.

[22] Y.W. Wong, S. Pellegrino, "Wrinkles in square membranes", *Computational Methods in Applied Sciences: Textile Composites and Inflatable Structures*, Vol. 3, 2005, pp. 109–122.

[23] S. Wang, J. Song, D. Kim, Y. Huang, J. A. Rogers, "Local versus global buckling of thin films on elastomeric substrates", *Applied Physics Letters*, Vol. 93, 2008, Article No. 023126.

[24] M. Watanabe, "Striped–pattern formation of a thin gold film deposited onto a stretched elastic silicone substrate", *Journal of Polymer Science Part B: Polymer Physics*, Vol. 43, 2005, pp. 1532–1537.

[25] Z. Whitman, M. Worley, V. La Saponara, V. Ghate, "Experimental and numerical analysis of notched stitched sandwich structures", *Proceedings of International SAMPE*

Symposium and Exhibition, Vol. 50, Long Beach, Canada, May 1– 5, 2005, pp. 1221–1233.

[26] Y. Yamamoto, S. Sasaki, H. Furukawa, A. Oyama, N. Endo, T. Sugihara, Y. Furuta, "Anchoring correction of eyebrow ptosis in facial palsy", *Plastic and Reconstructive Surgery*, Vol. 108(5), 2001, pp. 1297–1299.

[27] http://emedicine.medscape.com/article/1824895–overview #a15

Chapter 4

4 Instability of a Functionally Graded Material (FGM) Thin Film[1]

The instability of a functionally graded material (FGM) strip as a free standing film or a substrate–bonded film is studied in this chapter, in which the stiffness of the film is assumed to change exponentially along the length. The buckling load and the buckling mode shapes for the free standing FGM film are determined analytically. For the substrate–bonded film, the substrate is modeled as a Winkler foundation and the wrinkling load and wrinkling pattern are determined numerically by using a finite difference method and a series solution. In contrast with the wrinkling of homogenous thin films in which the wrinkles propagate in the entire domain, the wrinkles of the FGM films accumulate around the location with the least bending rigidity. The results of this work show that the sensitivity of the wrinkle accumulation around the weak locations of the system with lower stiffness is very high. This work is expected to provide a better understanding for localization of wrinkles around a region of substrate –bonded thin films in thin film technology.

4.1 Introduction

The instability problem of a mechanical system (i.e. buckling and wrinkling) is studied using the bifurcation theory [Bloom and Coffin, 2001] as finding the eigenvalues of the differential equation of the system. Free standing films under compressive loading undergo buckling, while for deposited films on the substrate a fine wavy pattern dominates on the film called wrinkling [Genzer and Groenewold, 2006]. Many patterns for wrinkling of a deposited film on the substrate are considered [Wang *et al.*, 2008] among them uniaxial wrinkling is a common pattern in which wrinkles propagate on the film span uniaxially [Huang and Im, 2006].

---

[1] The results of this chapter were accepted to publish as "Buckling and wrinkling of a functionally graded material (FGM) thin film" in *International Journal of Applied Mechanics*, D–12–00013R1, Accepted 17 March 2012.

Most of the existing theoretical works on the substrate–bonded films used the homogenous material properties for the film with a uniform wrinkling pattern along the entire span. For example, Cerda and Mahadevan [2003], Chen and Hutchinson [2004] and Niu and Talreja [1999] determined the wavelength and amplitude of sinusoidal wrinkles by using the uniform amplitude assumption for the wrinkles all over the span without considering the boundary effects. However, for thin film structure with finite length, the effect of the boundary conditions of the edge of the film disturbs the uniformity of the wrinkling pattern along the span. On the other hand, in thin film structures deposited on the substrate by using various deposition techniques, the assumption of the material homogeneity of the film is very flabby due to the importance of the microstructure at the small scale. Besides, techniques such as doping of the film with dopant elements or other impurities which locally alter the properties of the system attract especial attention in thin film technology [Chen *et al.*, 2007; Stashans, 2004]. Therefore, some concerns may arise about the importance of the variation of the material properties of the film and its effect on the wrinkling of the film–substrate system, which need further investigation.

In order to consider the effect of the variable material properties on the mechanical behavior of the film, a model of a functionally graded material (FGM) is used here, which has been commonly adopted by many researchers to investigate the behavior of functionally graded beams and plates in static, vibration and buckling analyses [Yang and Chen, 2008; Ke *et al.*, 2010; Zenkour, 2010; Shen and Wang, 2010]. In contrast with sandwich composite structures made by reinforcing fibbers in the matrix, the microstructure of the FGM changes gradually so that there is no clear distinction or border in the domain. Hence the material properties vary continuously with position due to the gradual change of the material composition. In other words, the gradually change of the volume fraction of the materials results in corresponding changes in the material properties continuously. In coating technology, the residual stress of the thin film may lead to the failure of the film and detachment from the substrate due to the material mismatch from the substrates. Using the FGM film with gradual change of the material properties through the thickness leads to decreasing the residual stresses and safe–failure design of the system [Khor *et al.*, 2000; Teixeira, 2001; Zhao *et al.*, 2008]. However, to

the author's knowledge, the effect of the material gradient of the film along the length span upon the wrinkling behavior has not been investigated for a substrate–bonded film with a finite length thus far. Therefore, the current work focuses on the assumptions of the finite length of the film, non–uniformity of the wrinkling pattern along the span and non–uniformity of the film properties, which have been ignored by the other researchers.

In this chapter, the buckling and uniaxial wrinkling problem of an FGM film with finite length is considered. To make the problem more mathematical tractable, an exponential profile is assumed for the elastic modulus of the film, which demonstrates the softening or stiffening of the film along the length span. The buckling problem of the free standing film is investigated by proposing a closed form analytical solution. For the substrate–bonded film, the eigenvalue problem of the differential equation of the system is solved by using a finite difference method and a series solution. The effect of the material gradient of the film and the substrate stiffness are considered on the instability parameters (i.e. load and pattern). A regression analysis is also conducted for parametric studies, which provides explicit expressions for the instability parameters. In contrast with the other works in the instability of thin film with homogenous material properties, the results of this work show that the effect of the material gradient along the length span is very significant in wrinkling localization. For a FGM film deposited on a substrate, it is shown that the wrinkles accumulate around the weakest location of the film which has the lowest stiffness. The importance of the problem increases especially in thin film technology, where the homogeneity of the film is uncontrollable due to effect of the microstructure of the system. The results of the analysis are expected to be helpful in the instability analysis of the non–homogenous film–substrate systems and their potential applications.

4.2 Modeling

The problem envisaged is a functionally graded thin film deposited on an elastic substrate subjected to a constant in–plane load $\bar{N}_x$ as shown in figure 4-1, where t, b and L represent the thickness, width and length of the film, respectively. In order to characterize the instability of the system, the classical beam/strip theory with small deformation is used to model the film. The substrate is modeled as a Winkler foundation [Birman and

Bert, 2004; Cerda and Mahadevan, 2003; Niu and Talreja, 1999], in which the interaction between the film and the foundation is represented by a linear spring system with the stiffness $\bar{K}$. The substrate should be thick enough and also compliant in order to apply Winkler model. For this uniaxial deformation of the film, the governing equation is given as [Ugural, 1999, pp. 298],

$$\frac{d^2}{dx^2}\left[D\frac{d^2\bar{w}}{dx^2}\right] + \bar{N}_x\frac{d^2\bar{w}}{dx^2} + b\bar{K}\bar{w} = 0 \tag{4-1}$$

where $\bar{w}$ is the out–of–plane displacement and D refers to the bending stiffness of the film defined by,

$$D = \frac{1}{12}\bar{E}bt^3 \tag{4-2}$$

where $\bar{E}=E/(1-\nu^2)$ with E and ν being the Young's modulus and the Poisson's ratio. In this work, the Young's modulus of the FGM film is assumed to vary along the length span as,

$$\bar{E}(x) = \bar{E}_0\,E(x) \tag{4-3}$$

and $\bar{E}_0$ is a constant Young's modulus of the film when x=0 and and $E(x)$ is the shape function of the varying Young's modulus along the length span x such that $E(x=0)$ =1. Correspondingly, the bending stiffness of the film is rewritten as,

$$D = D_0E(x) \tag{4-4}$$

where $D_0 = \frac{1}{12}\bar{E}_0 b\,t^3$. By Substituting equation (4-4) into (4-1) and introducing the non–dimensional variable ξ defined as $\xi = x/L$ and the normalized deflection $w = \frac{\bar{w}}{Max\,(\bar{w})}$, the dimensionless governing equation in (4-1) is derived as,

$$[E(\xi)\,]\frac{d^4w}{d\xi^4} + \left[2\,\frac{d}{d\xi}E(\xi)\,\right]\frac{d^3w}{d\xi^3} + \left[\,\frac{d^2}{d\xi^2}E(\xi) + N\right]\frac{d^2w}{d\xi^2} + Kw = 0 \tag{4-5}$$

in which

$$N = \frac{\bar{N}_xL^2}{D_0} \tag{4-6-A}$$

and

$$K = \frac{\bar{K}\,bL^4}{D_0} \tag{4-6-B}$$

The Young's modulus of the FGM film may have an arbitrary distribution pattern along the length span. In the current work, the stiffness stiffening and softening effects on the buckling and wrinkling of the FGM film will be investigated in comparison with the

homogenous film. Among various patterns proposed for the varying Young's modulus of an isotropic FGM in literature [Yang and Chen, 2008; Ke *et al.*, 2010], the exponential function is a common pattern that is used here to describe the stiffening or softening of the film, i.e.,

$$E(\xi) = \mathrm{EXP}(\alpha\xi) \tag{4-7}$$

Obviously, a positive value of material gradient α stiffens the film gradually along the length span, while a negative one softens the film along the span. For a homogenous film, the material properties are constant along the entire span of the film corresponding to $\alpha = 0$ (Figure 4-2).

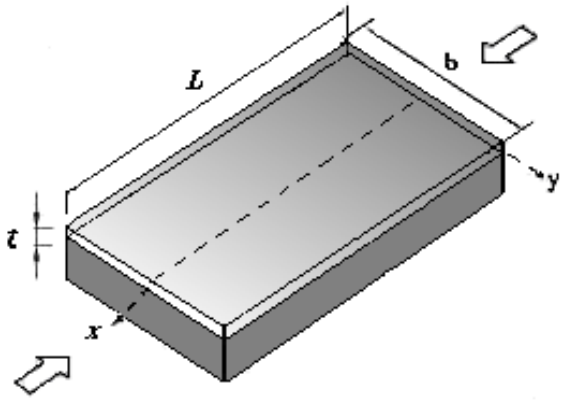

Figure 4-1: A substrate–bonded FGM film under compressive in–plane loading

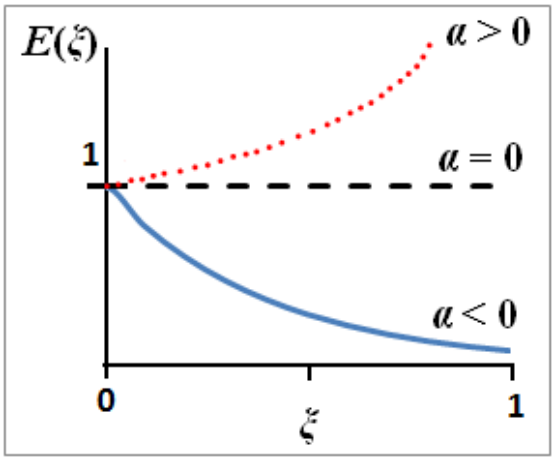

Figure 4-2: The profile of the elastic modulus of the film along the length span

4.3 Buckling

For a free standing FGM film, the governing equation of the instability reduces to

$$\frac{d^2}{d\xi^2}\left[E(\xi)\ \frac{d^2w}{d\xi^2}\right] + N\frac{d^2w}{d\xi^2} = 0 \qquad (4\text{-}8)$$

where $E(\xi)$ is the Young's modulus pattern assumed with the exponential function in equation (4-7). For $\alpha \neq 0$, the manipulation of the forth order differential equation in (4-8) by using a change of variable as $u = \sqrt{\frac{4N}{\alpha^2}\mathrm{EXP}(-\alpha\xi)}$ results in the Bessel differential equation as [Abramowitz and Stegun, 1972, pp. 358],

$$u^2\frac{d^2w}{du^2} + u\frac{dw}{du} + (u^2 - p^2)w = 0 \qquad (4\text{-}9)$$

with parameter $p = 0$. Therefore, a closed form analytical solution for the differential equation in (4-8) is derived for $\alpha \neq 0$ as

$$w(\xi) = m_1 J(\xi) + m_2 Y(\xi) + m_3\xi + m_4 \qquad (4\text{-}10)$$

where m_i (i=1...4) are unknown constants and

$$J(\xi) = J_0\left(\sqrt{\frac{4N}{\alpha^2}\ \mathrm{EXP}(-\alpha\xi)}\right) \qquad (4\text{-}11\text{-A})$$

$$Y(\xi) = Y_0\left(\sqrt{\frac{4N}{\alpha^2}\ \mathrm{EXP}(-\alpha\xi)}\right) \qquad (4\text{-}11\text{-B})$$

with $J_0(\xi)$ and $Y_0(\xi)$ being Bessel functions of the first and second type of order zero, respectively. For the case of a homogenous free standing film, the solution of the governing equation (4-8) is derived by replacing $J(\xi)$ and $Y(\xi)$ by $\sin(\xi\sqrt{N})$ and $\cos(\xi\sqrt{N})$ in equation (4-10).

In order to find the unknown constants m_i (i=1...4) in equation (4-10), boundary conditions of the film are imposed. The clamped–clamped boundary conditions at the edges ξ=0 and ξ=1 are given as

$$w = 0 \text{ and } \frac{dw}{d\xi} = 0 \qquad (4\text{-}12)$$

By imposing these boundary conditions into equation (4-10) and after some mathematical treatments, the characteristic equations and mode shapes of the buckling of the film are obtained respectively by the following equations,

$$\frac{J(1)-J(0)-J'(0)}{J'(1)-J'(0)} = \frac{Y(1)-Y(0)-Y'(0)}{Y'(1)-Y'(0)} \qquad (4\text{-}13\text{-A})$$

$$w = \frac{J(\xi) - J(0) - \xi\, J'(0)}{J'(1) - J'(0)} - \frac{Y(\xi) - Y(0) - \xi\, Y'(0)}{Y'(1) - Y'(0)} \tag{4-13-B}$$

Alternatively, these equations can be written in terms of Bessel functions as

$$\frac{J_0\left(\sqrt{\frac{4N}{\alpha^2}\,\mathrm{EXP}(-\alpha)}\right) - J_0\left(\sqrt{\frac{4N}{\alpha^2}}\right) - \alpha\sqrt{\frac{N}{\alpha^2}}\, J_1\left(\sqrt{\frac{4N}{\alpha^2}}\right)}{J_1\left(\sqrt{\frac{4N}{\alpha^2}\,\mathrm{EXP}(-\alpha)}\right) - J_1\left(\sqrt{\frac{4N}{\alpha^2}}\right)} = \frac{Y_0\left(\sqrt{\frac{4N}{\alpha^2}\,\mathrm{EXP}(-\alpha)}\right) - Y_0\left(\sqrt{\frac{4N}{\alpha^2}}\right) - \alpha\sqrt{\frac{N}{\alpha^2}}\, Y_1\left(\sqrt{\frac{4N}{\alpha^2}}\right)}{Y_1\left(\sqrt{\frac{4N}{\alpha^2}\,\mathrm{EXP}(-\alpha)}\right) - Y_1\left(\sqrt{\frac{4N}{\alpha^2}}\right)} \tag{4-14-A}$$

$$w = \frac{J_0\left(\sqrt{\frac{4N}{\alpha^2}\,\mathrm{EXP}(-\alpha\xi)}\right) - J_0\left(\sqrt{\frac{4N}{\alpha^2}}\right) - \alpha\sqrt{\frac{N}{\alpha^2}}\,\xi\, J_1\left(\sqrt{\frac{4N}{\alpha^2}}\right)}{J_0\left(\sqrt{\frac{4N}{\alpha^2}\,\mathrm{EXP}(-\alpha)}\right) - J_0\left(\sqrt{\frac{4N}{\alpha^2}}\right) - \alpha\sqrt{\frac{N}{\alpha^2}}\, J_1\left(\sqrt{\frac{4N}{\alpha^2}}\right)} - \frac{Y_0\left(\sqrt{\frac{4N}{\alpha^2}\,\mathrm{EXP}(-\alpha\xi)}\right) - Y_0\left(\sqrt{\frac{4N}{\alpha^2}}\right) - \alpha\sqrt{\frac{N}{\alpha^2}}\,\xi\, Y_1\left(\sqrt{\frac{4N}{\alpha^2}}\right)}{Y_0\left(\sqrt{\frac{4N}{\alpha^2}\,\mathrm{EXP}(-\alpha)}\right) - Y_0\left(\sqrt{\frac{4N}{\alpha^2}}\right) - \alpha\sqrt{\frac{N}{\alpha^2}}\, Y_1\left(\sqrt{\frac{4N}{\alpha^2}}\right)} \tag{4-14-B}$$

By solving these equations, the corresponding buckling load N and mode shapes are obtained.

Particularly, for the case of a homogenous free standing film (α = 0), the characteristic buckling equation for clamped–clamped film is represented as,

$$\sin\left(0.5\sqrt{N}\right)\left[\tan\left(0.5\sqrt{N}\right) - 0.5\sqrt{N}\right] = 0 \tag{4-15}$$

which leads to the symmetric and antisymmetric buckling modes with buckling loads and mode shapes presented in table 4-1.

Table 4-1: The buckling parameters for homogenous film with clamped edges

Buckling mode	Characteristic equation	Critical load	Mode shape
Symmetric	$\sin\left(0.5\sqrt{N}\right) = 0$	$N = 4\,\pi^2$	$1 + \cos\left(\sqrt{N}\xi\right)$
Anti-symmetric	$\tan\left(0.5\sqrt{N}\right) = 0.5\sqrt{N}$	$N = 8.183\,\pi^2$	$\sin\left(\sqrt{N}\xi\right) - 2\xi\sin\left(0.5\sqrt{N}\right)$

4.4 Wrinkling

The governing equation (4-5) of the system is a forth order linear ordinary differential equation with variable coefficients which has no closed form analytical solution even for simple functions of $E(\xi)$. Hence, approximate analytical solutions as well as numerical methods are pursued to characterize the wrinkling problem of the FGM film.

4.4.1 Series Solution

In order to get the approximate analytical solution for the governing equation (4-5) of the FGM film–substrate system, a series solution is constructed with power functions of η^m and unknowns coefficients c_m as,

$$w(\eta) = \sum_{m=0}^{m\to\infty} c_m \, \eta^m \tag{4-16}$$

where $\eta = \xi - 0.5$ such that $-0.5 \leq \eta \leq 0.5$. The proposed power series is a convergent series because η does not exceed the radius of convergence which is unit (i.e. $|\eta| < 1$).

On the other hand, a power series for the Young's modulus $E(\eta)$ based on Taylor expansion is introduced by

$$E(\eta) = \sum_{m=0}^{m\to\infty} E_m \, \eta^m \tag{4-17}$$

where

$$E_m = \frac{\alpha^m}{m!} \, \mathrm{EXP}\left(\frac{\alpha}{2}\right) \tag{4-18}$$

By plugging $w(\eta)$ and $E(\eta)$ from equations (4-16) and (4-17) into differential equation (4-5) and using the recurrence relations, the coefficients c_m (m=4,5,…) can be determined in terms of c_0, c_1, c_2 and c_3. Hence, the wrinkling pattern is represented as

$$w(\eta) = \varphi_0(\alpha, K, N, \eta)c_0 + \varphi_1(\alpha, K, N, \eta)c_1 + \varphi_2(\alpha, K, N, \eta)c_2 + \varphi_3(\alpha, K, N, \eta)c_3 \tag{4-19}$$

In the current study, the clamped–clamped boundary conditions are imposed at the edges of the film as,

$$w(\eta = \pm 0.5) = \frac{dw}{d\eta}(\eta = \pm 0.5) = 0 \tag{4-20}$$

Using these boundary conditions, the eigenvalue problem of the system is derived and the characteristic wrinkling equation and wrinkling pattern of the system are determined in terms of the material parameters (i.e. K and α) of the substrate and film.

4.4.2 Finite Difference Method (FDM)

The finite difference method (FDM) discretizes the domain by introducing nodes as shown in figure 4-3. The derivatives of the field variable (here deflection *w*) are approximated by the finite differences of the variable using the difference quotient formula [Hildebrand, 1968]. Here the central difference approach with 6th order of accuracy is used to solve the problem. By using an N–point stencil configuration (here N=9), one can obtain the finite difference formula for a 2M–order central finite difference approximation (here M=3) [Zhao and Wei, 2009]. The approximated derivatives of any function are represented by the values of the function at the neighborhood nodes (the stencil points) with coefficients given in table 4-2. For example, the second derivative of function $G(u)$ is represented by,

$$\frac{d^2}{du^2}G(u) = \frac{\frac{1}{90}G_{i-3} - \frac{3}{20}G_{i-2} + \frac{3}{2}G_{i-1} - \frac{49}{18}G_i + \frac{3}{2}G_{i+1} - \frac{3}{20}G_{i+2} + \frac{1}{90}G_{i+3}}{h^2} + O(h^6) \qquad (4\text{-}21)$$

where $h = u_{i+1} - u_i$ is the grid spacing and $G_i = G(u_i)$ refers to the exact value of the function $G(u)$ at node i.

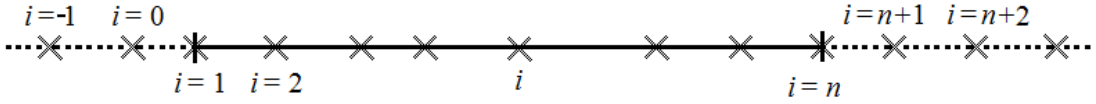

Figure 4-3: Discretized length span of the film by introducing nodes for finite difference analysis

Table 4-2: Finite difference coefficients of the 6th order of accuracy

Derivative	*i*-4	*i*-3	*i*-2	*i*-1	*i*	*i*+1	*i*+2	*i*+3	*i*+4
1	0	–1/60	3/20	–3/4	0	3/4	–3/20	1/60	0
2	0	1/90	–3/20	3/2	–49/18	3/2	–3/20	1/90	0
3	–7/240	3/10	–169/120	61/30	0	–61/30	169/120	–3/10	7/240
4	7/240	–2/5	169/60	–122/15	91/8	–122/15	169/60	–2/5	7/240

Applying the difference formulas into the governing equation of the system in equation (4-5) represents the equation of the node *i* as,

$$R_{i-4}^{(i)} w_{i-4} + R_{i-3}^{(i)} w_{i-3} + R_{i-2}^{(i)} w_{i-2} + R_{i-1}^{(i)} w_{i-1} + R_{i}^{(i)} w_{i} + R_{i+1}^{(i)} w_{i+1} + R_{i+2}^{(i)} w_{i+2} + R_{i+3}^{(i)} w_{i+3} + R_{i+4}^{(i)} w_{i+4} = 0 \quad (4\text{-}22)$$

while *i* covers all of the internal nodes of the system (i.e. i=2,3,…n–1) and coefficients R_α are obtained from the finite difference formula and differential equation (4-5).

On the other hand, applying the boundary conditions introduces the displacement value for the boundary nodes i=1 and i=n and also the virtual nodes i=0, –1, –2, … and n+1, n+2,… in figure 4-3. For the clamped edge, the symmetric extension assumption is applied on the boundaries [Zhao and Wei, 2009] which leads to w_1= w_n= 0, w_0= w_2 and w_{n+1}= w_{n-1} and so on.

Applying Equation (4-22) to all of the nodes and incorporating the boundary conditions, an algebraic system of equations for the governing equation of the system is derived as,

$$[A]\{w\} + N[B\,]\{w\} = 0 \quad (4\text{-}23)$$

in which $\{w\} = \{w_1, \dots, w_n\}^{\mathrm{T}}$ is the vector of the nodal displacement, $[A]$ and $[B]$ are square matrices. This is a general eigenvalue problem with the eigenvalues corresponding to the wrinkling loads of the system and the eigenvectors representing the pattern of the wrinkling.

4.5 Results and Discussions

In this section, the results obtained from the analytical and numerical methods presented in the previous chapters for the buckling of a free standing FGM film and the wrinkling of a FGM film deposited on the substrate are discussed. The effect of the gradient of the FGM film on the instability parameters (load, buckling mode shapes, wrinkling wave number …) is considered and compared with the instability of a homogenous film.

4.5.1 Buckling of a Free Standing Film

The buckling loads and mode shapes of the free standing FGM film are investigated to see the material gradient effect. Figure 4-4 plots the variation of the normalized buckling

load N/N^0_B with the material gradient α, where $N^0_B = 4\pi^2$ is the critical buckling load of a free standing homogenous film. Both the first and the second buckling loads increase with the material gradient α. When the material gradient α is approaching zero, the first and second buckling loads are obtained as the corresponding buckling loads of the homogenous film in table 4-1 as expected. Similar to the buckling of a homogeneous beam structure discussed by Timoshenko and Gere [1961], it is understood that the second buckling mode may be produced for a very slender FGM film by applying external constraints at the inflection points to prevent lateral deflection. Otherwise such a higher mode of buckling is unstable because the structure develops large deflection when the first (lower) buckling load is reached. For positive values of the material gradient α, the stiffness of the film increases, hence the buckling load of the FGM film is bigger than the buckling load of a homogenous film. On the other hand, for negative values of the parameter α, the compliance of the system increases which leads to decreasing of the buckling loads with respect to the buckling load of a homogenous film.

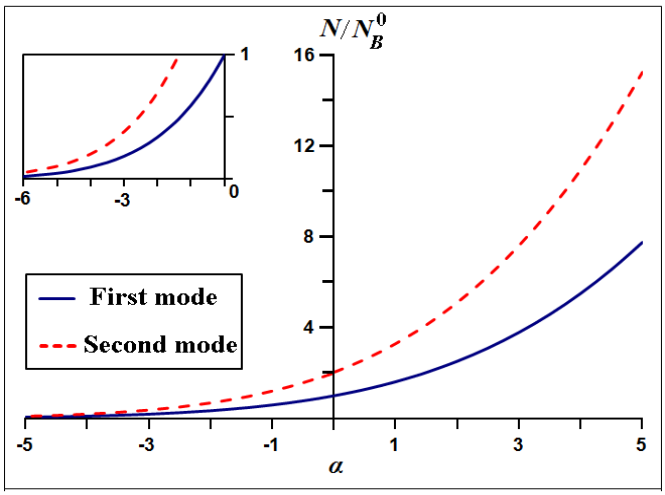

Figure 4-4: Variation of the first and the second normalized buckling load N/N^0_B of the free standing film with the material gradient α

In order to propose an explicit expression for the critical buckling load of the FGM film with exponential material distribution, a regression analysis [Kahane, 2008] is performed on the buckling load data obtained from buckling analysis. The critical buckling load $N_{cr.}$ is shown to follow an exponential relation with the material gradient α as,

$$N_{cr.} = N_{\mathrm{B}}^{0}\ \mathrm{EXP}(m_0\alpha) \qquad (4\text{-}24)$$

where m_0 is a constant parameter to be determined by the regression analysis. The results of the regression analysis for 50 datapoints with R^2 =0.995 and standard error less than 0.5% are presented in table 4-3 which shows a high accuracy for the proposed relation in (4-24) for a range of $-5 < \alpha < 5$. For α outside this range, the change in the material properties of the FGM film is too big (i.e. in the order of magnitude bigger than EXP (5) ≈ 150) which is not physically meaningful, and therefore it is ignored in the analysis.

Table 4-3: Regression analysis for the critical buckling load of the system in relation (4-24)

Parameter	Estimate	Std. Error	95% Confidence Interval		R^2
			Lower Bound	Upper Bound	
m_0	.418	.002	.415	.422	0.995

On the other hand, the first and the second buckling mode shapes are shown in figures 4-5-A and B, respectively for different material gradient parameters α. For a homogenous film ($\alpha = 0$) the mode shapes are symmetric or antisymmetric according to the results in table 4-1. However, for a FGM film ($\alpha \neq 0$), the position of the maximum amplitude moves toward the softer end along the span with increasing of the material gradient α as shown in the figures for both mode shapes. Also, for the second buckling mode the peak near the softer region grows while the other one diminishes as figure 4-5-B shows.

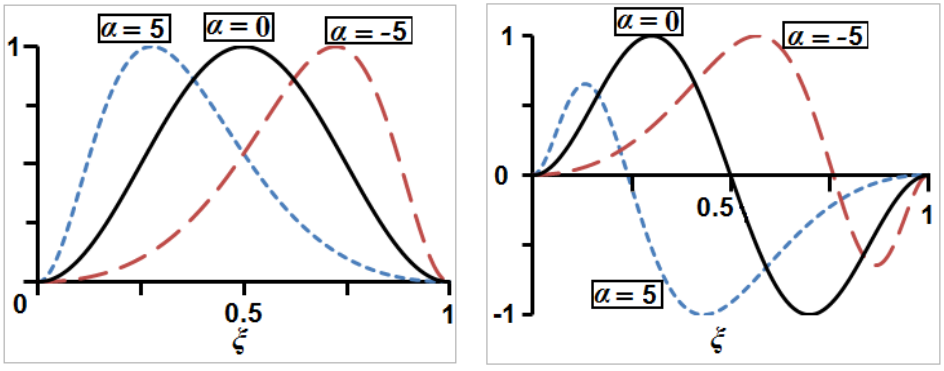

A) First mode shape B) Second mode shape

Figure 4-5: Buckling mode shapes of a free standing FGM film

4.5.2 Wrinkling of a Substrate–bonded Film

For a homogenous isotropic film in which the stiffness is uniformly distributed along the entire span (α=0), the governing equation of the film–substrate system in (4-5) is simplified to a forth order differential equation with constant coefficients. For a clamped–clamped beam on a soft foundation [Ratzerdorfer, 1936; CRCJ, 1971, pp. A–1–27], the wavelength of the flexures is not tiny and the corresponding critical compressive load is represented as the combination of the Euler buckling load and the substrate effect, i.e. $N= N^0{}_B+2\sqrt{K}$ where $N^0{}_B=4\pi^2$. Obviously, by increasing the substrate stiffness parameter K defined in (4-6-B) which is a function of the foundation stiffness $\overline{K}$ and slender ratio of the film (i.e. L/t), especially for thin film structure with tiny thickness, the effect of the substrate is several orders of magnitude bigger than the Euler buckling load $N^0{}_B$. Therefore, the critical compressive load $N^0{}_W$ and wave number $\beta^0{}_W$ of the wrinkling are represented in terms of the non–dimensional substrate stiffness K as

$$N_{\mathrm{W}}^{0} = 2\sqrt{K} \tag{4-25}$$

$$\beta_{\mathrm{W}}^{0} = \sqrt[4]{K} \tag{4-26}$$

These relations are the well–known relations of the wrinkling of a thin film deposited on a substrate in the literature [CRCJ, 1971, pp. A–1–27; Cerda and Mahadevan, 2003; Birman and Bert, 2004; Pocivavsek et al., 2008]. The finite difference analysis and series solution method lead to exactly the same results for wrinkling load and wave number. The critical load of the homogenous film on the substrate form the finite difference solution and the analytical formula of Ratzerdorfer [1936] are shown in figure 4-6.

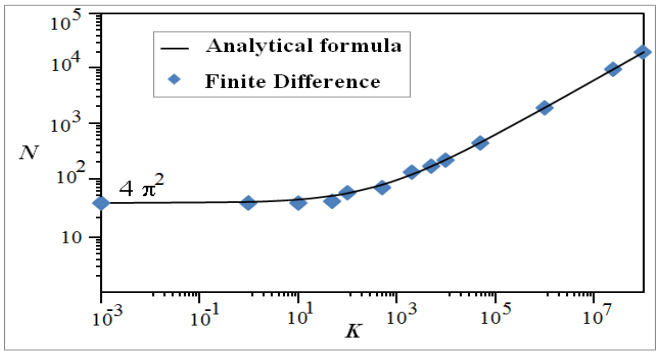

Figure 4-6: The critical load N of the homogenous film deposited on the substrate with stiffness K from Finite difference solution compared with analytical formula [Ratzerdorfer, 1936]

In contrast with the buckling of a free standing film which is influenced by the boundary conditions, the wrinkling load and wave number of the wrinkled homogenous film are influenced only by the substrate stiffness according to the equations (4-25) and (4-26). However, the boundary conditions of the film change the wrinkling pattern of the system. For a film–substrate system with very long or infinite length, the wrinkles propagate uniformly all over the domain and the effects of the boundary conditions are completely vanished [Cerda and Mahadevan, 2003; Chen and Hutchinson, 2004; Niu and Talreja, 1999] as shown in figure 4-7-A. While for a film–substrate system with finite length, the boundary conditions of the film affect the wrinkling pattern. For example, figure 4-7-B shows the wrinkling pattern of a homogenous film with clamped–clamped edges, in which the wrinkling amplitude decreases with the approach of the edges.

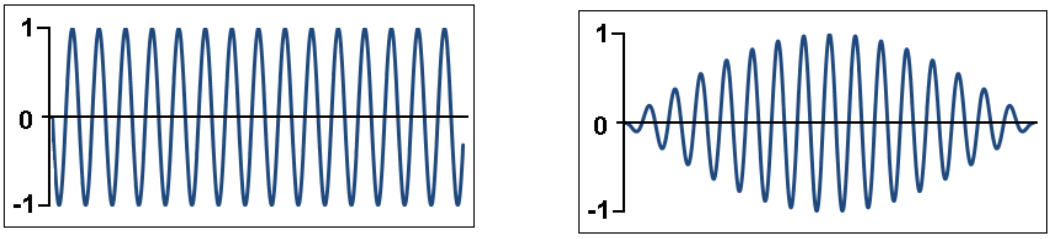

A) Infinite length B) Finite length model with clamped edges

Figure 4-7: Diagram of the wrinkling pattern of a homogenous film deposited on the substrate

For a FGM film deposited on the substrate, the critical wrinkling load are calculated for various values of the substrate stiffness K and gradient modulus α and are compared with the results of the homogenous film. For different substrate stiffness K_n ($K_n = 10^{-9}K$), figure 4-8 plots the normalized wrinkling load $F_n = \frac{N}{N^0_W}$ of the FGM film–substrate system versus material gradient α, where N^0_W is the wrinkling load for a homogenous film–substrate system in equation (4-25). It is observed in the figure that for a stiffening film (α>0), the normalized wrinkling load F_n (i.e. The wrinkling load of the FGM film relative to the wrinkling load of a homogenous film) is greater than one and decreases with the increasing of the substrate stiffness. However the wrinkling load itself increases for stiffer substrate, while with a lower rate than a homogeneous film bonded to the substrate. In addition, the dependence of the critical buckling load on the material

gradient α becomes less sensitive for a stiffer substrate as indicated by the flatter curves in figure 4-8 when K_n is getting bigger. Increasing the material gradient α stiffens the system and hence the normalized wrinkling load increases with an ascending function. In addition, for softer substrate with lower K_n, the wrinkling load of the FGM film decreases similar to the case of the homogenous film in equation (4-25) but with a faster rate, consequently the normalized critical wrinkling load increases in figure 4-8. On the other hand, for a softening film (α<0) the substrate stiffness has negligible effect on the wrinkling load of the FGM film–substrate, which is less than the wrinkling load of the homogenous film–substrate system (as expected).

These observations help to propose an appropriate relation between the normalized wrinkling load and the material gradient α for stiffening and softening films respectively by,

$$F_n^{(\alpha>0)} = 1 + m_1 K_n^{-m_2}\, \alpha^{m_3} \qquad \text{(4-27-A)}$$

$$F_n^{(\alpha<0)} = \mathrm{EXP}(m_4 \alpha) \qquad \text{(4-27-B)}$$

where the constant parameters m_1, m_2, m_3 and m_4 could be obtained from a regression analysis [Kahane, 2008]. The results of the regression analysis with 60 and 75 datapoints of the FDM solution for $0< \alpha <5$ and $-5< \alpha <0$, respectively, within the range of $0.01<K_n<10$ are shown in table 4-4. The constant parameters in equations (4-27-A,B) are determined with a high accuracy as $R^2= 0.99$ and a standard error less than ± 1% for the estimated parameters. Obviously, imposing $\alpha = 0$ in relations (4-27-A,B) leads to $F_n =1$ corresponding with the wrinkling load of a homogenous film. For values of K and α outside the above range, the stiffness of the substrate and film are too large or too small, which are not considered in this work. The series solution method leads to almost similar results obtained from finite difference analysis.

Table 4-4: The parameters of the relations (4-27-A, B) for wrinkling load obtained from regression analysis

Model Summary		R^2= 0.99		
Parameter	Estimate	Std. Error	95% Confidence Interval	
			Lower Bound	Upper Bound
m_1	.059	.000	.058	.059
m_2	.174	.001	.172	.176
m_3	.692	.004	.684	.699
m_4	.450	.004	.442	.458

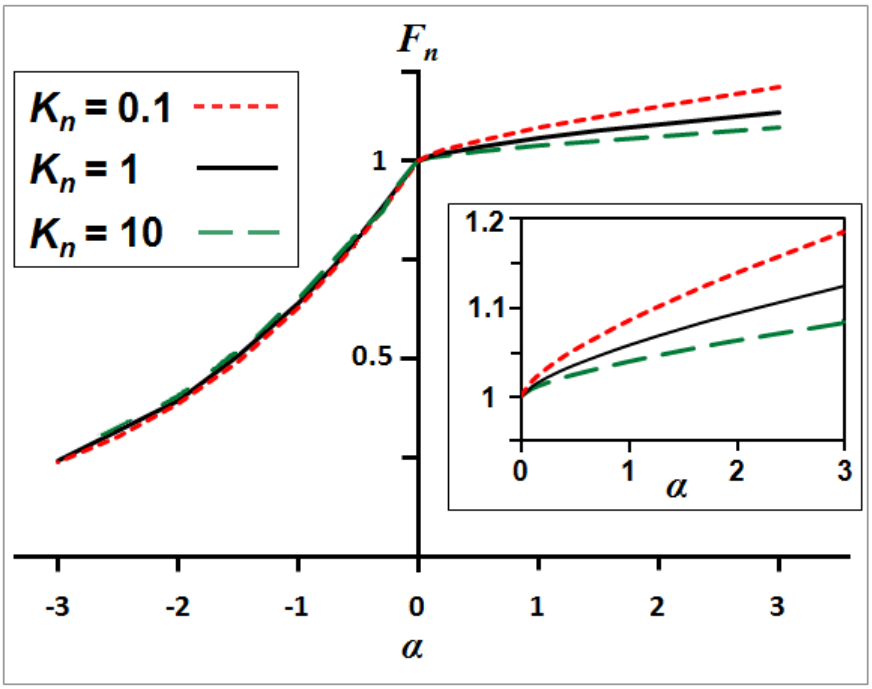

Figure 4-8: Normalized wrinkling load F_n versus gradient modulus α for different substrate stiffness K_n

Similarly, the wrinkling pattern of the FGM film bonded to the substrate is found to be affected by the material gradient of the FGM film as shown in figures 4-9-A-E from the FDM solution. For a homogenous film with uniform stiffness, the wrinkles propagate all over the length span; while for the case of a FGM film where the stiffness is variable along the span, the wrinkles accumulate around the weakest location of the system. In order to characterize the wrinkling pattern two parameters are introduced: the footprint of the wrinkling that shows the size of the region on the film influenced by the wrinkles and the wave number of the wrinkles which shows the number of the wrinkles in the affected area. More wave number on shorter footprint indicates a denser wrinkling pattern. The variation of the stiffness of the film accumulates wrinkles around the location with minimum stiffness, and by increasing the material gradient α as figures 4-9-B-E show, the footprint of the wrinkles decreases and the number of wrinkles decreases as well.

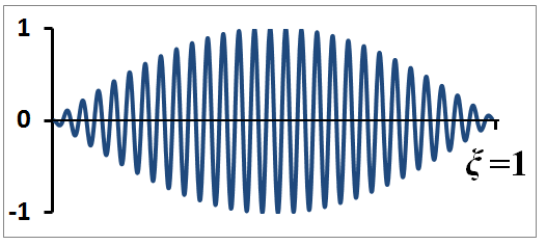

A) Homogenous film α =0

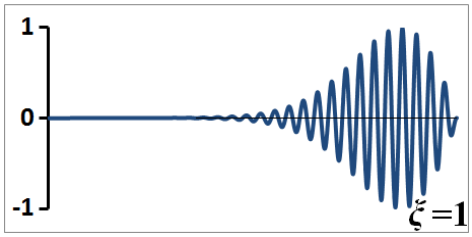

B) Softening FGM film α = –0.1

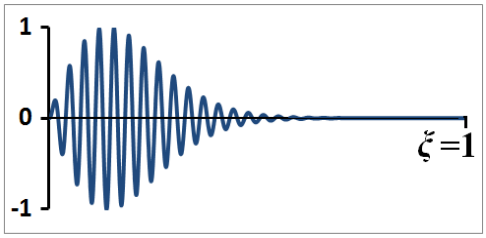

C) Stiffening FGM film α = 0.1

D) Softening FGM film α = –1

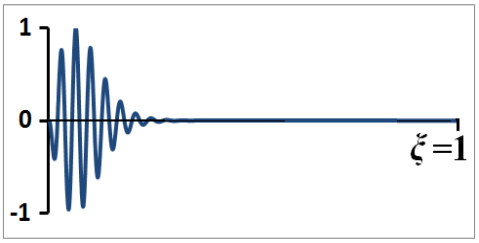

E) Stiffening FGM film α = 1

Figure 4-9: Wrinkling pattern of the FGM film with variable stiffness on the same substrate

The normalized wave number $\beta_n = \frac{\beta}{\beta_W^0}$ of the wrinkling for the FGM film–substrate system versus the material gradient α for different substrate stiffness K is plotted in figure 4-10 from the finite difference solution, where $\beta^0{}_W$ is the wrinkling wave number for a homogenous film–substrate system in equation (4-26). Obviously, all the curves approach to β_n =1 for a homogenous film corresponding with α =0. For positive and negative values of the material gradient α, the curves of the normalized wave number in this figure are almost symmetric. With the increasing of the material gradient α, the normalized wave number decreases, which indicates the accumulative effect of the wrinkling with less wave number. For stiffer substrates, the wave number of the wrinkling of the FGM film increases with slower rate compared to that of the homogenous film in Equation (4-26), therefore, the normalized wave number decreases as shown in figure 4-10.

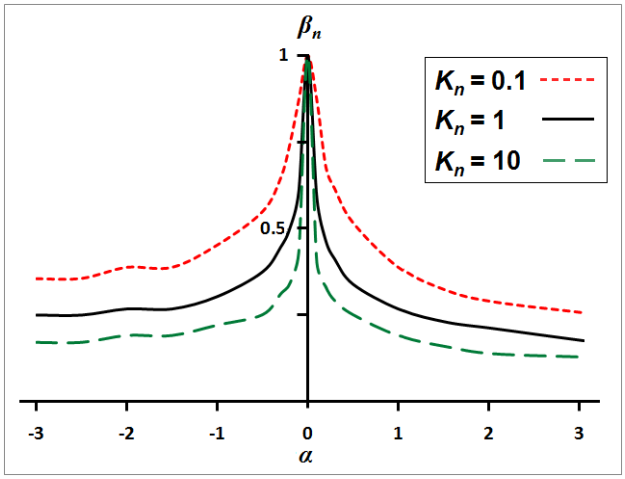

Figure 4-10: Normalized wave number β_n versus material gradient α for different substrate stiffness K_n

From the numerical simulation results of the finite difference method, the normalized wave number of the wrinkling for the FGM film–substrate system is proposed as a function of the substrate stiffness K and material gradient α in the following format,

$$\beta_n = \mathrm{EXP}(-m_1|\alpha|^{m_2})\, K_n^{-m_3[1-\mathrm{EXP}(m_4|\alpha|^{m_5})]} \qquad (4\text{-}28)$$

where m_i (i=1...5) are constant parameters and "$|\alpha|$" is the absolute value of the material gradient α. The best approximation of the normalized wave number in (4-28) is

obtained numerically by using m_4= –8 and m_5= 0.5. Hence, the equation (4-28) is rewritten as

$$\beta_n = \mathrm{EXP}(-m_1|\alpha|^{m_2})\, K_n^{-m_3\left[1-\mathrm{EXP}\left(-8\sqrt{|\alpha|}\right)\right]} \quad (4\text{-}29)$$

Clearly, equation (4-29) reduces to the result for a homogenous film with $\beta^0{}_W = \beta_0$ in (4-26) by substituting $\alpha = 0$. With the increase of the material gradient α, the normalized wave number of the wrinkling decreases exponentially as represented by equation (4-29) and figure 4-10. Applying a regression analysis with 65 datapoints for –1.5< α <3 and 0.01< K_n <10, the constant parameters m_1, m_2 and m_3 in (4-29) are determined, which are given in table 4-5. These results show a high accuracy for the proposed relation of the wave number in equation (4-29) with R^2=0.975 and a standard error about ± 4% for estimated parameters.

Table 4-5: The parameters of the equation (4-29) for normalized wave number β_n obtained from a regression analysis

Model Summary		R^2 = 0.975		
Parameter	Estimate	Std. Error	95% Confidence Interval	
			Lower Bound	Upper Bound
m_1	1.262	.027	1.207	1.317
m_2	.423	.014	.395	.450
m_3	.154	.007	.140	.168

The plot of the equation (4-29) in figure 4-11 shows that the variation of the material properties along the length span has a significant effect on the wave number of the wrinkling, which is more effective than the substrate stiffness on the wrinkling pattern due to accumulative effect imposed on the system. In other words, the effect of the first exponential term corresponding with the FGM gradient α in the equation (4-29) is more important than the second power term of substrate stiffness K.

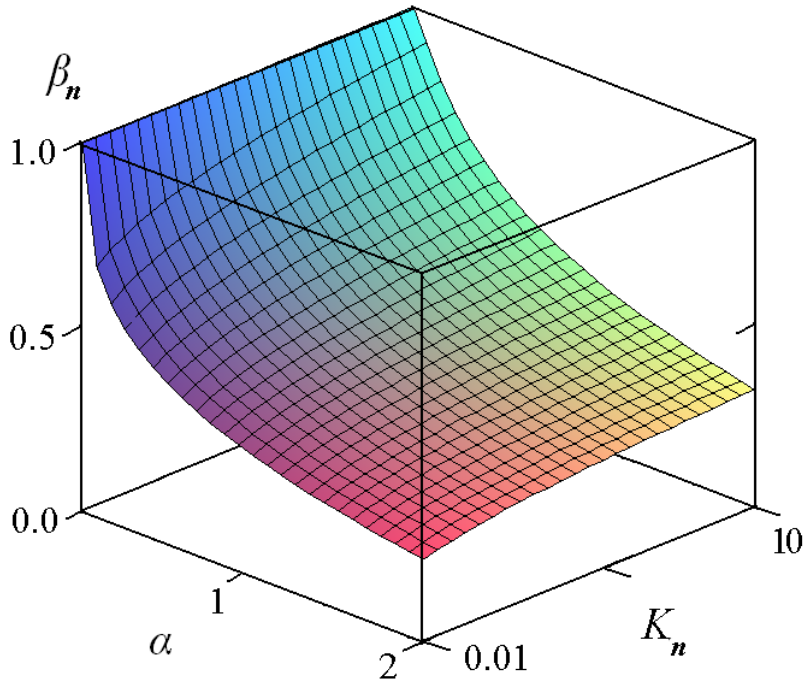

Figure 4-11: The normalized wave number β_n of the wrinkling versus material gradient α and the substrate stiffness K

Figure 4-12 shows the observed values of the wave number obtained from the finite difference solution of the eigenvalue problem versus the predicted values from (4-29), and histogram of the residual errors is plotted in figure 4-13. From these figures, it is concluded that the presented relation in (4-29) predicts the wrinkling wave number very well.

The normalized wave number predicted by finite difference method is compared with that from the series solution in figure 4-14 for a sample substrate stiffness K. It is observed that the finite difference method proposes a stiffer film with less wave number. The difference between the results increases especially with the increasing of the material gradient α for stiffer substrate with higher values of K. This may caused by the truncation error due to the discretization of the domain by finite difference formulation, which is intensified by growing α and K. Using the finite difference formulation with higher accuracy will decrease the truncation error.

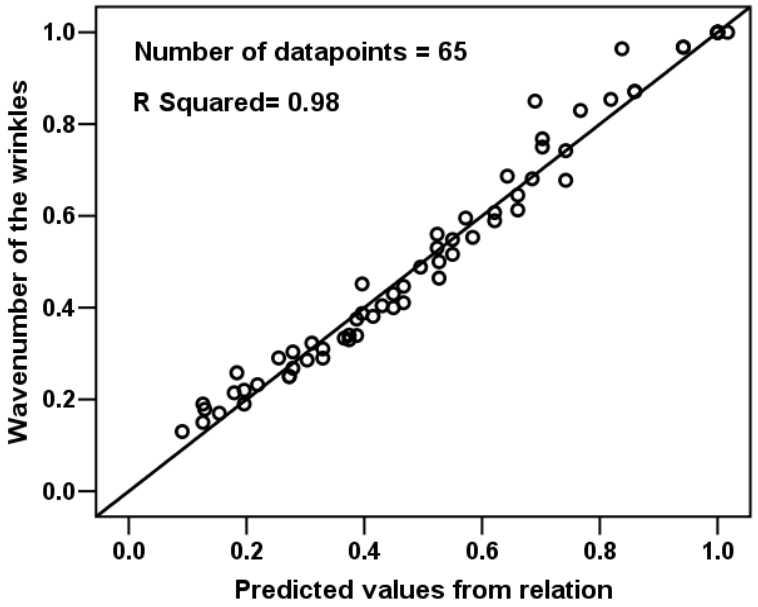

Figure 4-12: Normalized wave number compared with the predicted values from the proposed relation in (4-29)

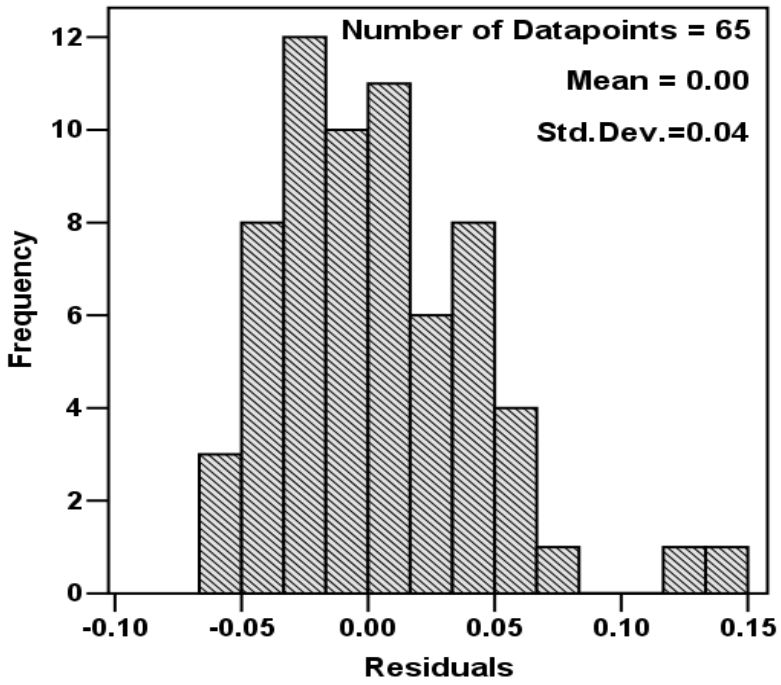

Figure 4-13: Histogram of the residual errors of the relation (4-29) for predicting the wave number

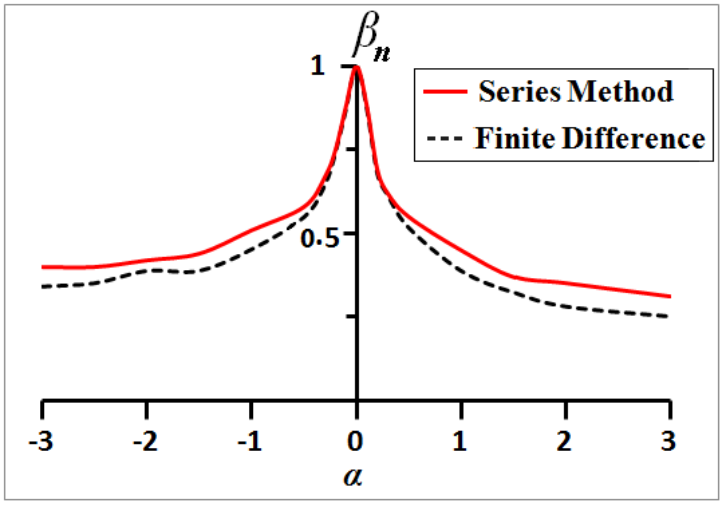

Figure 4-14: Comparison of the finite difference and series solution for the normalized wave number β_n of the wrinkling versus material gradient α

The change of the substrate stiffness K and material gradient α not only affects on the wave number of the wrinkling of the film, but also changes the effective length along the span which undergoes wrinkling. As discussed in figures 4-9-A-E, wrinkles accumulate at the location with minimum stiffness (the softer edge of the film). In order to consider the localization of the wrinkles along the length span, a non–dimensional parameter is introduced as the footprint of the wrinkles on the film which represents the effective length of the film influenced by the wrinkles. The footprint of the wrinkling is defined as the ratio of the length of the film subjected by the wrinkles to the entire length of the film, which varies from zero to one. When the footprint equals to one, the entire length span of the film is affected by the wrinkles corresponding to the case of the wrinkling of a homogenous film ($\alpha = 0$).

A regression analysis for the relation between the footprint and the wave number of the wrinkles shows that these parameters are proportional to each other by a linear function as

$$Footprint = m_0 \beta_n \qquad (4\text{-}30)$$

The regression analysis between the footprint and the normalized wave number proposes estimation for the coefficient m_0 as presented in table 4-6, which is very close to unity. The footprint parameter versus the corresponding normalized wave number for 75 datapoints from FDM solution is plotted in figure 4-15, in which datapoints are located

around the reference line in (4-30). This result indicates that the relation between the footprint and the wave number agrees well with the proposed relation.

Table 4-6: The regression analysis results for linear relation of the footprint with normalized wave number

Model summary		$R^2 = 0.974$		
Parameter	Estimate	Std. Error	95% Confidence Interval	
			Lower Bound	Upper Bound
m_0	.979	.009	.961	.998

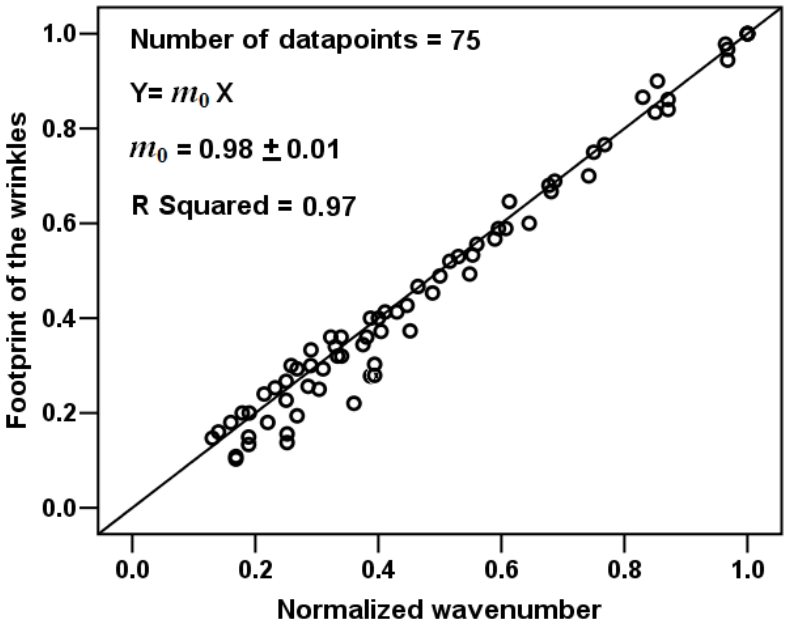

Figure 4-15: The linear relation between footprint and normalized wave number β_n of the wrinkling

The high sensitivity of the footprint parameter (as well as wrinkling wave number) with respect to the variation of the stiffness (i.e. material gradient α) indicates that even with small disturbances of the uniformity of the film stiffness, wrinkles accumulate densely at the weakest location along the length span (Figure 4-16). On the other hand, the importance of the microstructure of thin film systems besides the limitations of the

manufacturing process increases the effects of the mechanical properties variation which intensifies the abovementioned accumulative effect. Therefore, the wrinkles behave completely different in comparison with the uniform wrinkling of the system with homogenous material properties. Hence, this study is expected to be helpful for understanding the wrinkling phenomenon of a non–homogeneous film–substrate system.

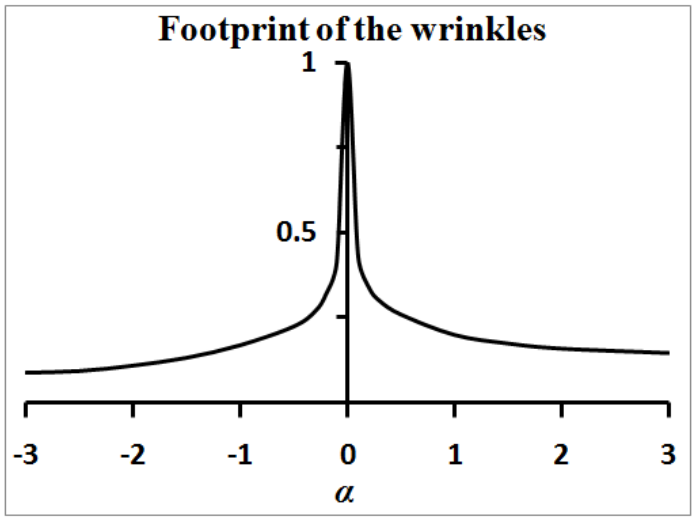

Figure 4-16: Footprint of the wrinkling versus material gradient α

4.6 Summary

The buckling of a free standing FGM film and the uniaxial wrinkling of a deposited FGM film on the Winkler substrate with finite length are investigated. Critical load and pattern at the onset of instability are derived according to the characteristic parameters of the system (i.e. substrate stiffness and variation of the film stiffness). The eigenvalue problem of the differential equation of the film–substrate system is solved by using finite difference method and series solution. It is observed that for a homogenous film the wrinkles propagate the entire length span, while for the FGM film the wrinkles accumulate around the weakest location of the film with the lowest stiffness. In comparison with a homogenous film, for stiffer substrate and higher material gradient of the FGM film, the rate of the increasing of the wave number and wrinkling load decreases and the wrinkles shrink more around the weakest location of the FGM film. The results of this analysis are expected to help in predicting and controlling the wrinkle pattern in experimental works, MEMS/NEMS applications and sensor/actuator systems.

4.7 References

[1] M. Abramowitz, I.A. Stegun, *Handbook of Mathematical Functions*, 1972, Dover Publications, New York.

[2] V. Birman, C.W. Bert, "Wrinkling of composite–facing sandwich panels under biaxial loading", *Journal of Sandwich Structures and Materials*, Vol. 6 (3), 2004, pp. 217–237.

[3] F. Bloom, D. Coffin, *Handbook of Thin Plate Buckling and Postbuckling*, 2001, Chapman & Hall CRC.

[4] E. Cerda, L. Mahadevan, "Geometry and physics of wrinkling", *Physical Review Letters*, Vol. 90 (7), 2003, pp. 074302/1–4.

[5] X. Chen, J. W. Hutchinson, "A family of herringbone patterns in thin films", *Scripta Materialia*, Vol. 50, 2004, pp. 797–801.

[6] W. Chen, J. Wang, M.–r. Wang, "Influence of doping concentration on the properties of ZnO:Mn thin films by sol–gel method", *Vacuum*, Vol. 81(7), 2007, pp. 894–898.

[7] CRCJ Column Research Committee of Japan, *Handbook of Structural Stability*, 1971,Corona, Tokyo, Japan.

[8] J.Genzer, J.Groenewold, "Soft matter with hard skin: From skin wrinkles to templating and material characterization", *Soft Matter*, Vol. 2 (4), 2006, pp. 310–323.

[9] R. Huang, S. H. Im, "Dynamics of wrinkle growth and coarsening in stressed thin films", *Physical Review E*, Vol. 74 (2), 2006, Article No. 026214.

[10] L.H. Kahane, *Regression Basics*, 2nd. Ed., 2008, Sage Publications Inc.

[11] L. L. Ke, J. Yang, S. Kitipornchai, "An analytical study on the nonlinear vibration of functionally graded beams", *Meccanica*, Vol. 45 (6), 2010, pp.743–752.

[12] K. A. Khor, Z. L. Dong, Y. W. Gu, "Influence of oxide mixtures on mechanical properties of plasma sprayed functionally graded coating", *Thin Solid Films*, Vol. 368 (1), 2000, pp. 86–92.

[13] K. Niu, R. Talreja, "Modeling of wrinkling in sandwich panels under compression", *Journal of Engineering Mechanics,* Vol. 125(8), 1999, pp. 875–883.

[14] L. Pocivavsek, R. Dellsy, A. Kern, S. Johnson, B. Lin, K. C. Lee, E. Cerda, "Stress and fold localization in thin elastic membranes", *Science*, Vol. 320 , 2008, pp. 912–916.

[15] J. Ratzerdorfer, *Die Knickfestigkeit von staben und stabwerken*, 1936, Springer, Wien.

[16] H.S. Shen, Z.X. Wang, "Nonlinear bending of FGM plates subjected to combined loading and resting on elastic foundations", *Composite Structures*, Vol. 92 (10), 2010, pp. 2517–2524.

[17] A. Stashans, "Defects in titanates", *International Journal of Nanotechnology*, Vol. 1 (4), 2004, pp. 399–430.

[18] V. Teixeira, "Mechanical integrity in PVD coatings due to the presence of residual stresses", *Thin Solid Films*, Vol. 392 (2), 2001, pp. 276–281.

[19] A.C. Ugural, *Stresses in Plates and Shells*, 1999, McGraw–Hill Book Company, Inc.

[20] S.P. Timoshenko, J.M. Gere, *Theory of Elastic Stability*, 1961, McGraw–Hill Book Company, Inc.

[21] S. Wang, J. Song, D. Kim, Y. Huang, J. A. Rogers, "Local versus global buckling of thin films on elastomeric substrates", *Applied Physics Letters*, Vol. 93, 2008, Article No. 023126.

[22] J. Yang, Y. Chen, "Free vibration and buckling analyses of functionally graded beams with edge cracks", *Composite Structures*, Vol. 83 (1), 2008, pp. 48–60.

[23] A.M. Zenkour, "Hygro–thermo–mechanical effects on FGM plates resting on elastic foundations", *Composite Structures*, Vol. 93 (1), 2010, pp. 234–238.

[24] J. Zhao, Y. Li, X. Ai, "Analysis of transient thermal stress in sandwich plate with functionally graded coatings", *Thin Solid Films*, Vol. 516 (21), 2008, pp. 7581–7587.

[25] S. Zhao, G. W. Wei, "Matched interface and boundary (MIB) for the implementation of boundary conditions in high–order central finite differences", *International Journal for Numerical Methods in Engineering*, Vol. 77, 2009, pp. 1690–1730.

Chapter 5

5 Buckling and Wrinkling of a Thin Solid Film with Quadratic Thickness Pattern

The instability of a beam/strip with variable thickness as a free standing film or a deposited film on the substrate is investigated. The thickness pattern is assumed with a quadratic profile with its minimum at the middle of the length span. For the free standing film, the buckling loads and mode shapes are derived analytically by using a closed form solution. For the substrate–bonded film, the substrate is modeled by using Winkler foundation and the effect of the non–uniform thickness of the film on the wrinkling parameters is considered. Unlike the film with uniform thickness, the wrinkles accumulate around the location with the minimum thickness along the span of the film with non–uniform thickness.

5.1 Introduction

Buckling and wrinkling of thin solid film structures under compressive loading are categorized as mechanical instability of the system first introduced by *Leonard Euler* for buckling of columns. The instability of the system is considered by using the bifurcation theory, such that the branch points (or equivalently bifurcation points) at the instability onset are corresponding with the eigenvalues and eigenfunctions of the eigenvalue problem for the differential equation of the system [Bloom and Coffin, 2001]. Different patterns have been introduced to study the wrinkling of thin films [Huang and Im, 2006; Wang et al. 2008], among which uniaxial wrinkling pattern attracts great attention from many researchers [Chen and Hutchinson, 2004].

In literature, the uniform thickness assumption of the film is mostly used for the wrinkling problem of films. Among others, Cerda and Mahadevan (2003), Chen and Hutchinson (2004) and Niu and Talreja (1999) calculated the wavelength and amplitude of the sinusoidal wrinkling by assuming the uniform amplitude for the wrinkles all over the span, but several questions remained unanswered. In thin film structures that the thickness of the film is tiny, even small variations of the thickness attract a lot of concerns about the effect of the thickness variation on the system. In contrast with the

uniform thickness film, during deposition of the film on the substrate, the thickness cannot be attributed uniformly all over the span, hence it is necessary to consider the effect of the film thickness variations on the critical load and pattern (i.e. amplitude and wave number) of the wrinkling.

In this chapter, the buckling and uniaxial wrinkling problem of a film with variable thickness deposited on a Winkler substrate is considered. By modeling the profile of the film thickness with a quadratic profile, the eigenvalue problem for the differential equation of the system is solved and the corresponding parameters of the wrinkling (i.e. load and pattern) are determined. The effect of the substrate stiffness and variation of the film thickness on the instability parameters are considered. In contrast with other works of the instability of the thin films which usually assume a uniform thickness for the film and neglect the effect of the thickness variation, the current work shows that this effect is very important in wrinkling localization. The tiny thickness of the film increases the importance of the problem in which the uniformity of the thickness of the film is uncontrollable.

5.2 Modeling

The buckling of a free standing film and the uniaxial wrinkling of a thin film deposited on the substrate are investigated with the classical beam/strip theory with small deformation. The non–uniform film deposited on a Winkler substrate with modulus $\bar{K}$ under an in–plane loading $\bar{N}_x$ is shown in figure 5-1 with thickness $t(x)$, width b and length L. The substrate should be thick enough and also compliant in order to apply Winkler model [Birman and Bert, 2004; Cerda and Mahadevan, 2003; Niu and Talreja, 1999]. The governing equation for a film under a uniaxial deformation like a strip is given as [Ugural, 1999, pp. 298]

$$\frac{d^2}{dx^2}\left[D\frac{d^2\bar{w}}{dx^2}\right] + \bar{N}_x\frac{d^2\bar{w}}{dx^2} + b\bar{K}\bar{w} = 0 \qquad (5\text{-}1)$$

in which $\bar{w}$ is the deflection and D is the bending stiffness of the film as

$$D = \frac{1}{12}\bar{E}bt^3 \qquad (5\text{-}2)$$

where $\bar{E}$ is the elastic modulus E for a plane stress beam or $E/(1-\nu^2)$ for a plane strain strip with ν being the Poisson's ratio. In the current work, the thickness is considered as a variable parameter along the length span of the strip/beam and is defined by

$$t = t_0\big(1 + \epsilon\, f(x)\big) \tag{5-3}$$

where t_0 is the minimum thickness of the film, ϵ is the amplitude of the variation of the thickness introduced as the amplitude parameter and $f(x)$ is the shape function of the variation of the thickness along the length span x such that Max $[f(x)] = 1$. Correspondingly, the bending stiffness is rewritten as

$$D = D_0 D(x) = D_0\big(1 + \epsilon\, f(x)\big)^3 \tag{5-4}$$

where $D_0 = \frac{1}{12}\bar{E}bt_0{}^3$. Imposing (5-4) into (5-1) and introducing the non–dimensional variable ξ defined as $\xi = x/L$ and the normalized deflection $w = \frac{\bar{w}}{Max\,(\bar{w})}$ leads to the dimensionless equation of (5-1) as

$$[D(\xi)\,]\frac{d^4w}{d\xi^4} + \Big[2\,\frac{d}{d\xi}D(\xi)\,\Big]\frac{d^3w}{d\xi^3} + \Big[\,\frac{d^2}{d\xi^2}D(\xi) + N\Big]\frac{d^2w}{d\xi^2} + Kw = 0 \tag{5-5}$$

in which $D(\xi) = \big(1 + \epsilon\, f(\xi)\big)^3$ is the bending stiffness modulus profile and

$$N = \frac{\bar{N}_x}{D_0}L^2 \tag{5-6-A}$$

and

$$K = \frac{\bar{K}}{D_0}bL^4 \tag{5-6-B}$$

For simulation purpose, a quadratic function is assumed as the profile of the thickness pattern with its minimum located at the middle of the span as shown in figure 5-2. In the following, the effect of the thickness variation of the film is considered on the buckling and wrinkling parameters (load and pattern) and the results are compared with the results of a classical film with uniform thickness.

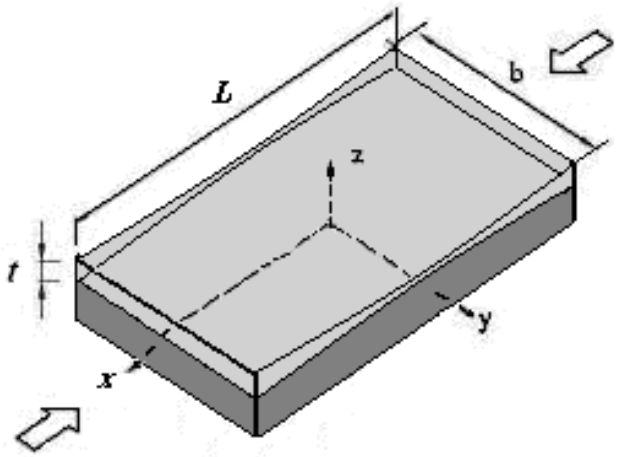

Figure 5-1: Deposited film with variable thickness on the substrate

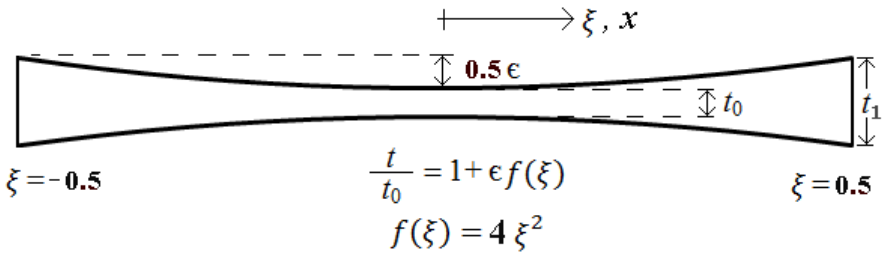

Figure 5-2: The profile of the thickness of the film along the length span

5.3 Buckling Analysis

For a free standing film with variable thickness, the governing equation of the system at the onset of buckling is represented by

$$\frac{d^2}{d\xi^2}\left[D(\xi)\,\frac{d^2w}{d\xi^2}\right] + N\frac{d^2w}{d\xi^2} = 0 \qquad (5\text{-}7)$$

while $D(\xi)$ is the bending stiffness modulus profile. For the non–uniform thickness film ($\epsilon \neq 0$), the manipulation of the forth order differential equation (5-7) by using a change of variable $u = \frac{1}{\sqrt{1+\epsilon\,\xi^2}}$ results in the algebraic form of the Mathieu differential equation as [Abramowitz and Stegun, 1972]

$$(1-u^2)\frac{d^2w}{du^2} - u\frac{\mathrm{d}w}{\mathrm{d}u} + [a + 2\,q(1-2u^2)]\,w = 0 \qquad (5\text{-}8\text{-}A)$$

which can be converted to the canonical form of Mathieu differential equation by substituting u=cos(η) as

$$\frac{d^2w}{d\eta^2} + [a - 2\,q\cos(2\eta)]\,w = 0 \tag{5-8-B}$$

where $a = 1 + \frac{N}{2\,\epsilon}$ and $q = -\frac{N}{4\,\epsilon}$. It should be noted that MathieuC (a, q, η) and MathieuS (a, q, η), the even and odd Mathieu functions of parameter η, are solutions of the Mathieu differential equation in (5-8-A,B). Furthermore, MathieuC and MathieuS are normalized such that MathieuC (a, q, 0) = 1 and $\frac{d}{d\eta}$MathieuS (a, q, η=0) = 1 [Abramowitz and Stegun, 1972]. Therefore, the governing equation (5-7) has a general solution as

$$w(\xi) = m_1\mathrm{C}(\xi) + m_2\mathrm{S}(\xi) + m_3\xi + m_4 \tag{5-9}$$

in which $\mathrm{C}(\xi)$ and $\mathrm{S}(\xi)$ are even and odd functions as

$$\mathrm{C}(\xi) = \sqrt{1+\epsilon\,\xi^2}\ \mathrm{MathieuC}\left[1 + \frac{N}{2\,\epsilon}\,, -\frac{N}{4\,\epsilon}, \arctan\left(\xi\sqrt{\epsilon}\right)\right] \tag{5-10-A}$$

$$\mathrm{S}(\xi) = \sqrt{1+\epsilon\,\xi^2}\ \mathrm{MathieuS}\left[1 + \frac{N}{2\,\epsilon}, -\frac{N}{4\,\epsilon}, \arctan\left(\xi\sqrt{\epsilon}\right)\right] \tag{5-10-B}$$

and m_i (i=1...4) are unknown constants to be determined from the boundary conditions. For the case of a free standing film with uniform thickness (ϵ=0), the solution of the governing equation of the buckling problem is represented by substituting $\sin(\xi\sqrt{N})$ and $\cos(\xi\sqrt{N})$ to replace functions $\mathrm{S}(\xi)$ and $\mathrm{C}(\xi)$ in (5-9), respectively.

The boundary conditions of the film are applied for clamped–clamped edges at ξ= ±½ to determine the unknown constants m_i (i=1...4) in equation (5-9) as

$$w = 0 \text{ and } \frac{dw}{d\xi} = 0 \tag{5-11}$$

Therefore, the characteristic equations and mode shapes of the buckling of the film are obtained for symmetric and antisymmetric modes, respectively as

$$\mathrm{C}'\left(\frac{1}{2}\right)\left[\mathrm{S}'\left(\frac{1}{2}\right) - \mathrm{S}\left(\frac{1}{2}\right)\right] = 0 \tag{5-12-A}$$

$$w = \frac{\mathrm{C}(\xi) - \mathrm{C}\left(\frac{1}{2}\right)}{\mathrm{C}'\left(\frac{1}{2}\right)} - \frac{\mathrm{S}(\xi) - \xi\mathrm{S}\left(\frac{1}{2}\right)}{\mathrm{S}'\left(\frac{1}{2}\right) - \mathrm{S}\left(\frac{1}{2}\right)} \tag{5-12-B}$$

Alternatively, these equations are rewritten in terms of Mathieu functions as

$$\left[\sqrt{\epsilon}\mathrm{MC}\left(\xi = \frac{1}{2}\right) + \mathrm{MC}'\left(\xi = \frac{1}{2}\right)\right]\left[\mathrm{MS}\left(\xi = \frac{1}{2}\right) - \sqrt{\epsilon}\mathrm{MS}'\left(\xi = \frac{1}{2}\right)\right] = 0 \tag{5-13-A}$$

$$w(\xi) = \frac{\sqrt{1+\epsilon\,\xi^2}\ \mathrm{MC}\,[\xi] - \sqrt{1+.25\epsilon}\ \mathrm{MC}\left[\xi=\frac{1}{2}\right]}{\sqrt{\epsilon}\mathrm{MC}\left(\xi=\frac{1}{2}\right) + \mathrm{MC}'\left(\xi=\frac{1}{2}\right)} - \frac{\sqrt{1+\epsilon\,\xi^2}\ \mathrm{MS}\,[\xi] - \xi\sqrt{1+.25\epsilon}\ \mathrm{MS}\left[\xi=\frac{1}{2}\right]}{\mathrm{MS}\left(\xi=\frac{1}{2}\right) - \sqrt{\epsilon}\mathrm{MS}'\left(\xi=\frac{1}{2}\right)} \tag{5-13-B}$$

where $\mathrm{MC}(.)$ and $\mathrm{MS}(.)$ are used for $\mathrm{MathieuC}\left[1+\frac{N}{2\,\epsilon}, -\frac{N}{4\,\epsilon}, \arctan\left(\xi\sqrt{\epsilon}\right)\right]$ and $\mathrm{MathieuS}\left[1+\frac{N}{2\,\epsilon}, -\frac{N}{4\,\epsilon}, \arctan\left(\xi\sqrt{\epsilon}\right)\right]$ in (5-13-A,B) respectively and ( )' stands for the derivative of MathieuC(a, q, η) and MathieuS(a, q, η) with respect to η. Therefore, the corresponding buckling load N and mode shapes are obtained in terms of the parameter ϵ numerically.

Particularly, for the film with uniform thickness ($\epsilon = 0$), the characteristic buckling equation for the boundary conditions of both clamped edges is represented as

$$\sin\left(0.5\sqrt{N}\right)\left[\tan\left(0.5\sqrt{N}\right) - 0.5\sqrt{N}\right] = 0 \qquad (5\text{-}14)$$

which leads to the symmetric and antisymmetric buckling modes with buckling loads and mode shapes being presented in table 5-1.

Table 5-1: The buckling parameters for homogenous film with clamped edges

Buckling mode	Characteristic equation	Critical load	Mode shape
Symmetric	$\sin\left(0.5\sqrt{N}\right) = 0$	$N = 4\,\pi^2$	$1 + \cos\left(\sqrt{N}\xi\right)$
Anti-symmetric	$\tan\left(0.5\sqrt{N}\right) = 0.5\sqrt{N}$	$N = 8.183\,\pi^2$	$\sin\left(\sqrt{N}\xi\right) - 2\xi\,\sin\left(0.5\sqrt{N}\right)$

5.4 Wrinkling Analysis

The governing equation of the film–substrate system in equation (5-5) is a forth order linear ordinary differential equation with variable coefficients which has no analytical closed form solution even for simple functions of $f(\xi)$; hence semi–analytical or numerical methods are used to solve the equation.

5.4.1 Series Solution Method

In order to solve the forth order differential equation (5-5), a series solution is constructed with power functions of ξ^i and unknowns coefficients c_i as

$$w(\xi) = \sum_{i=0}^{i\to\infty} c_i\,\xi^i \qquad (5\text{-}15)$$

Plugging $w(\xi)$ from (5-15) into differential equation (5-5), making shift on the power and index of the terms and rearranging them with the same power leads to the recurrence relations of the differential equation as

$$c_4 = p_0(4)[Kc_0 + (12\epsilon + 2N)c_2] \quad (5\text{-}16\text{-A})$$

$$c_5 = p_0(5)[Kc_1 + (108\epsilon + 6N)c_3] \quad (5\text{-}16\text{-B})$$

$$c_i = p_0(i)[p_1(i-2)c_{i-2} + p_2(i-4)c_{i-4} + p_3(i-6)c_{i-6}] \quad (5\text{-}16\text{-C})$$

where parameters $p_0(i)$, $p_1(i)$, $p_2(i)$ and $p_3(i)$ are introduced by

$$p_0(i) = \frac{-1}{i^4 - 6i^3 + 11i^2 - 6i} \quad (5\text{-}17\text{-A})$$

$$p_1(i) = 3(i^2 - i)^2\,\epsilon + (i^2 - i)N \quad (5\text{-}17\text{-B})$$

$$p_2(i) = K + 3i(i+2)(i^2 - 1)\,\epsilon^2 \quad (5\text{-}17\text{-C})$$

$$p_3(i) = (i^4 + 6i^3 + 5i^2 - 12i)\,\epsilon^3 \quad (5\text{-}17\text{-D})$$

For a symmetric solution of the wrinkling pattern, it is concluded that all the coefficients c_i with the odd index vanish and only the even index coefficients corresponding with the terms with even power remain. Thus, by using the recurrence relations (5-16-A, B and C), all of the coefficients can be determined versus c_0 and c_2 and the symmetric wrinkling pattern is represented as

$$w(\xi) = \varphi_0(\epsilon, K, N, \xi)c_0 + \varphi_2(\epsilon, K, N, \xi)c_2 \quad (5\text{-}18)$$

Also, the boundary conditions of the system for clamped edges are represented as

$$w(\xi = \pm 0.5) = \frac{dw}{d\xi}(\xi = \pm 0.5) = 0 \quad (5\text{-}19)$$

where the conditions $w(\xi = -0.5) = 0$ and $\frac{dw}{d\xi}(\xi = -0.5) = 0$ are already satisfied for the symmetric pattern by ignoring odd index coefficients in (5-15). By substituting $w(\xi)$ from (5-18) into the boundary conditions (5-19), the characteristic wrinkling equation of the system and wrinkling pattern are derived versus the critical wrinkling load N and structural parameters (i.e. K and ϵ).

5.4.2 Finite Difference Method

The finite difference method is used to solve the differential equation (5-5) numerically. The domain is discretized by introducing some nodes (Figure 5-3). By using the central difference method with 2nd order of accuracy, the approximated derivatives of a function $G(u)$ are defined as [Hildebrand, 1968; Timoshenko, 1940]

$$\frac{d}{du}G(u) = \frac{G_{i+1}-G_{i-1}}{2h} + O(h^2) \quad (5\text{-}20\text{-A})$$

$$\frac{d^2}{du^2}G(u) = \frac{G_{i+1}-2G_i+G_{i-1}}{h^2} + O(h^2) \quad (5\text{-}20\text{-B})$$

$$\frac{d^3}{du^3}G(u) = \frac{G_{i+2}-2G_{i+1}+2G_{i-1}-G_{i-2}}{2h^3} + O(h^2) \quad (5\text{-}20\text{-C})$$

$$\frac{d^4}{du^4}G(u) = \frac{G_{i+2}-4G_{i+1}+6G_i-4G_{i-1}+G_{i-2}}{h^4} + O(h^2) \quad (5\text{-}20\text{-D})$$

where $h = u_{i+1} - u_i$ is the length step between two neighbourhood nodes and $G_i = G(u_i)$ refers to the exact value of function $G(u)$ at node i while i=1,2,…n is the number of the nodes of the system.

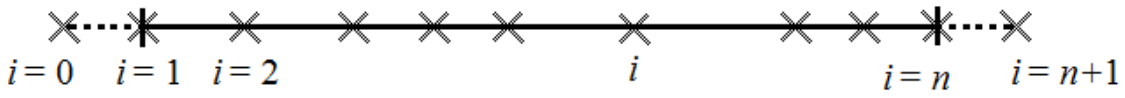

Figure 5-3: Discretized length span of the film in finite difference method

Imposing the difference formulas from (5-20) into the differential equation (5-5) represents the governing equation of the node i (i=2,3,…n–1) as

$$R_{i-2}^{(i)} w_{i-2} + R_{i-1}^{(i)} w_{i-1} + R_i^{(i)} w_i + R_{i+1}^{(i)} w_{i+1} + R_{i+2}^{(i)} w_{i+2} = 0 \quad (5\text{-}21)$$

where coefficients R_α are obtained from the governing equation and finite difference formula.

On the other hand, the boundary conditions of the system provide the information of the deflection of the boundary nodes (i=1,n) and virtual nodes (i=0,n+1). For the clamped–clamped film, according to the symmetrical extension of the domain it is inferred that $w_1 = w_n = 0$, $w_0 = w_2$ and $w_{n+1} = w_{n-1}$.

In this way, a set of algebraic equations is replaced for the governing equation of the system as

$$[A]\{w\} + N[B]\{w\} = 0 \quad (5\text{-}22)$$

in which $\{w\} = \{w_0, w_1, \dots, w_n, w_{n+1}\}^T$ is the vector of the nodal displacement of nodes i=0,1,…n+1 and $[A]$ and $[B]$ are square matrices. This general eigenvalue problem with eigenvector $\{w\}$ and eigenvalue parameter N has a straight forward solution. The eigenvalues of the problem correspond to the wrinkling loads, while the eigenvectors represent the wrinkling pattern of the system.

5.5 Results and Discussions

In this section, for the free standing film, the buckling loads and mode shapes are determined analytically and for the deposited film on the substrate the wrinkling load of the system is determined from finite difference and series solution methods. The parameters (i.e. load and wrinkle pattern) corresponding with the first eigenvalue and eigenfunction of the eigenvalue problem of the differential equation are considered as the critical parameters of the instability. The effects of the change in the thickness of the film and stiffness of the substrate on the wrinkling are also investigated.

5.5.1 Buckling of a Free Standing Film

The buckling loads of the free standing film with variable thickness for symmetric and antisymmetric buckling modes numerically calculated are shown in figure 5-4 for various amplitude parameters ϵ. The critical buckling mode corresponding with the symmetric mode has smaller buckling loads than the antisymmetric mode. Both of the symmetric and antisymmetric buckling loads are ascending versus the amplitude parameter ϵ. When the amplitude parameter ϵ approaches zero, the symmetric and antisymmetric buckling loads approach to the corresponding buckling load of the uniform thickness film in table 5-1 as expected (i.e. $N=4\pi^2$ and $N=8.18\pi^2$ for the symmetric and antisymmetric modes, respectively).

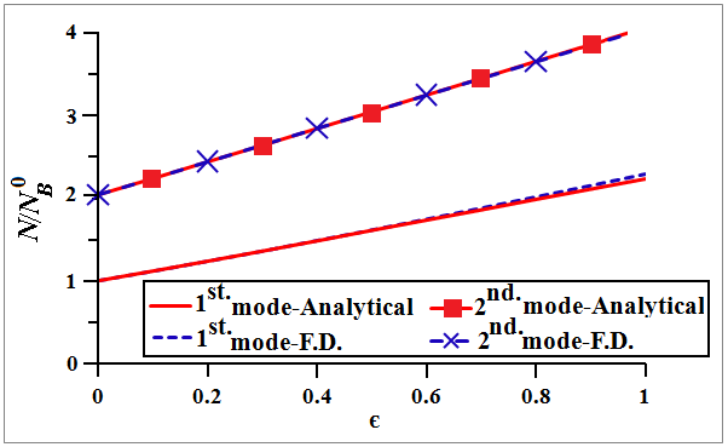

Figure 5-4: Symmetric and antisymmetric buckling load of the clamped–clamped free standing film from analytical and finite difference (F.D.) solution

The critical buckling load of the free standing film with variable thickness in figure 5-4 follows a linear relation with the amplitude parameter ϵ as

$$N = N_B^0(1 + m_0\epsilon) \qquad (5\text{-}23)$$

where $N^0{}_B=4\pi^2$ is the critical buckling load of the clamped–clamped film with uniform thickness (ϵ=0) and m_0 = 1.273 ± 0.008 is a constant parameter determined by a regression analysis [Kahane, 2008]. The results of the regression analysis for 50 datapoints with R^2 =0.999 and standard error less than 1% show a high accuracy for the proposed linear relation in equation (5-23) for 0< ϵ <1.

On the other hand, the symmetric buckling mode shapes are shown in figure 5-5 for different amplitude parameters ϵ. For the film with uniform thickness (ϵ = 0), the results in the figure 5-5 correspond with the symmetric buckling mode in table 5-1. By increasing the amplitude parameter ϵ, the film thickness at the edges increases which leads to increasing the stiffness of the system, so that the mode shapes are compressed with less deflection at the edges.

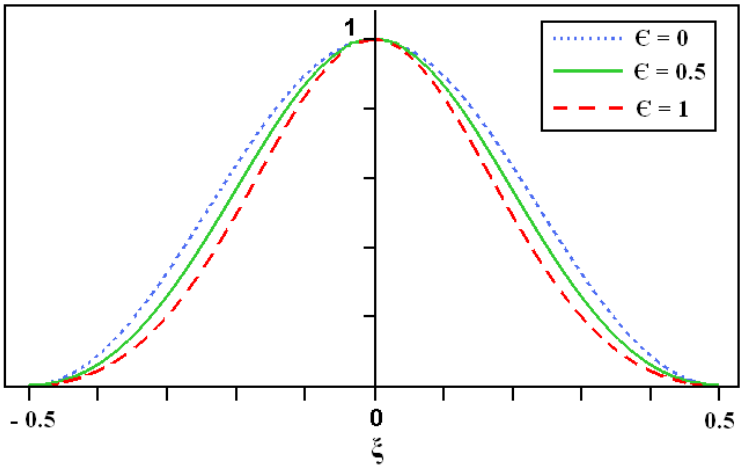

Figure 5-5: Symmetric buckling mode shapes of the free standing film

5.5.2 Wrinkling of a Substrate–bonded Film

For a film with uniform thickness ($\epsilon = 0$) on a substrate, the governing equation of the film–substrate system is simplified to a forth order differential equation with constant coefficients. For a clamped–clamped beam on a soft foundation [Ratzerdorfer, 1936; CRCJ, 1971, pp. A–1–27], the wavelength of the flexures is not tiny and the corresponding critical compressive load is represented as the combination of the Euler buckling load N^0_B and the substrate effect, i.e. $N = N^0_B + 2\sqrt{K}$ where $N^0_B = 4\pi^2$. Obviously, for a stiff substrate with larger foundation stiffness $\bar{K}$ and thin film structure with tiny thickness and big slender ratio (i.e. L/t), the stiffness parameter K defined in (5-6-B) increases so that the effect of the substrate is several orders of magnitude bigger than the Euler buckling load N^0_B. Therefore, the critical compressive load N^0_W and wave number β^0_W of the wrinkling are independent of the boundary conditions of the film, which can be expressed in terms of the non–dimensional substrate stiffness K as

$$N^0_W = 2\sqrt{K} \tag{5-24}$$

$$\beta^0_W = \sqrt[4]{K} \tag{5-25}$$

Similar results are obtained in the work of Cerda and Mahadevan [2003], Birman and Bert [2004] and Pocivavsek [2008]. For this special case, our finite difference analysis and series solution method lead to the same results for the load and the wave number of the wrinkling. However, the effect of the boundary conditions of the film influences the wrinkling pattern in a different manner.

For a film–substrate system with infinite length, the wrinkles propagate uniformly all over the domain and the effects of the boundary conditions completely vanish [Chen and Hutchinson, 2004; Niu and Talreja, 1999] as shown in figure 5-6-A. While for a film–substrate system with finite length, the boundary conditions of the edges of the film affect the wrinkling amplitude. Figure 5-6-B shows the wrinkling pattern on the film with uniform thickness for clamped–clamped boundary conditions, in which the effect of the clamped boundary conditions on the edges of the film is obvious.

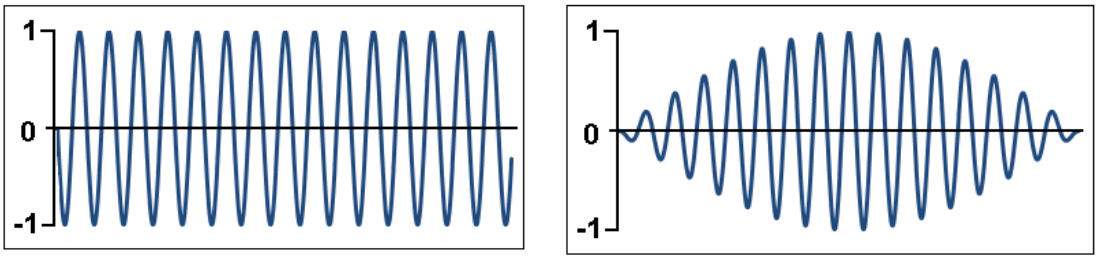

A) Infinite length model B) Finite length model with clamped edges

Figure 5-6: The wrinkling pattern of a film with uniform thickness (ϵ = 0) deposited on the substrate

For the film with variable thickness, the critical load of the wrinkling is calculated for various values of the substrate stiffness K and amplitude parameter ϵ and compared with the wrinkling load of the film with uniform thickness. For different substrate stiffness K_n (K_n=$10^{-9}K$), the wrinkling load N is normalized with the wrinkling load of a uniform film $N^0{}_W$ in equation (5-24) as $F_n = \frac{N}{N_W^0}$ and shown in figure 5-7. According to this figure, the variation of the wrinkling load N is negligible for most values of parameters K_n and ϵ, while some deviations from F_n =1 occur for very soft substrates. For films with uniform thickness, the critical load of the system decreases with the decreasing of the substrate stiffness K, while the corresponding deviation is slightly intensified for non–uniform film. By considering these small deviations, a relation for the normalized wrinkling load is proposed as

$$F_n = 1 + m_1 K_n^{-m_2}\, \epsilon^{m_3} \qquad (5\text{-}26)$$

where the constant parameters m_1, m_2 and m_3 are obtained from a regression analysis [Kahane, 2008]. The results of the regression analysis with 85 datapoints for 0< ϵ <1 and 0.001<K_n<100 are shown in table 5-2 and the constant parameters in (5-26) are determined with a high accuracy as R^2=0.99 and a standard error less than ± 4% for the estimated parameters. Clearly, imposing ϵ=0 in equation (5-26) leads to F_n =1 corresponding with the wrinkling load of a film with uniform thickness. For values of K outside the above range, the substrate stiffness is too large or too small corresponding to the solid or too flabby substrates which are not considered in this work. The finite

difference method and series solution method lead to the same results as shown in figure 5-8.

Table 5-2: The parameters of the relation (5-26) for wrinkling load obtained from regression analysis

Model Summary		$R^2 = 0.99$		
Parameter	Estimate	Std. Error	95% Confidence Interval	
			Lower Bound	Upper Bound
m_1	.024	.001	.022	.025
m_2	.213	.004	.206	.220
m_3	.775	.020	.736	.814

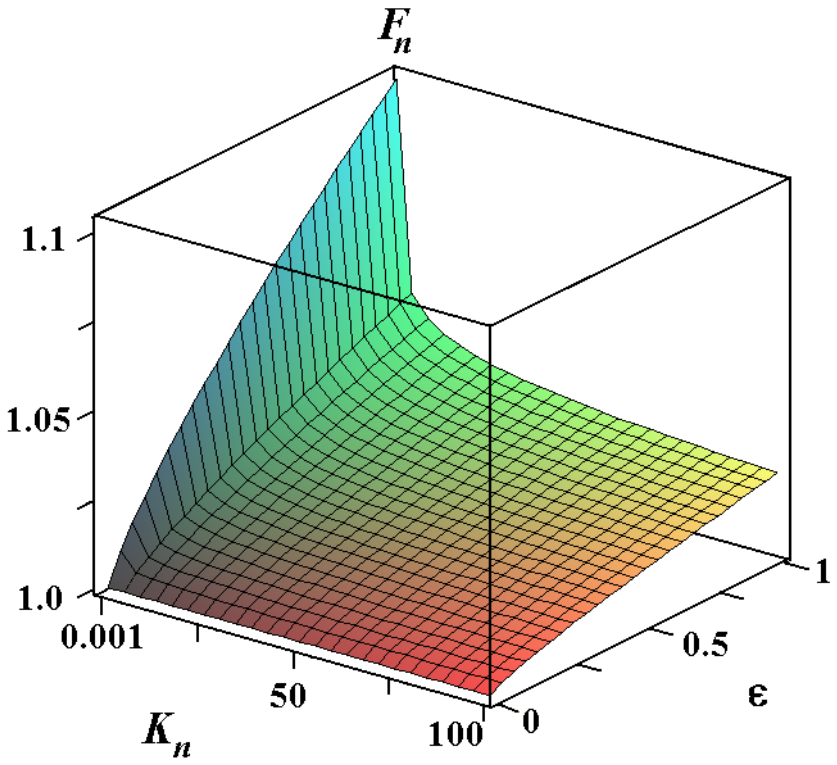

Figure 5-7: Normalized wrinkling load F_n versus amplitude parameter ϵ and logarithmic substrate stiffness K_n

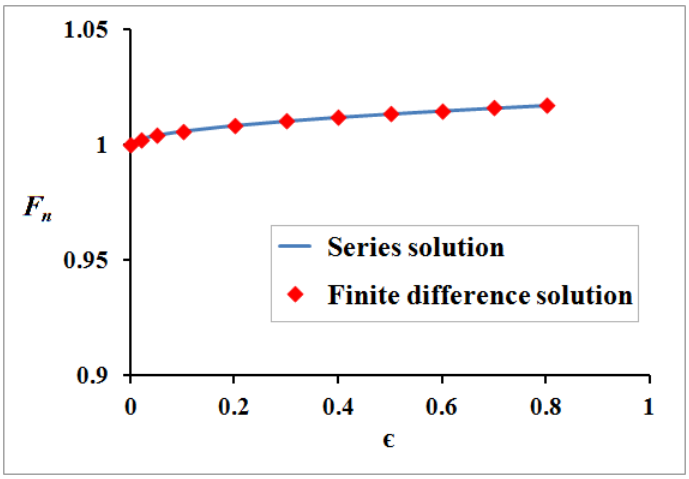

Figure 5-8: Normalized wrinkling load F_n versus amplitude parameter ϵ from finite difference method and series solution

In contrast with the critical load which remains slightly changed under the variation of the thickness and substrate stiffness, the pattern of the wrinkling changes highly as shown in figures 5-9-A-C. For a film with uniform thickness, the wrinkles propagate all over the length span, while for the films with variable thickness the wrinkles accumulate around the weakest location of the system with minimum thickness (at the middle of the length span). The wrinkling pattern is characterized by monitoring two parameters: the wave number of the wrinkling and the footprint of the wrinkling that shows the size of the region on the film influenced by the wrinkles. The accumulative effect of the wrinkling on the non–uniform film is intensified by increasing the thickness amplitude parameter ϵ such that the wrinkles are compressed more and the wrinkle number becomes less (Figures 5-9-A-C).

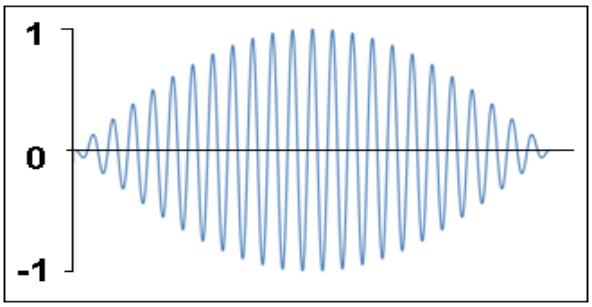

A) Wrinkling on the uniform thickness film ϵ =0

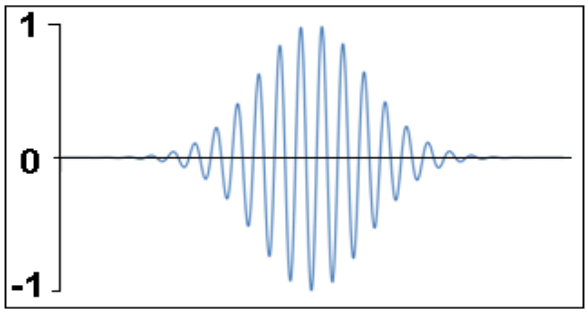

B) Wrinkling on the variable thickness film with ϵ =0.2

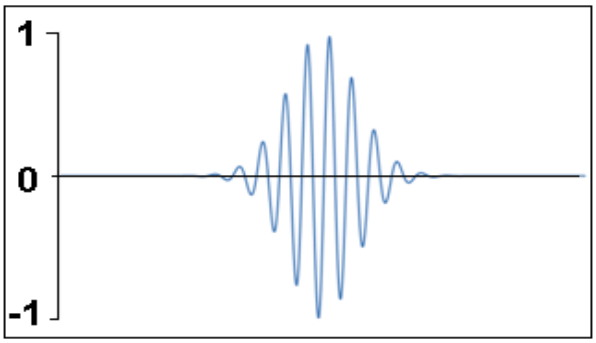

C) Wrinkling on the variable thickness film with ϵ =0.8

Figure 5-9: Wrinkling of the film with variable thickness and the effect of the different amplitude parameters ϵ

The normalized wave number $\beta_n = \frac{\beta}{\beta_W^0}$ of the wrinkling versus the substrate stiffness K and amplitude parameter ϵ is shown in figure 5-10, where $\beta^0{}_W$ is the wrinkling wave number for a uniform thickness film (ϵ =0) in equation (5-25). Obviously, the wave number is highly affected by the change of the parameters K and ϵ especially the later one. Similar to the case of a uniform thickness film based on equation (5-25), the wave

number of the wrinkling of a non–uniform film increases with the increasing of the substrate stiffness. However, the rate of the change of the wave number with parameter K for the uniform thickness film is much faster than that for the film with variable thickness. Therefore, the normalized wave number β_n decreases by increasing K as shown in figure 5-10. On the other hand, by increasing the amplitude parameter ϵ of the variable thickness, the wave number of the wrinkles decreases effectively and they accumulate around the weakest position of the film as discussed in figures 5-9-A-C.

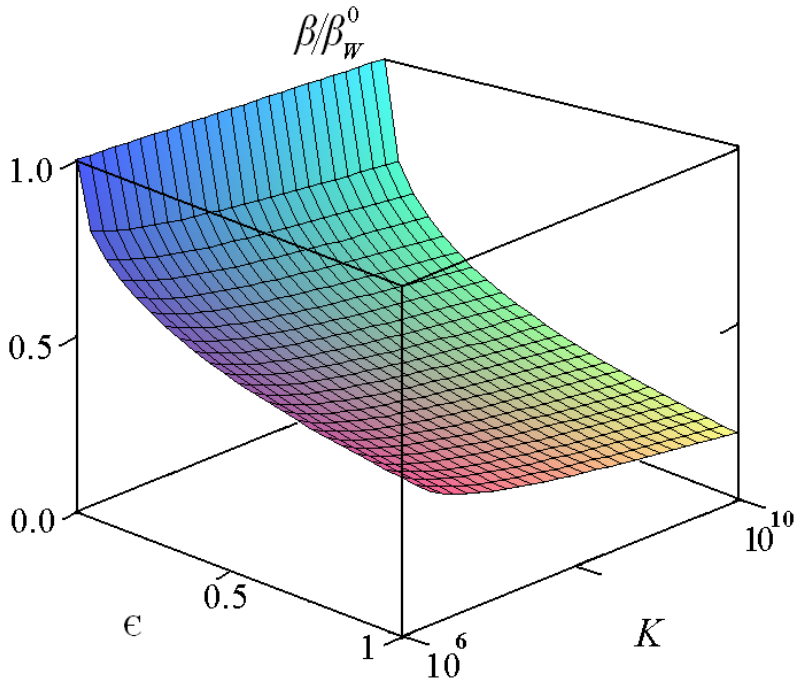

Figure 5-10: Normalized wave number β_n versus substrate stiffness K and amplitude parameter ϵ

The abovementioned observation proposes an explicit relation for the normalized wave number of the wrinkling as

$$\beta_n = \mathrm{EXP}(-m_1\epsilon^{m_2})K_n^{-(m_3\epsilon^{m_4})} \tag{5-27}$$

where m_i (i=1...4) are constant parameters. The best approximation of the normalized wave number in (5-27) is introduced by choosing m_4= 1/3. Hence, the equation (5-27) is rewritten as

$$\beta_n = \mathrm{EXP}(-m_1\epsilon^{m_2})\, K_n^{-(m_3\sqrt[3]{\epsilon})} \tag{5-28}$$

Clearly, imposing $\epsilon=0$ in equation (5-28) simplifies it to the case of a uniform thickness pattern with $\beta = \beta^0_W$. On the other hand, the effect of the amplitude parameter ϵ is more important than the substrate stiffness K on the normalized wave number (Figure 5-10). Thus, the corresponding term with the power of K_n in equation (5-28) could be ignored for a simpler approximation.

By using a regression analysis with 68 datapoints for $0< \epsilon <1$ and $0.01< K_n <10$, the constant parameters m_1, m_2 and m_3 in equation (5-28) are determined. The results of the regression analysis presented in table 5-3 show a high accuracy for the proposed relation of the wave number in equation (5-28) with $R^2=0.98$ and a standard error about ± 3% for the estimated parameters. The predicted values of the equation (5-28) are compared with the observed normalized wave number in figure 5-11 with a reference line. Also, figure 5-12 shows the histogram of the residual errors of the regression analysis. The error in counting the number of the wrinkles along the film span, attributing a natural number to them and predicting the discrete wave number of the wrinkles by a continuous function are considered as sources of error.

Table 5-3: The parameters of the equation (5-28) for wave number obtained from a regression analysis

Model Summary		$R^2 = 0.980$		
Parameter	Estimate	Std. Error	95% Confidence Interval	
			Lower Bound	Upper Bound
m_1	.841	.017	.808	.874
m_2	.470	.015	.440	.500
m_3	.122	.004	.114	.130

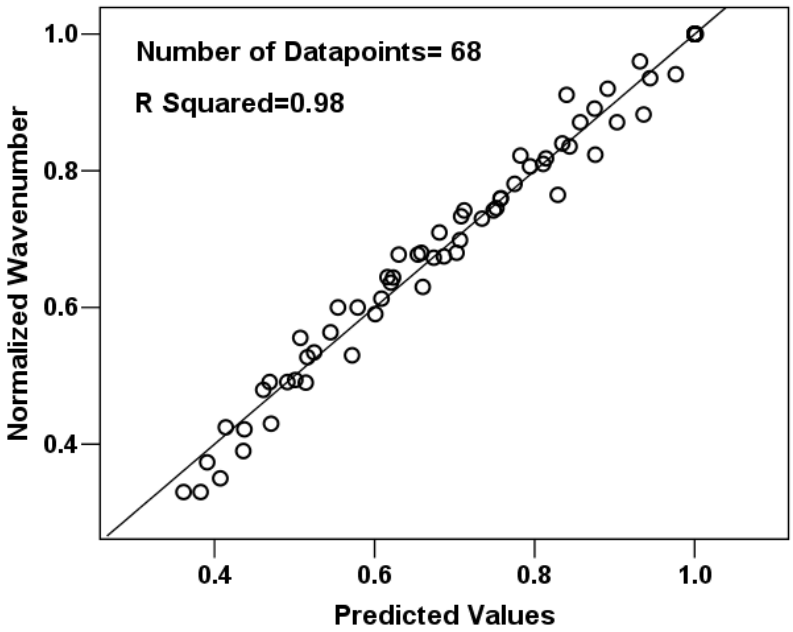

Figure 5-11: Normalized wave number β_n compared with the predicted values obtained from the proposed relation in (5-28)

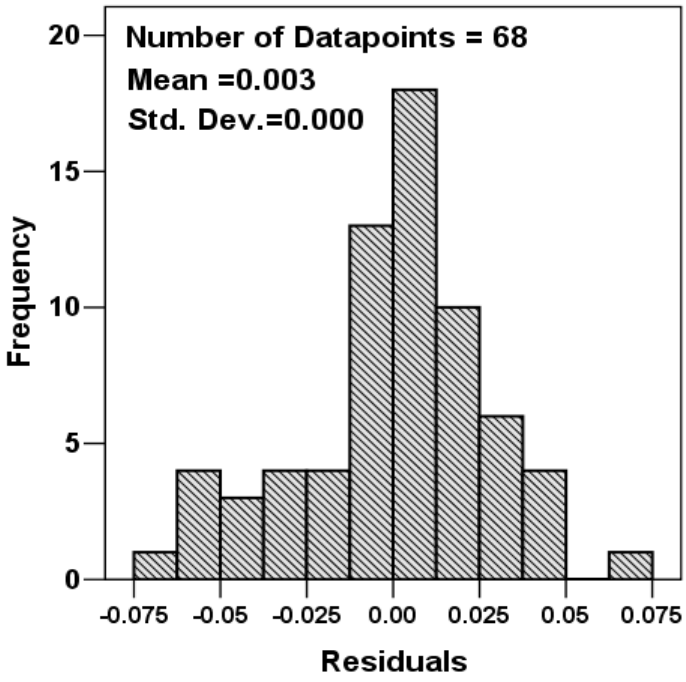

Figure 5-12: Histogram of the residual errors of the equation (5-28) for predicting the wave number

Figures 5-13-A,B show the normalized wave number from the finite difference method compared with the series solution. The finite difference method proposes a stiffer film with less wave number accumulated more densely around the middle of the film. Using the finite difference formulation with higher accuracy decreases the truncation error and hence the results get more compatible with the results of the series solution method.

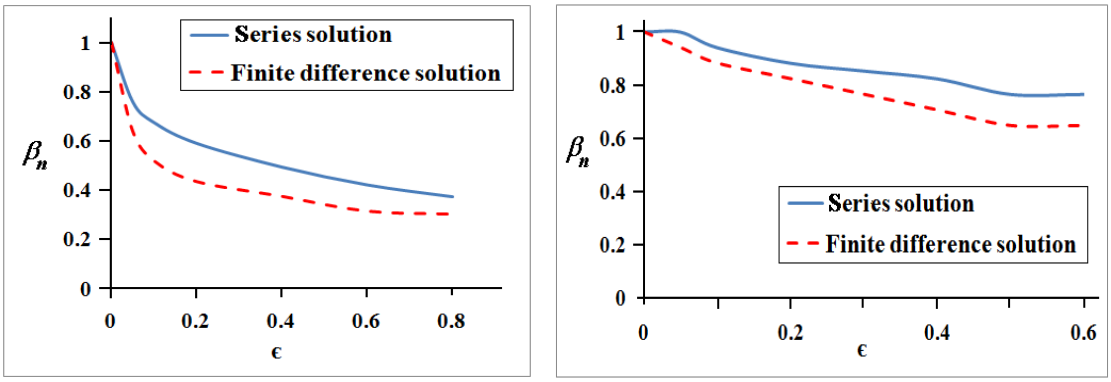

A) Film on a stiff substrate B) Film on a soft substrate

Figure 5-13: Comparison of the finite difference and series solution for the wrinkling wave number

Not only the wave number of the wrinkling of the film, but also the footprint of the wrinkles is influenced by the substrate stiffness K and amplitude parameter ϵ. Increasing the amplitude parameter ϵ accumulate the wrinkles at the location with minimum thickness (here, at the middle of the system) as figures 5-9-A-C show. The footprint of the wrinkles defined as the effective length of the film influenced by the wrinkles changes between zero and one. For wrinkling of the film with uniform thickness (ϵ=0), the footprint equals to one and the whole length span is affected by the wrinkles.

A regression analysis for the relation between the footprint and the normalized wave number of the wrinkling shows that these parameters are strongly proportional to each other linearly as

$$Footprint = m_0 + m_1 \beta_n \qquad (5\text{-}29)$$

Figure 5-14 shows the footprint parameter versus the corresponding normalized wavenumebrs for 60 datapoints. The datapoints are located around the reference line in equation (5-29) which shows that the footprint and wave number parameters identically

follow the same behavior. The regression analysis between the footprint and the normalized wave number yield the values of the parameters m_0 and m_1 which are presented in table 5-4.

The finite difference method proposes a stiffer system with more compressed wrinkles. Based on the finite difference results, the footprint parameter is obtained to follow exactly the wave number pattern with the relation of $Footprint = \beta_n$ with R^2=0.99 for the available database with 60 datapoints. According to the abovementioned results, by increasing the wave number of the wrinkling along the film span, the effective length of the film subjected to the wrinkling increases.

Table 5-4: The regression analysis results for linear relation of the footprint versus wave number

Model Summary		$R^2 = 0.958$		
Parameter	Estimate	Std. Error	95% Confidence Interval	
			Lower Bound	Upper Bound
m_0	.268	.015	.238	.298
m_1	.736	.020	.696	.777

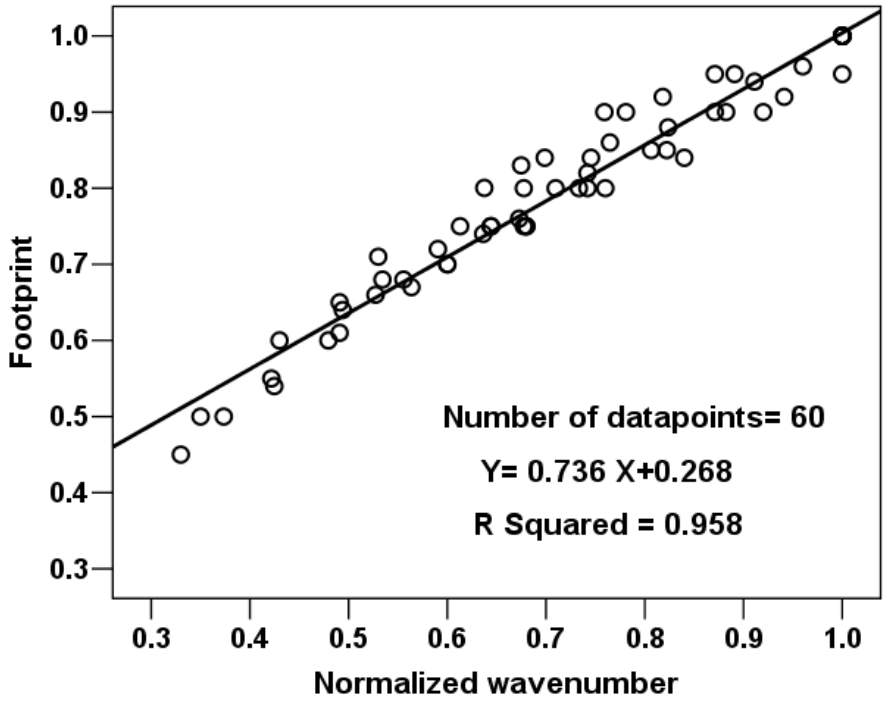

Figure 5-14: The linear relation between footprint and normalized wave number β_n

High sensitivity of the footprint parameter with respect to the amplitude parameter ϵ as shown in figure 5-15 indicates that even under small disturbances in the uniformity of the film thickness, wrinkles accumulate densely at the weakest location of the film (i.e., the middle of the length span which is the thinnest location). Also, the tiny thickness of the thin film increases the importance of the thickness variation of the film and intensifies the abovementioned accumulative effect. Therefore, it is concluded that for the deposited film on the substrate, the small variation of the thickness of the film which unavoidably exist on the film due to limitations of the manufacturing process may lead to the accumulation of the wrinkles around a region. Hence, the wrinkles behave completely different from the uniform wrinkling of a film with uniform thickness.

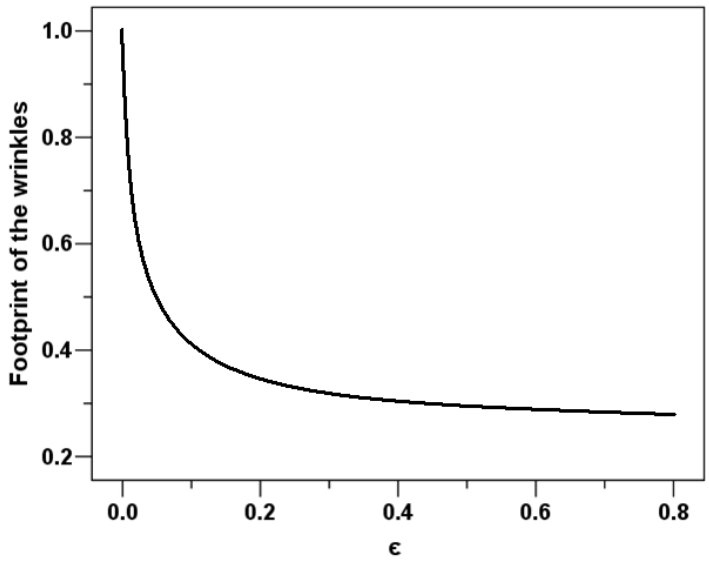

Figure 5-15: Footprint of the wrinkles versus thickness variation parameter

5.6 Summary

The buckling of a free standing film and the uniaxial wrinkling of a substrate–bonded film were investigated. The thickness of the homogenous isotropic film was assumed with a quadratic pattern with a minimum located at the middle of the length span. The buckling problem was solved analytically and it was shown that the variation of the thickness linearly changes the buckling load. For the wrinkling of a film with variable thickness, the results of both the finite difference method and the series solution show that in contrast with a film with uniform thickness in which the wrinkles propagate along the entire length span, the wrinkles accumulate around the weakest location with minimum thickness. Stiffer substrate and higher thickness variation shrink wrinkles even more around the thinnest location on the film. The high sensitivity of the wrinkling accumulation around the thin locations of the system especially for thin film structures in which controlling the uniformity of the thickness is very difficult opens new avenues in the application of thin solid films. The results of this analysis bring more insights into the physics of wrinkling in science and provide effective tools for the development of the wrinkling applications in different fields such as MEMS technology and sensor/actuator systems.

5.7 References

[1] M. Abramowitz, I.A. Stegun, *Handbook of Mathematical Functions*, 1972, Dover Publications, New York.

[2] F. Bloom, D. Coffin, *Handbook of Thin Plate Buckling and Postbuckling*, 2001, Chapman & Hall CRC.

[3] E. Cerda, L. Mahadevan, "Geometry and physics of wrinkling", *Physical Review Letters*, Vol. 90 (7), 2003, pp. 074302/1–4.

[4] X. Chen, J. W. Hutchinson, "A family of herringbone patterns in thin films", *Scripta Materialia*, Vol. 50, 2004, pp. 797–801.

[5] CRCJ Column Research Committee of Japan, *Handbook of Structural Stability*, 1971,Corona, Tokyo, Japan.

[6] F.B. Hildebrand, *Finite Difference Equations and Simulations*, 1968, Prentice Hall Inc.

[7] R. Huang, S. H. Im, "Dynamics of wrinkle growth and coarsening in stressed thin films", *Physical Review E*, Vol. 74 (2), 2006, Article No. 026214.

[8] L.H. Kahane, *Regression Basics*, 2nd. Ed., 2008, Sage Publications Inc.

[9] K. Niu, R. Talreja, "Modeling of wrinkling in sandwich panels under compression", *Journal of Engineering Mechanics,* Vol. 125(8), 1999, pp. 875–883.

[10] L. Pocivavsek, R. Dellsy, A. Kern, S. Johnson, B. Lin, K. C. Lee, E. Cerda, "Stress and fold localization in thin elastic membranes", *Science*, Vol. 320 , 2008, pp. 912–916.

[11] J. Ratzerdorfer, *Die Knickfestigkeit von staben und stabwerken*, 1936, Springer, Wien.

[12] S.P. Timoshenko, *Theory of Plates and Shells*, 1940, McGraw–Hill Book Company, Inc.

[13] A.C. Ugural, *Stresses in Plates and Shells*, 1999, McGraw–Hill Book Company, Inc.

[14] S. Wang, J. Song, D. Kim, Y. Huang, J. A. Rogers, "Local versus global buckling of thin films on elastomeric substrates", *Applied Physics Letters*, Vol. 93, 2008, Article No. 023126.

Chapter 6

6 Buckling and Wrinkling of Thin Film with Wavy Thickness Pattern

The effect of the fluctuation of the thickness on the instability parameters of a thin film with variable thickness is considered by using a finite difference method. The thickness profile is modeled with a wavy function and the buckling and wrinkling behavior of the system are investigated. According to the results of the instability analysis, the fluctuations of the thickness strongly influence on the buckling and wrinkling parameters.

6.1 Introduction

The instability problem of a thin solid film structure under compressive loading is considered and the buckling/wrinkling loads, buckling mode shape and wrinkling pattern are determined. The profile of the thickness is modeled as a wavy pattern with multiple crests and troughs completely different from the quadratic pattern discussed in chapter 5. Therefore, the effect of the fluctuation of the thickness on the instability parameters is studied. The instability of the film is considered for the uniaxial pattern in which the buckling modes/wrinkling pattern develop on the film in one direction.

In order to analyze the instability problem, the eigenvalue problem of the differential equation of the system is solved by using the finite difference method similar to the previous chapters. The buckling load and buckling mode shapes are determined for a free standing film. For a film–substrate system with uniform thickness, a highly ordered pattern develops uniformly on the system, however for the case of a film with variable thickness such as the one in chapter 5, the thickness profile affects on the wrinkling pattern along the span. This chapter deals with the cases in which the thickness of the film fluctuates along the length span, and considers the effect of the fluctuation profiles on the instability behavior.

Obviously, the importance of this chapter is not limited to a purposely–made wavy thickness film. In fact, there are many unavoidable factors during the manufacturing processes and applications of films that influence the uniformity of the thickness which are known as flaws or defects of the system. These defects are intensified especially in

thin film technology when the thickness of the film is tiny. The results of this chapter show the importance of considering the non–uniformity of film thickness on the instability (i.e. buckling/wrinkling) of the thin film system.

6.2 Formulation

For a film with variable thickness, it was shown in chapter 5 that under uniaxial buckling/wrinkling the governing equation of the system follows a differential equation as

$$[D(\xi)]\frac{d^4w}{d\xi^4} + \left[2\,\frac{d}{d\xi}D(\xi)\right]\frac{d^3w}{d\xi^3} + \left[\frac{d^2}{d\xi^2}D(\xi) + N\right]\frac{d^2w}{d\xi^2} + Kw = 0 \qquad (6\text{-}1)$$

in which w is the normalized deflection, K is the non–dimensional Winkler modulus of the substrate stiffness and N is the non–dimensional compressive in–plane load on the film which is constant, and $0<\xi<1$ is the longitudinal coordinate of the film. Parameter D refers to the bending stiffness of the film represented by

$$D(\xi) = \left(1 + \epsilon\, f(\xi)\right)^3 \qquad (6\text{-}2)$$

while the thickness changes along the length span is assumed to follow with a profile as

$$t = t_0\left(1 + \epsilon\, f(\xi)\right) \qquad (6\text{-}3)$$

where t_0 is the average thickness of the film, ϵ is introduced as the amplitude parameter representing the variation of the thickness amplitude and $f(\xi)$ is the shape function of the variations of the thickness along the length span such that Max $[f(\xi)] = 1$.

Figure 6-1 shows different wavy patterns for the thickness of the film by using a sine function as $f(\xi) = \sin(P\pi\xi)$ for P= 2, 3, 6 and 10. For different fluctuation parameters P in the figure, different numbers of the fluctuation appear on the film, while the amplitude of all these configurations is assumed same as each other.

By considering the eigenvalue problem of the differential equation of the system using the finite difference method described in chapter 5, the buckling/wrinkling load and pattern are obtained and the effects of the film thickness variation parameters and substrate stiffness on the instability parameters are studied.

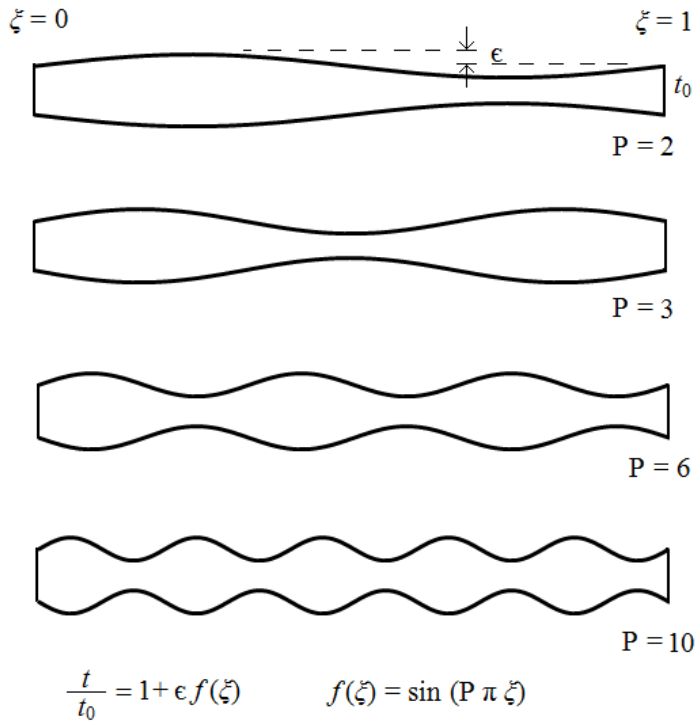

Figure 6-1: The profile of the variable thickness film along the length span

6.3 Results and Discussions

The buckling of a free standing film and the wrinkling of a substrate–bonded film are considered for the film with wavy thickness. The effect of the thickness fluctuation (i.e. the amplitude parameter ϵ and the fluctuation number P) on the instability load and mode shapes is studied.

6.3.1 Buckling of a Free Standing Film

With the increase of the amplitude parameter ϵ, the localized compliance at some locations along the film length span increases as expected from equation (6-2), numerical results of the buckling analysis show that for a free standing film with variable thickness, the buckling load decreases. In addition, the variation of the thickness affects on the mode shapes of the system such that the buckling profiles tend to accumulate to weaker areas where the system has less thickness and less bending rigidity. It is also found that a buckling mode is replaced with another one on the film due to the wavy thickness. The

change of the buckling modes results in the large variation of buckling load of the system. Following cases exemplify two samples to describe this behavior.

For a free standing film with fluctuation number P=2 in figure 6-1, the numerical results show that the buckling load of the film with clamped–clamped edges follows a quadratic relation to mode number n like the Euler buckling formula $N= N^0_B\, n^2\, E_{P=2}(\epsilon)$ where $N^0_B=4\pi^2$ is the critical buckling load of a uniform thickness film ($\epsilon=0$) and $E_{P=2}(\epsilon)$ is a descending function of the amplitude parameter ϵ. The normalized critical buckling load N/N^0_B versus the amplitude parameter ϵ is shown in the figure 6-2, which indicates that this buckling load decreases smoothly by increasing the amplitude parameter ϵ. In fact, decreasing the bending rigidity of the system for bigger amplitude parameter ϵ leads to the decreasing of the critical buckling load as expected. According to figure 6-3, the first mode shape has one peak similar to the half–sine pattern; however the position of the maximum deflection approaches to the location with the minimum thickness with the increasing of the amplitude parameter ϵ.

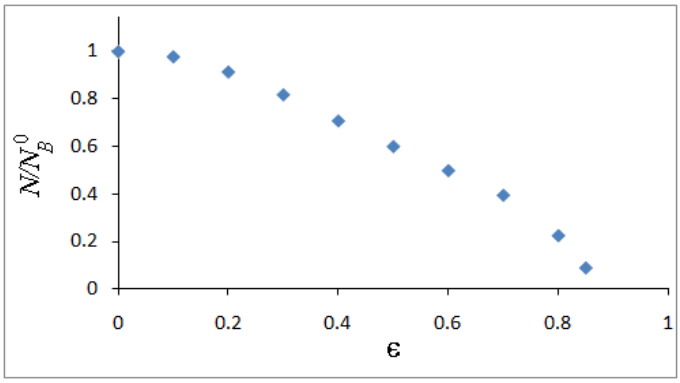

Figure 6-2: The buckling load of the film with P=2 versus amplitude parameter ϵ

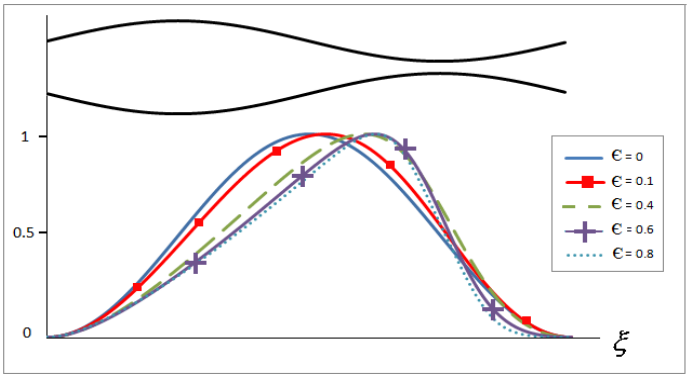

Figure 6-3: First mode shape of the film with P=2 for different amplitude parameters ϵ

Similarly, for the system with two crests and one trough corresponding with P=3 in figure 6-1, the buckling load of a clamped–clamped strip (or beam) follows the similar relation of the Euler buckling formula as $N= N^0_B\, n^2\, E_{P=3}(\epsilon)$ where $E_{P=3}(\epsilon)$ is a function of the parameter ϵ. The function $E_{P=3}(\epsilon)$ versus amplitude parameter ϵ is shown in figure 6-4 which has a fall off behavior. For example, when ϵ<0.3 the function $E_{P=3}(\epsilon)$ is almost constant, then increases with ϵ to reach a maximum value, while decreases with the increasing of ϵ when ϵ >0.5. These different regimes in this figure are in agreement with the mode shapes of the system in figures 6-5-A,B. For ϵ <0.5 the first mode shape of the system is a half–sine with single crest, while for ϵ >0.5 it is a full–sine with a crest and a trough (Figure 6-5-A). The second mode shape has an opposite behavior such that it has a full–sine pattern for ϵ <0.5, while a half–sine pattern for ϵ >0.5 (Figure 6-5-B).

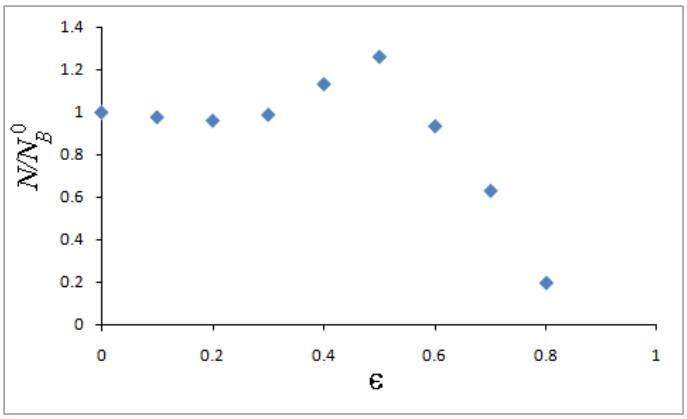

Figure 6-4: The normalized critical buckling load N/N^0_B versus amplitude parameter ϵ for P=3

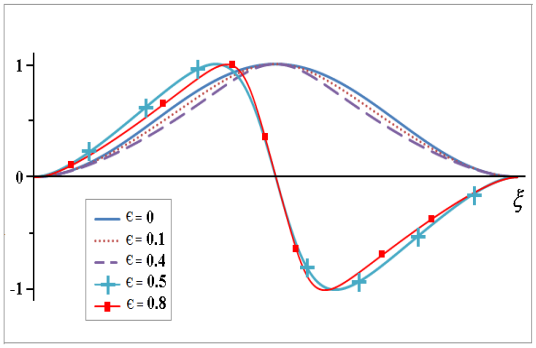

A) The first mode shape

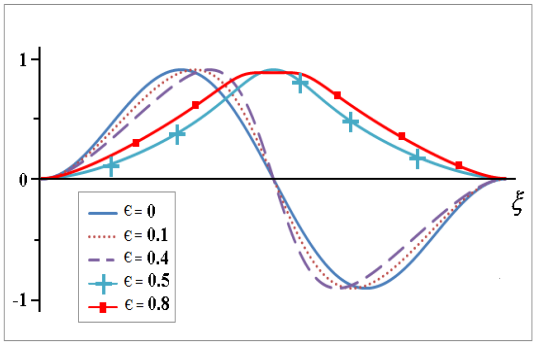

B) The second mode shape

Figure 6-5: The buckling mode shapes of the variable thickness film with P=3

When the fluctuation number P of the wavy thickness changes (under constant parameter ϵ), the critical buckling load undergoes some variations. Figure 6-6 shows the normalized critical buckling load N/N^0_B for different odd and even fluctuation numbers P with ϵ=0.3. In general, the critical buckling load of the system increases with the increasing of the fluctuation number P. It is found that for both odd and even fluctuation numbers P, the critical buckling loads follow a quadratic relation. When the fluctuation number P is sufficient large, the curves according to odd and even fluctuation numbers coincide with each other (as expected).

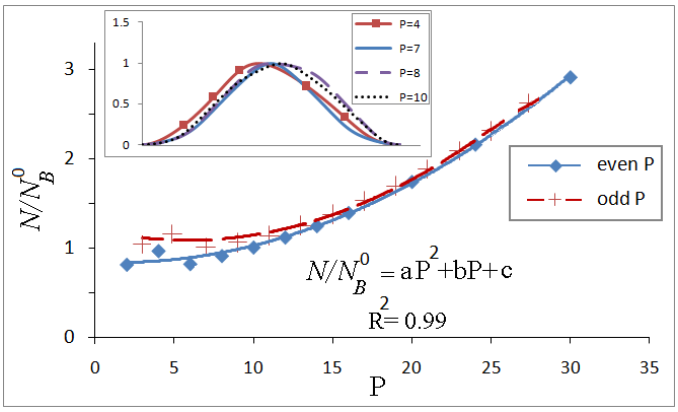

Figure 6-6: The normalized critical buckling load N/N^0_B versus fluctuation number P for ϵ =0.3

6.3.2 Wrinkling of a Substrate–bonded Film

For a thin film with uniform thickness on a compliant substrate, wrinkles propagated along the length span under a wrinkling load N^0_W with a wave number β^0_W as explained in pervious chapters, given by

$$N^0_W = 2\sqrt{K} \tag{6-4}$$

$$\beta^0_W = \sqrt[4]{K} \tag{6-5}$$

For a non–uniform film with the fluctuation number P=3 deposited on a substrate, the effect of the amplitude parameter ϵ on the wrinkling pattern is shown in figure 6-7. Obviously the wrinkles accumulate where the film has less bending rigidity, i.e., the positions with smallest thickness (for fluctuation number P=3 wrinkles accumulate at the

middle length span of the film). This accumulative effect is intensified by increasing the amplitude parameter ϵ.

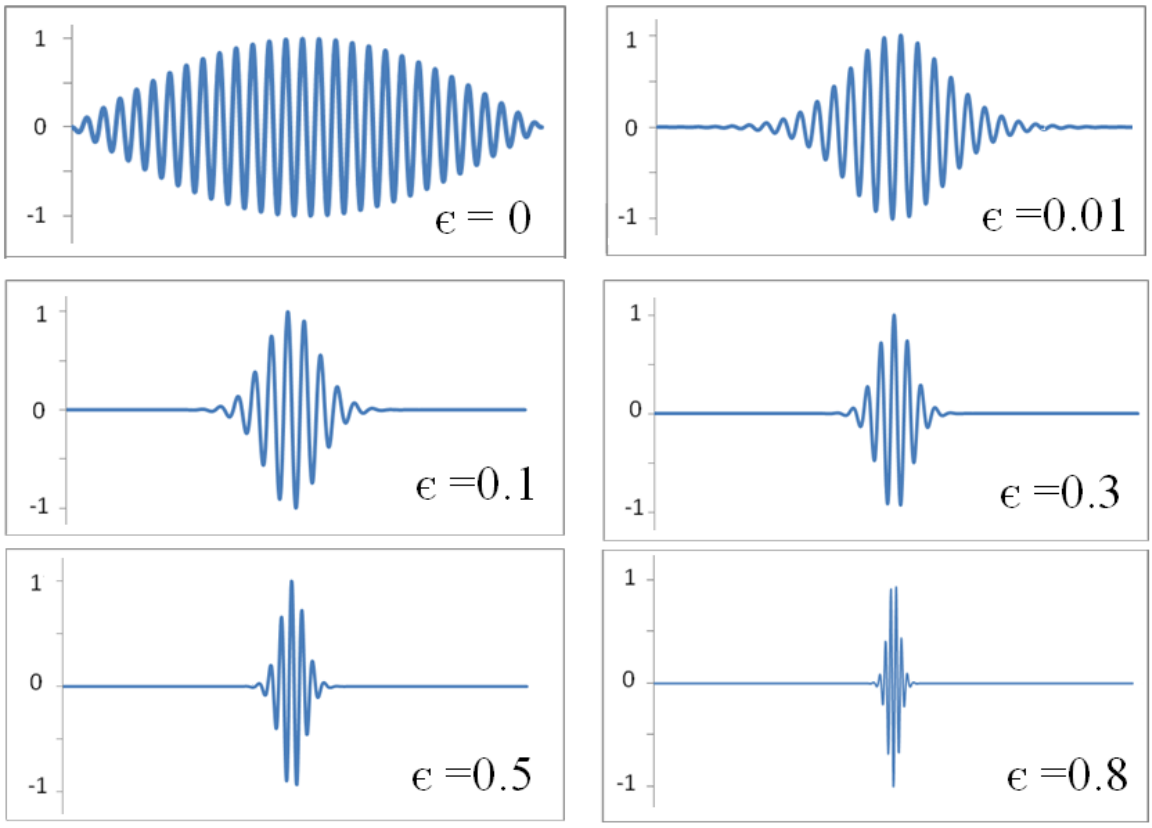

Figure 6-7: Wrinkling pattern for a variable thickness film with the fluctuation number P=3

Figure 6-8 shows the wrinkling patterns of the film deposited on the substrate for different fluctuation numbers P. Unlike the strip (or beam) with uniform thickness in which wrinkles propagate all over the length span, the fluctuation of the thickness leads to the localization of wrinkles at the positions with less thickness where the bending rigidity of the film is smaller than other positions. Hence these special locations along the length span are vulnerable to the wrinkling. For odd fluctuation numbers P wrinkles accumulate symmetrically over the length span at the thinner positions, while for even values of P (P>2) they propagate on the narrowest positions along the film span except the nearest trough to the edges. When P=2, wrinkles accumulate around the single trough of the film.

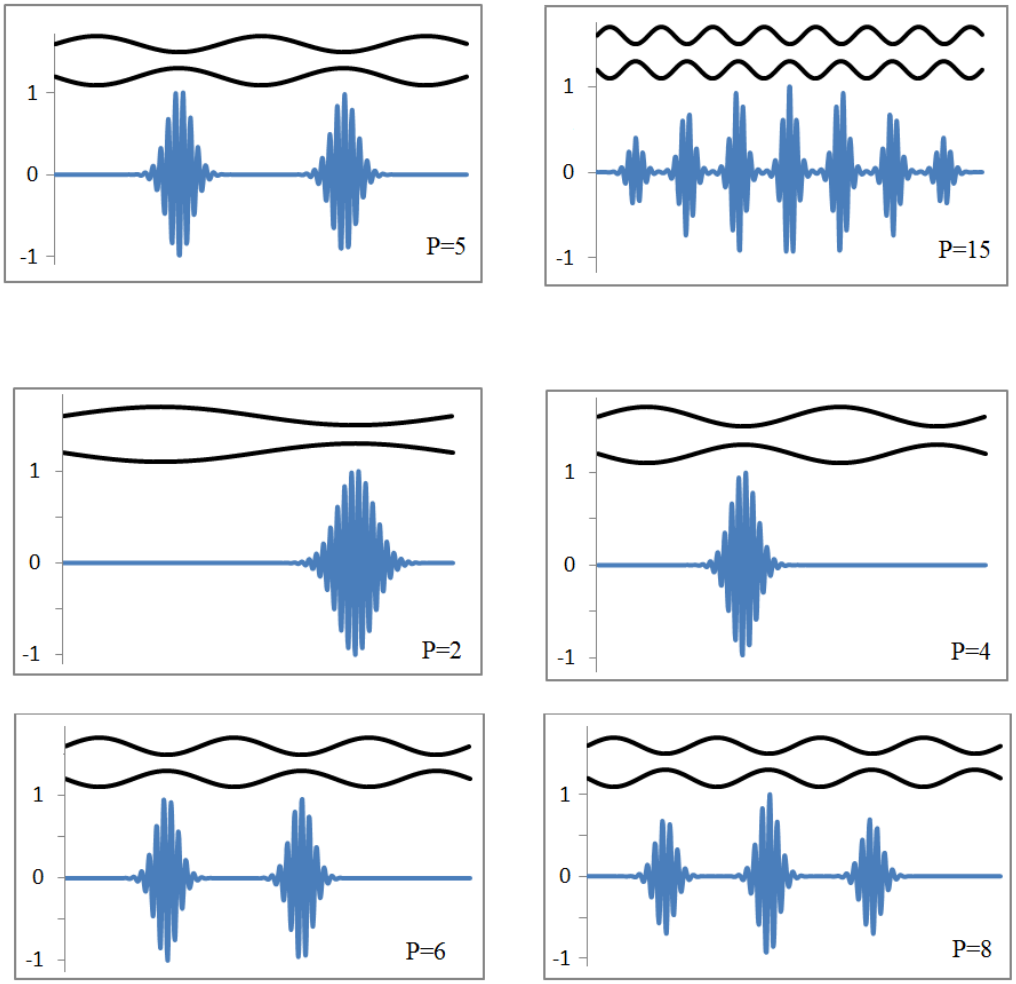

Figure 6-8: Wrinkling pattern for odd and even fluctuation number P for $\epsilon = 0.1$

In comparison with a film of uniform thickness, the wrinkling load and wave number of a film with variable thickness are also affected by the amplitude parameter ϵ and fluctuation number P in addition to the substrate stiffness as shown in equations (6-4) and (6-5). Numerical results in figure 6-9 suggest that the wave number of the wrinkling is a descending function of the amplitude parameter ϵ which follows an exponential relation. High sensitivity of the wave number with respect to the amplitude parameter ϵ leads that even for small variation of the thickness, the wave number changes significantly.

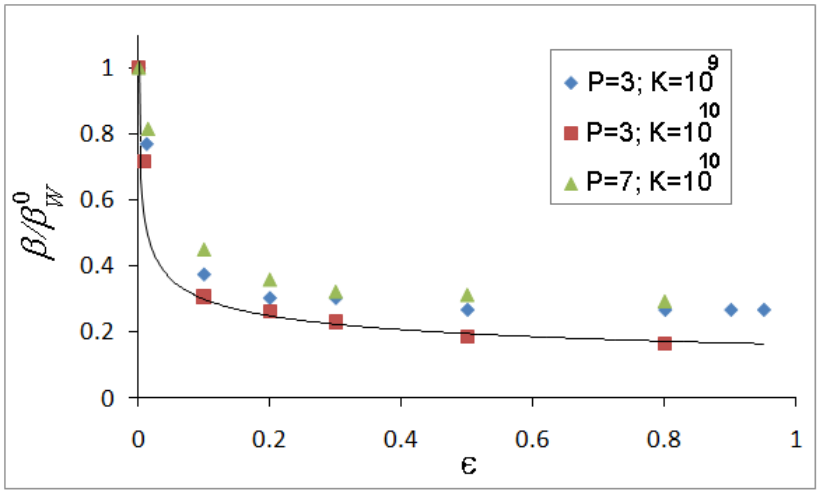

Figure 6-9: The normalized wave number $\beta/\beta^0{}_W$ versus amplitude parameter ϵ

Similarly, it is shown that the normalized wave number $\beta/\beta^0{}_W$ follows a power function of the substrate stiffness *K*. For the case of P=3 with one trough at the middle of the length span, the wave number of the wrinkling is approximated by

$$\frac{\beta_{(P=3)}}{\beta^0_W} = \mathrm{EXP}(-m_1\,\epsilon^{m_2})\,K^{-m_3\,\epsilon^{m_4}} \qquad (6\text{-}6)$$

where $\beta^0{}_W$ is the wave number of the uniform thickness film in the equation (6-5). By performing a regression analysis using the data of the numerical analysis, the constant parameters m_i (i=1..4) are obtained as presented in table 6-1 with a high accuracy as R^2= 0.95 for 70 data–points. Obviously, imposing ϵ=0 in equation (6-6) leads to $\beta = \beta^0{}_W$ as expected for a uniform film. Figure 6-10 shows the diagram of the predicted values of the equation (6-6) in comparison with the numerical data of the normalized wave number $\beta/\beta^0{}_W$ for 70 records. The predicted values clearly follow the observed values from numerical calculation.

For the case of P>3, the wave number of the wrinkling is easily obtained from the wave number of the P=3 in equatin (6-6) combined with the effect of P, therefore, for odd and even flactuation numbers P the wave number are simply multiplied by factors (P–1)/2 and P/2–1, respectively as shown in figure 6-8.

Table 6-1: The results of the regression analysis for normalized wave number in equation (6-6)

Model Summary		$R^2 = 0.95$		
Parameter	Estimate	Std. Error	95% Confidence Interval	
			Lower Bound	Upper Bound
m_1	1.885	.086	1.712	2.057
m_2	.352	.018	.316	.388
m_3	.183	.029	.124	.242
m_4	.167	.037	.093	.242

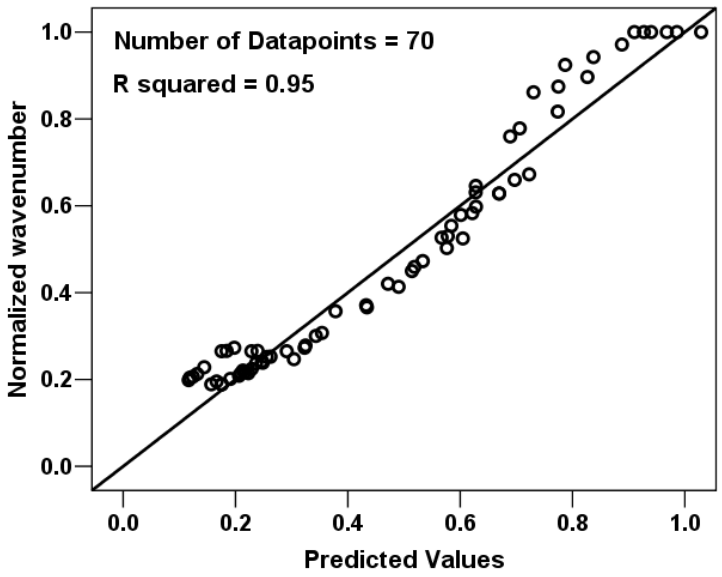

Figure 6-10: The plot of the normalized wave number versus predicted values of equation (6-6)

On the other hand, the effect of the substrate stiffness K, the amplitude parameter ϵ and the fluctuation number P on the wrinkling load of the system is considered as shown in figures 6-11, 12 and 13. Similar to the uniform film with wrinkling load N^0_W in equation (6-4), it is found in figure 6-11 that for stiffer substrate with bigger stiffness K,

the wrinkling load increases. On the other hand, by increasing the amplitude parameter ϵ the critical wrinkling load decreases, which is also shown by the normalized wrinkling load N/N^0_W in figure 6-12. From these figures, it is found that the normalized wrinkling load linearly decreases with the amplitude parameter ϵ, while it is independent of the substrate stiffness K as

$$\frac{N}{N^0_W} = 1 - C(\mathrm{P})\epsilon \qquad (6\text{-}7\text{-A})$$

where C(P) is a function of the fluctuatuin number P. Note that the sensitivity of the wrinkling load for big fluctuation numbers P is diminished exponentially as shown in figure 6-13, an exponential function is proposed for C(P) as

$$C(P) = m_1[1 + \mathrm{EXP}(m_2 - m_3 P)] \qquad (6\text{-}7\text{-B})$$

where m_1, m_2 and m_3 are constant parameters. The results of the regression analysis for 100 datapoints in the range of 2<P<150 and 0.1<ϵ<0.8 propose m_1=0.215 and m_2=1.55 and m_3=0.008 with a high accuracy as R^2=0.98 as shown in figure 6-14.

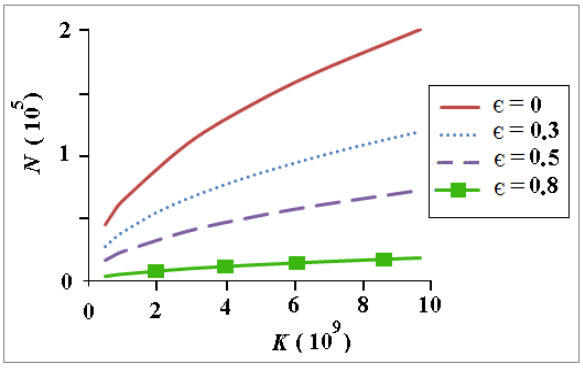

Figure 6-11: The wrinkling load N versus substrate stiffness K for P=3

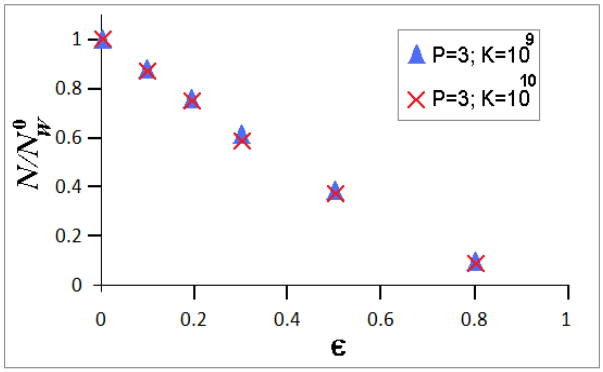

Figure 6-12: The normalized wrinkling load N/N^0_W versus the amplitude parameter ϵ for P=3

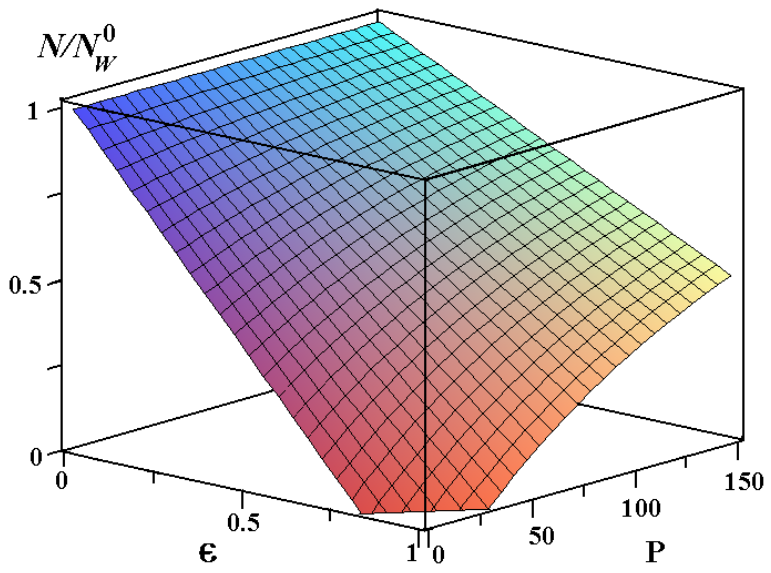

Figure 6-13: The normalized wrinkling load N/N^0_W versus various fluctuation number P and amplitude parameter ϵ

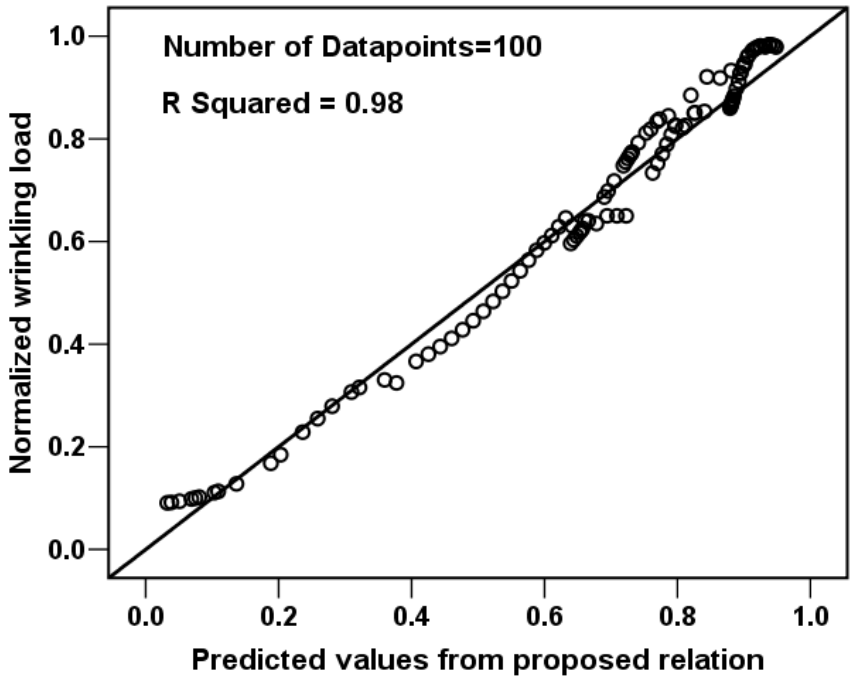

Figure 6-14: The plot of the normalized wrinkling load N/N^0_W versus predicted values of equation (6-7-A,B)

6.3.3 Convergence Criterion

In order to obtain an acceptable solution for the numerical analysis, a convergence criterion is monitored. Here, the number of the nodes of the finite difference method is controlled such that the outputs of the system (i.e. the load and mode shape) reach to a stable condition with small variation. With the sufficient number of the nodes attributed to the system, both of the load and mode shapes converge to the stable conditions, however increasing the nodes of the system increases the stiffness of the mathematical model as the result of the numerical errors.

For the buckling of a free standing film, the critical buckling load converges to the objective value by increasing the number of the nodes in system. The normalized buckling load (with respect to the objective value of the load) is plotted versus the number of the nodes per trough in figure 6-15 for various cases. Clearly, there is a lower limit for the number of the nodes for which the convergent solution is achieved. Therefore, for the buckling of the free standing film, the convergence criterion can be satisfied by controlling the number of the nodes of the system.

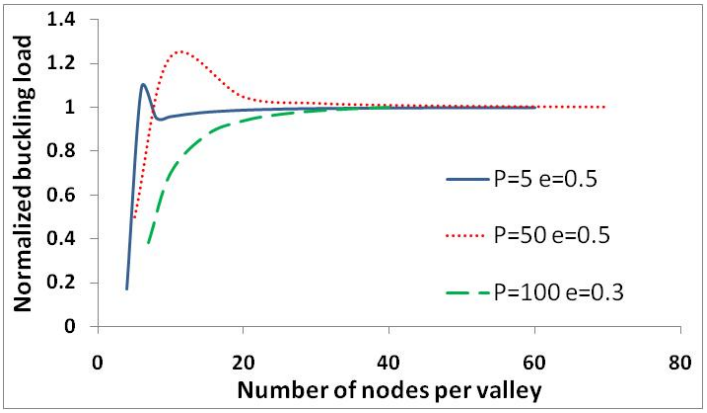

Figure 6-15: Convergence of the finite difference method for buckling analysis

In the wrinkling problem, the number of the nodes per trough should be much bigger than the number of the wrinkling fluctuations. Because the number of the wrinkles for each trough is proportional with $K^{1/4}$, then a lower limit for the number of the nodes is introduced. The lower bound decreases highly by increasing the amplitude parameter ϵ due to the accumulative effect. By controlling the number of the nodes, the convergence critetion is satisfied and the accuracy of the numerical solution is garaunteed.

6.4 Summary

The instability of a free standing film/deposited film on the substrate is investigated for uniaxial pattern while the thickness of the film fluctuates by a sine pattern. The eigenvalue problem for the differential equation of the system is solved by using a finite difference method. The results of the buckling analysis show that the critical load decreases by increasing the amplitude of the thickness variation. For film–substrate system, the fluctuation of the thickness accumulates the wrinkles at the positions with minimum thickness along the span. By growing the amplitude of the thickness variation, the wave number of the wrinkling decreases exponentially and the wrinkling load decreases linearly. For large fluctuation of the thickness, the sensitivity of the wrinkling with respect to the number of the fluctuations diminishes. The results of this chapter which consider the instability of the film with a wavy thickness generalize the results of the chapter 5 in which the thickness of the film undergoes only a local minimum. The results provide better understanding on the instability of the thin solid films when the thickness of the film cannot be assumed as a uniform pattern and promise more improvements in controlling and using of thin film technology effectively in applications.

Chapter 7

7 Post–Instability of a Thin Solid Film

The behavior of a beam/strip under a uniaxial deformation after the instability onset is considered by solving the nonlinear equation of large deflection theory. For a free standing film the buckling and postbuckling are considered, while for a deposited film on a substrate the wrinkling and post–wrinkling behavior are investigated by using numerical solution of finite difference method. Different issues such as wrinkling–folding transition and non–uniformity of the film are studied.

7.1 Introduction

The governing equation of the system around a bifurcation point corresponds with an eigenvalue problem of the differential equation which leads to the loads and modes at the instability onset [Bloom and Coffin, 2001]. For post–instability of the system, the large deformation theory is used to consider the nonlinear behavior of the structure. Two types of nonlinearities commonly encountered in the literature are geometric and material nonlinearity [Sathyamoorthy, 1998]. Geometric nonlinearity comes from the nonlinear strain–displacement relations due to large deformation of the structure. When the deflection/amplitude of the film is not small enough, then the geometric nonlinearity of the stretching causes the stretching of the median plane so that nonlinear terms appear in the differential equation of the system. On the other hand, material nonlinearity comes from nonlinear stress–strain relation such as plastic or viscoelastic behavior of the material of the film.

Linear instability problem of the film is considered by using the small deformation theory. Many researchers studied the wrinkling of a homogenous film with uniform thickness and infinite length using the linear instability analysis with a uniform amplitude sinusoidal pattern [Cerda and Mahadevan, 2003; Chen and Hutchinson, 2004]. Furthermore, the effect of the variation of the thickness and material properties of the film–substrate system on the wrinkling parameters was considered in the previous chapters.

On the other hand, the nonlinear analysis of the postbuckling has been commonly discussed in the literature [Timoshenko and Gere, 1961; Sathyamoorthy, 1998] by considering the geometric nonlinearity of the median plane stretching [Fertis, 1999]. As an example, Fang and Wickert (1994) considered the buckling and postbuckling behavior of a beam with both clamped boundary conditions. In contrast with the postbuckling problem which is usually represented by a closed form analytical solution from an elliptic integral [Wang *et al.*, 1997], the post–wrinkling of the film–substrate systems needs more investigations to be understood completely. For post–wrinkling case, usually there is no analytical solution (except for simple cases of uniform wrinkling pattern) and the toughness of the nonlinear analysis is intensified in accompany with the singularity of the mathematical model near the bifurcation point. Singh *et al*. (2009) developed a procedure for the nonlinear instability problem and applied it with a finite element method to propose a quadratic relation for load–amplitude relation of composite plates on a shear foundation. In some cases, the researchers restrain the amplitude of the beam/film by using external constrains [Cao and Boyce, 1997; Zhang *et al.*, 2010] which leads to wrinkling. Some other investigations were carried out on the instability of the composite beams analytically and numerically for infinite long system [Leotoing, 2002; Li *et al.*, 2009]. It was also found in literature [Pocivavsek *et al.*, 2008] that the wrinkling of a thin elastic film on a substrate is usually followed by folding such that all the wrinkles vanish on the film except on some positions that folds grow. However, the wrinkling of the systems with finite length with non–uniform thickness/stiffness needs more investigation.

In this chapter, the uniaxial buckling of a free standing film and the uniaxial wrinkling of a film deposited on a Winkler substrate are considered. By using a finite difference method combined with a successive procedure for solving the eigenvalue problem for a nonlinear differential equation, the buckling and wrinkling problems are investigated and the critical loads/mode shapes at the onset of instability and the load–amplitude relation of the post–instability phase are determined. The effect of the non–uniform material properties and variable thickness of the film on the instability parameters are discussed. The results of the buckling analysis including the buckling loads and mode shapes are consistent with the results in literature. For the film–substrate system, the wrinkles accumulate around the softest/thinnest position of the system with a

non–uniform pattern, and the effect of the substrate stiffness and film characteristics on the post–wrinkling behavior is discussed. It is shown that for buckling and wrinkling problem, the relation of the load–amplitude of the film after instability is quadratic. For a free standing film at the end of the post–buckling region, the stiffness of the system diminishes so that according to literature, the film undergoes a sudden failure mode, while for the film–substrate system the post–wrinkling region undergoes a folding phase in which the load–amplitude does not follow the quadratic relation and the wrinkling pattern changes correspondingly.

7.2 Modeling

In order to characterize the buckling/wrinkling of a thin film deposited on a substrate, the instability problem of the film–substrate system is investigated. For uniaxial buckling/wrinkling, the large deformation beam/strip theory is used to model the thin film. In wrinkling problem, the substrate is modeled by using a Winkler foundation such that the interaction between the film and the substrate is modeled by a spring system [Birman and Bert, 2004]. Therefore, the effect of the substrate is applied on the film as an external loading corresponding with the stiffness of the substrate and deflection of the film. Figure 7-1 shows a deposited film with non–uniform material properties and variable thickness on a substrate with length L, width b and thickness t. The loading is applied along the longitudinal direction x in which direction film undergoes a uniaxial deformation.

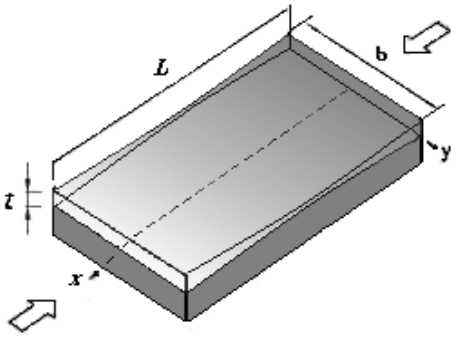

Figure 7-1: The film–substrate system under uniaxial loading

Figure 7-2 shows a deformed element of the beam/film with forces and moments acting on it, where N and Q are the longitudinal (i.e. axial) and transverse (i.e. shear) components of the force on a cross section and M is the bending moment. The changes in these parameters are shown by sign Δ as ΔN, ΔQ and ΔM and the deflection of the beam/film at each point in z direction is denoted by w. On the other hand, the external loading on the element is shown by distributed forces f_x and f_z and distributed moment m. By using a finite rotation around the y–axis perpendicular to the plane of the element, these components are introduced in curvilinear coordinate system along the centerline of the element and perpendicular to it, respectively shown by f_t and f_n.

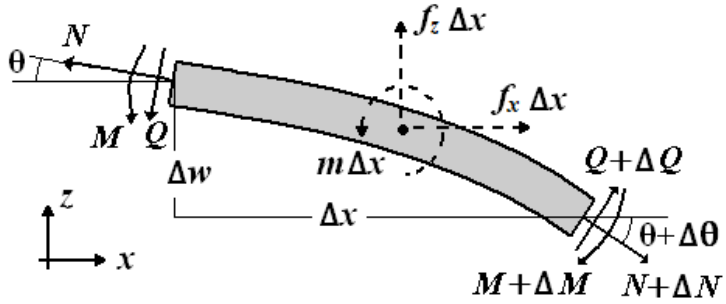

Figure 7-2: Free body diagram of an element of the beam/film in deformed configuration

For the element shown in figure 7-2, the assumption of neglecting the shear strain for thin elastic beam/film leads to a relation between the rotation angle θ and deflection w as

$$\theta = \tan^{-1}\left(\frac{dw}{dx}\right) \tag{7-1}$$

The equilibrium equations of the beam/film for a slightly deformed configuration in figure 7-2 are derived as,

$$\frac{dN}{dx} + Q\frac{d\theta}{dx} = f_t \tag{7-2-A}$$

$$N\frac{d\theta}{dx} - \frac{dQ}{dx} = f_n \tag{7-2-B}$$

$$\frac{dM}{dx} - \frac{Q}{\cos\theta} = m \tag{7-2-C}$$

In the absence of external distributed moment m, by substituting shear component Q from (7-2-C) into (7-2-B) one may find the governing equation of the system versus θ as

$$\frac{d}{dx}\left(\cos\theta\,\frac{dM}{dx}\right) - N\frac{d\theta}{dx} + f_n = 0 \tag{7-3}$$

On the other hand, based on the geometry of the deformed element, when R is the radius of curvature at each point and ds is the length of the element, it is clear that ds = ± R dθ and $(ds)^2=(dx)^2+(dw)^2$. Therefore, by using the equation (7-1) the curvature of the beam at each point is given by

$$\frac{1}{R}=\frac{M}{EI}=\pm\frac{\frac{d^2w}{dx^2}}{\left(1+\left(\frac{dw}{dx}\right)^2\right)^{1.5}} \tag{7-4}$$

where EI is the bending rigidity of the beam/strip. Substituting M and θ versus w in the equation (7-3) results in the governing equation of the system in terms of the deflection w and its derivatives as

$$\frac{d}{dx}\left(\frac{1}{\sqrt{1+\left(\frac{dw}{dx}\right)^2}}\frac{d}{dx}\left(EI\frac{\frac{d^2w}{dx^2}}{\left(1+\left(\frac{dw}{dx}\right)^2\right)^{1.5}}\right)\right)-N\frac{\frac{d^2w}{dx^2}}{1+\left(\frac{dw}{dx}\right)^2}+f_n=0 \tag{7-5}$$

Also the balance of the forces in tangential direction along the beam in equation (7-2-A) concludes that for the free external in–plane loading (i.e. f_t =0), the in–plane force N along the beam/film is constant and its variation due to higher order term $Q\frac{d\theta}{dx}=\cos\theta\frac{dM}{dx}\frac{d\theta}{dx}$ is negligible.

Note that when large deformation of the system is considered, the geometric nonlinearity affects on the moment–curvature relation and the longitudinal force due to stretching of the median plane of the system [Sathyamoorthy, 1998]. As shown in equation (7-4), due to the large deformation of the film, the parameter $\frac{dw}{dx}$ is not negligible and the moment –curvature nonlinearity appears in the governing equation of the system in equation (7-5). Obviously, for small values of parameter $\frac{dw}{dx}$ corresponding with the small deformation of the beam, the equations (7-4) and (7-5) are simplified to the linear equations by ignoring $\left(\frac{dw}{dx}\right)^2$ and nonlinearity of the moment–curvature relationship vanishes.

The geometric nonlinearity due to stretching occurs when the neutral axis of the beam/strip is stretched; hence, the relation between the strain and displacement becomes nonlinear. For a beam with length L_0 in its initial flat configuration before loading, applying compressive axial force leads to an axial deformation of the beam to length L_1 <

L_0. At the critical state of the compression, beam does not hold the axial configuration and deflects transversely and instability occurs. The length of the beam in the new deflected configuration is obtained by

$$L_2 = \int_{x=0}^{L_1} \sqrt{1 + \left(\frac{dw}{dx}\right)^2}\ dx \tag{7-6}$$

Therefore, the decreasing of the length of the beam in the deflected configuration with respect to the neutral state is given by

$$L_0 - L_2 = L_0 - \int_{x=0}^{L_1} \sqrt{1 + \left(\frac{dw}{dx}\right)^2}\ dx = L_0 - L_1 - \int_{x=0}^{L_1} \left(\sqrt{1 + \left(\frac{dw}{dx}\right)^2} - 1\right) dx \tag{7-7}$$

By changing the upper domain of integral to L_0 for small values of compression parameter $L_0 - L_1$, the change of the length of the system is obtained, and hence from the axial strain one can find the axial force on the system as

$$N = P - EA/L_0 \left[\int_{x=0}^{L_0} \left(\sqrt{1 + \left(\frac{dw}{dx}\right)^2} - 1\right) dx\right] \tag{7-8}$$

where $P = EA(1 - L_1/L_0)$ is the applied axial force and EA is the compressive rigidity of the beam.

Therefore, the governing equation of the beam/film undergoing a large deformation is obtained from equations (7-5) and (7-8) where the first one contributes the nonlinearity in the moment–curvature relation and the second one represents the nonlinear effect of the stretching of the neutral axis of the film. In buckling analysis of the system, researchers usually ignore the nonlinearity effect of the moment–curvature relation and only consider the stretching of the neutral axis [Fang and Wickert, 1994]. However, in wrinkling problem where a highly ordered wavy pattern dominates along the span, the variation of the curvature gets more important and needs to be considered.

For interaction of the beam/film and the substrate, the Winkler model is commonly used by many researchers, in which the substrate imposes a distributed loading on the film with an equivalent spring model. The force is applied perpendicular to the beam/film median plane so that there is no shear between the beam/film and its substrate. Therefore, the tangential component of the film–substrate interaction is neglected corresponding

with f_t =0 (due to zero shear) and the normal component perpendicular to the beam/film median plane is given by $f_n = bKw$ where K is the Winkler foundation modulus.

Finally, the governing equation of the system is normalized by substituting w by δw^* where δ is the maximum amplitude and w^* is the normalized mode shape (i.e. Max [w^*] = 1). Furthermore, non–dimensional parameters with superscript "*" are introduced as $x^*=x/L$, $\delta^*= \delta/L$ and $EI^*= EI/EI_0$ where EI_0 is the bending stiffness modulus for a uniform system and EI^* is a function of the length coordinate x^* corresponding with the variation of the bending stiffness modulus due to the change in thickness and/or material properties along the length span. Also $N^*=NL^2/EI_0$ and $K^*=bKL^4/EI_0$ are the dimensionless axial loading and Winkler foundation modulus of the substrate. Therefore, the governing equation of the beam/strip under uniaxial deformation in equation (7-5) is normalized as

$$\frac{d}{dx^*}\left(\frac{1}{\sqrt{1+\delta^{*2}\left(\frac{dw^*}{dx^*}\right)^2}}\frac{d}{dx^*}\left(EI^*(x^*)\frac{\frac{d^2w^*}{dx^{*2}}}{\left(1+\delta^{*2}\left(\frac{dw^*}{dx^*}\right)^2\right)^{1.5}}\right)\right) - N^*\frac{\frac{d^2w^*}{dx^{*2}}}{1+\delta^{*2}\left(\frac{dw^*}{dx^*}\right)^2} + K^*w^* = 0 \tag{7-9}$$

where the dimensionless axial load is derived from equation (7-8) as

$$N^* = P^* - \frac{EAL^2}{EI_0}\left[\int_{x^*=0}^{1}\left(\sqrt{1+\delta^{*2}\left(\frac{dw^*}{dx^*}\right)^2}-1\right)dx^*\right] \tag{7-10}$$

and $P^*=PL^2/EI_0$ is the dimensionless applied axial load on the system in the postbuckling/ post–wrinkling configuration. Solving the equation (7-9) leads to a relation between the amplitude of the system (i.e. δ^*) after instability and the loading parameter N^*, while the equation (7-10) provides the external loading P^* required to produce the corresponding amplitude on the system.

7.3 Solution Approach

For a system with small deformation, the assumption of $1+ \delta^{*2}\left(\frac{dw*}{dx^*}\right)^2 \approx 1$ is applied to linearize the governing equations of the system in (7-9) and (7-10) as

$$\frac{d^2}{dx^{*2}}\left(EI^*(x^*)\frac{d^2w*}{dx^{*2}}\right) - N^*\frac{d^2w*}{dx^{*2}} + K^*w^* = 0 \qquad (7\text{-}11)$$

while N^* is a constant parameter equal to the external in–plane loading applied at the edges of the system (i.e. $N^*=P^*$). Solving the eigenvalue problem for this linear forth order differential equation determines the onset of the instability.

The buckling problem of a free standing film under a large deformation is analyzed by simplifying the equation (7-9) to (7-11) by ignoring the effect of the moment–curvature nonlinearity, while keeping the nonlinearity due to the stretching of the neutral axis of the beam/strip [Sathyamoorthy, 1998; Fang and Wickert, 1994]. Therefore, by solving the eigenvalue problem in equation (7-11) one may find the buckling loads and mode shapes of the system. Consequently, the postbuckling behavior of the system is considered by using the relation of the applied external load P^* and amplitude δ^*in equation (7-10).

The wrinkling problem of a film–substrate system is studied at the onset of instability when the deflection and its variation are small. Hence, the nonlinear equation (7-9) is simplified to the linear eigenvalue equation (7-11) with a constant parameter N^*. However, in order to consider the post–wrinkling behavior of the system, first the equation (7-9) is solved and after finding the parameter N^* versus δ^*, the external applied load P^* is obtained from equation (7-10).

Equation (7-11) is the eigenvalue problem for linear differential equation at the onset of instability. As discussed in pervious chapters, for uniform and non–uniform films deposited on the substrate, where finding an analytical solution seems to be hard or impossible, numerical methods are used to solve the equation. By solving the equation, the eigenvalues and eigenfunctions corresponding with the buckling/wrinkling loads and mode shapes are determined. Finding the external load P^* is straight forward by substituting the parameters N^* and w^* into equation (7-10) represented by

$$P^*= N^*+C\,\delta^{*2} \qquad (7\text{-}12)$$

where P^* and δ^* follow a quadratic relation as reported by other researchers in literature [Timoshenko and Gere,1961; Brush and Almroth, 1975], and C is the constant curvature.

Equation (7-9) for post–wrinkling analysis is solved by a successive method in which the nonlinear terms are approximated with the known deflection obtained from the previous step [Singh *et al*., 2009]. Therefore, the nonlinear problem is changed to a linear one with straight forward solution. The procedure for solving the equation is described in the following steps:

1) The linear eigenvalue problem of the system is solved. The linear equation (7-11) is obtained by ignoring all the nonlinear coefficients in the nonlinear problem. The eigenvalues and eigenfunctions of the linear problem represent the wrinkling load and pattern on the onset of instability.
2) The nonlinear coefficients are estimated by substituting the mode shape values from the linear analysis of the previous step for a specific amplitude δ^*. Therefore the nonlinear equation changes to a linear differential equation.
3) The eigenvalue problem for the modified linear differential equation is solved and the new eigenvalues and eigenfunctions are obtained.
4) By comparing the eigenfunctions of the successive steps, the convergence criterion is considered. If the difference between these eigenfunctions exceeds the convergence criterion, then the steps (2) and (3) are repeated iteratively for a new modified eigenfunction until the convergence criterion is satisfied. The fulfillment of the convergence condition provides an eigenvalue and eigenfunction that satisfy the nonlinear equation corresponding with the specific value of the amplitude parameter δ^*.
5) The eigenvalue and eigenfunction obtained from the analysis for the specific δ^* are launched into the equation of stretching in (7-10) to find the corresponding applied external load P^*.
6) The procedure is repeated for another parameter of δ^*.

By following the successive procedure, the eigenvalue problem for the nonlinear differential equation is solved numerically. The equivalent equation in step 2 is given with a linear equation as

$$\frac{d}{dx^*}\left(f_1\ \frac{d}{dx^*}\left(f_2\ \frac{d^2w*}{dx^{*2}}\right)\right) - f_3 N^*\ \frac{d^2w*}{dx^{*2}} + K^* w^* = 0 \qquad (7\text{-}13\text{-A})$$

where f_1, f_2 and f_3 are obtained by substituting w^* from the linear analysis of the previous step by

$$f_1 = \frac{1}{\sqrt{1+\delta^{*2}\left(\frac{dw*}{dx^*}\right)^2}} \qquad (7\text{-}13\text{-B})$$

$$f_2 = \frac{EI^*(x^*)}{\left(1+\delta^{*2}\left(\frac{dw*}{dx^*}\right)^2\right)^{1.5}} \qquad (7\text{-}13\text{-C})$$

$$f_3 = \frac{1}{1+\delta^{*2}\left(\frac{dw*}{dx^*}\right)^2} \qquad (7\text{-}13\text{-D})$$

The procedure is stopped when the convergence criterion is satisfied. The convergence criterion is defined as the condition that the eigenfunction obtained from the solution at each step does not differ a lot in comparison with the previous step. For example the norm of the difference between the current eigenfunction and the previous one should be less than a number (i.e. 0.1%). Fulfilling this condition ensures that the solution of the nonlinear problem converges to the exact solution of the problem which satisfies the governing equation.

Therefore, the external loading on the system after instability is derived according to equation (7-10) as

$$P^* = N^* + \frac{EAL^2}{EI_0}\Phi^* \qquad (7\text{-}14\text{-A})$$

where N^* is directly obtained from the linearized eigenvalue problem and Φ^* is given by

$$\Phi^* = \int_{x^*=0}^{1}\left(\sqrt{1+\delta^{*2}\left(\frac{dw^*}{dx^*}\right)^2}-1\right)dx^* \qquad (7\text{-}14\text{-B})$$

which can also be approximated by using Taylor expansion for small variations of the amplitude as

$$\Phi^* = \delta^{*2}\int_{x^*=0}^{1}\frac{1}{2}\left(\frac{dw^*}{dx^*}\right)^2\ dx^* \qquad (7\text{-}14\text{-C})$$

Substituting parameters N^* and Φ^* into (7-14-A) leads to the relation between the applied load P^* with the amplitude of the system after the onset of instability.

In order to solve the differential equations numerically, a finite difference method with central difference formulation of 6th order of accuracy is used similar to the previous chapters [Hildebrand, 1968; Timoshenko and Gere, 1961]. Applying the difference formulation into the governing equation of the system discretizes the differential equation and replaces it by a set of algebraic equations. By imposing the boundary conditions, a complete system of the algebraic equations is derived as

$$[A]\{w^*\} + N^*[B\,]\{w^*\} = 0 \qquad (7\text{-}15)$$

in which $\{w^*\} = \{w_1^*, \dots, w_n^*\}^{\mathrm{T}}$ is the vector of the nodal displacement and $[A]$ and $[B]$ are square matrices. This general eigenvalue problem with eigenvector $\{w^*\}$ and eigenvalue parameter N^* has a straight forward solution. The eigenvalues of the problem correspond with the buckling/wrinkling loads and the eigenvectors represent the buckling mode shapes/wrinkling pattern of the system.

7.4 Results and Discussions

7.4.1 Buckling Problem

For a free standing film under uniaxial compressive in–plane loading, the system undergoes a buckling mode based on Euler buckling theory. The critical buckling load of the system with clamped edges at the onset of buckling is determined as $N_B^* = 4\pi^2$ corresponding with the mode shape $w^* = \frac{1}{2}[1 - \cos(2\pi x^*)]$ for $0 < x^* < 1$.

The postbuckling behavior of the clamped beam was investigated analytically by many researchers [Timoshenko and Gere,1961; Brush and Almroth, 1975]. The effect of the curvature–moment nonlinearity is usually ignored and only the stretching nonlinearity of the neutral axis is considered [Fang and Wickert, 1994]. Ignoring the curvature–moment nonlinearity corresponds with the relation $1 + \delta^{*2}\left(\frac{dw^*}{dx^*}\right)^2 \cong 1$ in equations (7-13-A-D) which leads to $f_1 = f_3 = 1$ and $f_2 = EI^*$, while the stretching nonlinearity in relations (7-14-A-C) remains unchanged. According to this simplification, by imposing the mode shape $w^* = \frac{1}{2}[1 - \cos(2\pi x^*)]$ in equations (7-13) and (7-14) one may find

$$P^* = N_B^* + \rho^2 \frac{EAL^2}{EI_0} \delta^{*2} \tag{7-16-A}$$

where ρ comes from the integration of the stretching nonlinearity (i.e. Φ^*) in equation (7-14-B,C). Since $N_B^* = 4\pi^2$, equation (7-16-A) can be equivalently rewritten as,

$$\delta^* = \frac{\pi}{2\rho} \sqrt{\left(\frac{4P}{\pi^2 EA} - \frac{16I_0}{AL^2}\right)} \tag{7-16-B}$$

which is derived by Fang and Wickert (1994) with an equivalent strain denoted by $\varepsilon = P/EA$. The quadratic relation between the loading and amplitude of the beam is derived as reported in literature [Timoshenko and Gere, 1961].

In order to check the accuracy and applicability of the finite difference code and the successive procedure for solving the nonlinear problem, the values of N_B^* and ρ are solved numerically when only the stretching nonlinearity (i.e. for $f_1 = f_3 = 1$ and $f_2 = EI^* = 1$) is considered and approximated by the first order Taylor expansion, which are $4\pi^2$ and $0.99\pi/2$, respectively. For the same problem, values of N_B^* and ρ were derived as $4\pi^2$ and $\pi/2$ analytically by Fang and Wickert (1994). These numerical results show a good agreement with the analytical solutions, which demonstrates the accuracy and applicability of the current numerical procedure. However, by using the equation (7-14-B) without considering the Taylor expansion approximation, the parameter ρ is calculated as $\rho = 0.92\ \pi/2$ which represents a difference of 7% with the approximate solution.

On the other hand, considering the effect of the bending nonlinearity (i.e. f_1, f_2 and f_3) in equations (7-13-A-D) by using the finite difference method results in a small deviation in the parameters N^* and Φ^*. These parameters also follow a quadratic relation as

$$\frac{N^*}{N_B^*} = 1 + 0.215\ \pi^2 \delta^{*2} \tag{7-17-A}$$

$$\Phi^* = 0.219\ \pi^2 \delta^{*2} \tag{7-17-B}$$

which leads to

$$P^* = N_B^* + \left(0.215 N_B^* + 0.219\ \frac{EAL^2}{EI_0}\right) \pi^2 \delta^{*2} \tag{7-17-C}$$

Usually $\frac{EAL^2}{EI_0} \gg N_B^*$, ignoring the first term in the parentheses in (7-17-C) and comparing it with the equation (7-16-A) represents the equivalent ρ in this case as $(0.219\pi^2)^{0.5} = 0.94\ \pi/2$ which has a 2% stiffening effect due to including the bending stiffness nonlinearity in

the postbuckling problem. . Due to the small difference, this nonlinearity was ignored in the postbuckling analysis by most researchers in literature.

For a buckled film, any small increase in the loading leads to a large amplitude of the system. Finally, the resistance of the post–buckled system against loading vanishes and the ascending quadratic relation of P–δ is replaced with a descending relation so that system collapses suddenly by the transition of the stable postbuckling phase to the unstable collapse phase [Timoshenko and Gere, 1961, page80; Singer *et al.*, 1998, page 134].

7.4.2 Wrinkling of an Infinite Length Beam/Film

For a homogenous isotropic film with uniform thickness, the bending stiffness modulus is constant all over the span (i.e. EI^*=1). For the film with constant bending stiffness modulus and infinite length, it is shown that the wrinkles propagate uniformly all over the domain with the same amplitude and a periodic function like $w^*= \cos(\beta_0^* x^*)$. The wave number of the wrinkling and the wrinkling load versus the substrate stiffness K^* is given by [Cerda and Mahadevan, 2003]

$$\beta_0^* = \sqrt[4]{K^*} \tag{7-18}$$

$$N_0^* = 2\sqrt{K^*} \tag{7-19}$$

In post–wrinkling phase, substituting w^*, β_0^* and N_0^* in equations (7-14-A,C) leads to the relation of the applied loading P^* with the amplitude of the wrinkling δ^* as

$$P^* = N_0^* \left(1 + \frac{EAL^2}{8EI_0}\delta^{*2}\right) \tag{7-20-A}$$

Equivalently, the amplitude of the wrinkles is given in terms of the applied loading by

$$\delta^* = \sqrt{\frac{8EI_0}{EAL^2}}\sqrt{\left(\frac{P^*}{N_0^*} - 1\right)} \tag{7-20-B}$$

According to the equation (7-20-B), for external load P^* less than the critical wrinkling load N_0^* in (7-19) the amplitude of the wrinkling is zero as expected for pre–wrinkling flat configuration. However, for the applied loading P^* bigger than the critical load, the nonzero amplitude of the wrinkles describes the post–wrinkling behavior of the system. Pocivavsek *et al*. (2008) and other researchers also showed that the amplitude of the wrinkles is the square root of the compressive loading.

7.4.3 Wrinkling of a Uniform Beam/Film with Finite Length

For a finite homogenous isotropic beam/film with uniform thickness (i.e. $EI^*=1$) deposited on a substrate, by using the finite difference method, it is shown that the forth order differential equation with constant coefficients in (7-11) undergoes a wavy pattern at the onset of wrinkling as discussed in the previous chapters. The wave number of the wavy pattern and the corresponding critical load of the wrinkling are obtained same as the equations (7-18) and (7-19) for various boundary conditions. In contrast with the buckling of a free standing film which is dominated by the boundary conditions, for the wrinkling of the film, the critical wrinkling load $N_0^*$and wave number β_0^* only depend on the substrate stiffness K^* in equations (7-18) and (7-19), since the substrate effect is more dominant than the boundary constraint as discussed in chapters 4 and 5. However, the boundary constraints influence the wrinkling pattern amplitude, for example the amplitude of the wrinkles is not uniform throughout the length span and is constrained to zero at the clamped ends.

In order to investigate the post–wrinkling behavior of the system, the finite difference method combined with the successive procedure is used to solve the eigenvalue problem for the nonlinear differential equation (7-9). The results of the linear analysis at the onset of the wrinkling are plugged into the nonlinear eigenvalue equation, and after solving the equation, the results of each step are used for running the next step for various values of amplitude δ^* and substrate stiffness parameter K^* to determine N^* and Φ^* in equations (7-14-A,B). The plots of these parameters for a fixed K^* are shown in figures 7-3-A and 7-3-B. As figures show, both parameters N^* and Φ^* firstly increase quadratically with the amplitude parameter δ^* starting from $N^*=N_0^*$ and $\Phi^*=0$ at the bifurcation point. The quadratic region is limited by an upper bound resulting in the decrease of N^* and Φ^* after this point. This ascending–descending behavior is completely in agreement with the postbuckling behavior of the beams considered by Timoshenko and Gere (1961, page 80) as discussed before.

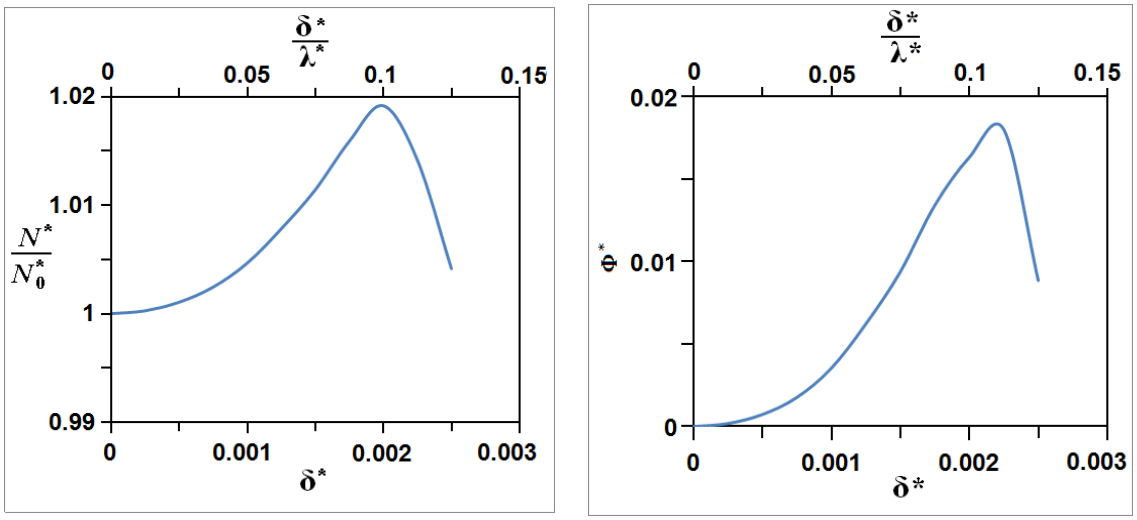

A) Loading parameter $\frac{N^*}{N_0^*}$ B) Loading parameter Φ^*

Figure 7-3: Loading parameters versus amplitude obtained from nonlinear analysis

Before the upper bound for N^* (and also Φ^*) is reached, the relation between the loading parameters N^* (and Φ^*) and δ^* is quadratic, and coefficients are determined by using a regression analysis [Kahane, 2008] for a set of substrate parameters K^*as,

$$\frac{N^*}{N_0^*} = 1 + C_N \delta^{*2} \tag{7-21-A}$$

$$\Phi^* = C_\Phi \, \delta^{*2} \tag{7-21-B}$$

where $N_0^* = 2\sqrt{K^*}$ is the critical wrinkling load in equation (7-19) and C_N, C_Φ are coefficients depending on the substrate stiffness K^*. The regression analysis provides an expression for the coefficients C_N and C_Φ in terms of the square root of K^* with an $R^2 \approx 0.99$. By introducing another parameter $\lambda^* = \pi/\beta_0^* = \lambda/L$ for wrinkling wavelength λ, equations (7-21-A,B) are rewritten as,

$$\frac{N^*}{N_0^*} = 1 + \pi^2 C_N^* \left(\frac{\delta^*}{\lambda^*}\right)^2 \tag{7-22-A}$$

$$\Phi^* = \pi^2 C_\Phi^* \left(\frac{\delta^*}{\lambda^*}\right)^2 \tag{7-22-B}$$

where C_N^* and C_Φ^* are constant post–wrinkling coefficients independent of the substrate stiffness parameters K^*, which are presented in table 7-1 with a high accuracy of $R^2 \approx 0.995$ and an standard error less than 2%.

Table 7-1: The post–wrinkling coefficients in the equations (7-22) obtained from a regression analysis

Model Summary		$R^2 = 0.995$		
Parameter	Estimate	Std. Error	95% Confidence Interval	
			Lower Bound	Upper Bound
C_N^*	.221	.004	.210	.230
C_Φ^*	.184	.002	.180	.190

Similar to the postbuckling of a free standing beam/film in which a small increase of the applied load above the critical buckling load results in a large amplitude of the buckled profile, the post–wrinkling path in figures 7-3-A,B demonstrates the same trend. By substituting equations (7-22-A,B) in equation (7-14-A), one may find the applied external loading on the post–wrinkling of the system versus amplitude–wavelength ratio for the post–wrinkling path as,

$$\frac{P^*}{N_0^*} = 1 + \pi^2 \left\{ C_N^* + \frac{EAL^2}{EI_0 N_0^*} C_\Phi^* \right\} \left(\frac{\delta^*}{\lambda^*}\right)^2 \qquad (7\text{-}23)$$

According to equation (7-23) the curvature of $\frac{P^*}{N_0^*} - \left(\frac{\delta^*}{\lambda^*}\right)$ depends on both the stretching and bending nonlinearity coefficients C_Φ* and C_N*. In contrast with the buckling problem in equation (7-17-C), where $\frac{EAL^2}{EI_0 N_0^*}$ is several order of magnitude bigger than one and the effect of the bending nonlinearity is negligible in comparison with the stretching nonlinearity, in wrinkling problem the order of magnitude of $\frac{EAL^2}{EI_0}\frac{1}{2\sqrt{K^*}}$ is equivalent with $\left(\frac{\lambda^*}{t^*}\right)^2$ (i.e. $t^*=t/L$) and therefore, for small wavelength of the wrinkling both of the bending and stretching nonlinearity sources need to be taken into account.

On the other hand, the analytical solution (7-20-A) for infinite length beam/film by ignoring the bending nonlinearity introduces the curvature of the $\frac{P^*}{N_0^*} - \left(\frac{\delta^*}{\lambda^*}\right)$ as $\frac{EAL^2}{EI_0\sqrt{K^*}}\frac{\pi^2}{8}$ and proposes the equivalent C_Φ* as ¼ (compare with the numerical results of C_Φ* in table

7-1). Besides, the curvature of $\Phi^* - \frac{\delta^*}{\lambda^*}$ for wrinkling of a finite length film is given by $\pi^2 C_\Phi{}^* = 0.184\ \pi^2 \pm 1\%$, which is similar to the curvature of $\Phi^* - \delta^*$ in buckling problem equal to $0.219\ \pi^2$ in equation (7-17-B). The similar magnitude of the curvature for post–wrinkling and postbuckling suggests that each wrinkle flexure can be treated as an equivalent beam with the effective length equal with the wavelength of the wrinkling.

In both of the postbuckling and post–wrinkling cases, there is an upper bound for load–amplitude of the postbuckling/post–wrinkling region. When the amplitude exceeds this upper bound, the loading parameters decrease and the corresponding mode shape obtained from numerical solution differs from the mode shape pattern on the onset of instability. In the buckling of a free standing beam/strip, the decrease of the applied load by increasing the amplitude results in the failure of the system [Timoshenko and Gere,1961; Singer *et al.*, 1998]. While in the wrinkling of substrate–bonded film, the wavy wrinkling pattern vanishes so that the amplitude of the wrinkles goes to zero all over the span except at some positions, where the amplitude increases and a fold initiates to grow. Pocivavsek *et al*. (2008) considered the transition between the wrinkling and the folding experimentally, such that, when the compression of the system increases more than a threshold value, a transition from the wrinkling to the folding occurs. Here, the threshold value is sought based on the numerical analysis by using the end point of the quadratic region in figure 7-3 for various parameters of K^*. The amplitude and loading parameters at the onset of transition phase (i.e. wrinkling to folding transition) follow the equations (7-22-A, B) with the parameters introduced in table 7-1. These threshold parameters depend on the substrate stiffness K^* from numerical results given by

$$\frac{N^*}{N_0^*} \leq \frac{N_{Tr.}^*}{N_0^*} = 1 + C_N^{*Tr.} \frac{1}{N_0^*} \tag{7-24-A}$$

$$\Phi^* \leq \Phi_{Tr.}^* = C_\Phi^{*Tr.} \frac{1}{N_0^*} \tag{7-24-B}$$

$$\frac{\delta^*}{\lambda^*} \leq \frac{\delta_{Tr.}^*}{\lambda^*} = C_\delta^{*Tr.} \frac{1}{\beta_0^*} \tag{7-24-C}$$

where $C_N{}^{*Tr.}$, $C_\Phi{}^{*Tr.}$ and $C_\delta{}^{*Tr.}$ are transition coefficients obtained from a regression analysis [Kahane, 2008] and are presented in table 7-2. Equations (7-24-A,B,C) define the conditions for the threshold value of wrinkling–folding transition, such that when the corresponding parameters of the system satisfy these equations, the system holds a

wrinkling profile, and when the equations (7-24) are violated, then the folds appear on the system. The condition for wrinkling–folding transition can be developed and derived for applied load P^* by substituting $C_N^{*Tr.}$, $C_\Phi^{*Tr.}$ in equation 7-23. The equations (7-24-A,B,C) are consistent such that any of them results in two other pairs by using the equations (7-22-A,B). On the other hand, combining equations (7-24-A,B,C) with (7-22-A,B) leads to a relation between the transition coefficients $C_N^{*Tr.}$, $C_\Phi^{*Tr.}$ and $C_\delta^{*Tr.}$ and the post–wrinkling coefficients C_N^* and C_Φ^* as

$$\frac{C_N^{*Tr.}}{C_N^*} = \frac{C_\Phi^{*Tr.}}{C_\Phi^*} = 2\left(\pi C_\delta^{*Tr.}\right)^2 \qquad (7\text{-}25)$$

Comparing the numerical results from regression analysis in tables 7-1 and 7-2 verifies numerically the equation (7-25) which is the relation between threshold parameters of the transition at the end of the quadratic region and the post–wrinkling coefficients (i.e. the curvature of the quadratic curve).

Table 7-2: The post–wrinkling coefficients in the equations (7-24) obtained from regression analysis

Model Summary		$R^2 = 0.98$		
Parameter	Estimate	Std. Error	95% Confidence Interval	
			Lower Bound	Upper Bound
$C_N^{*Tr.}$	657.58	25.39	597.53	717.63
$C_\Phi^{*Tr.}$	562.24	22.99	505.98	618.50
$C_\delta^{*Tr.}$	12.60	.27	11.96	13.23

Figure 7-4 shows the threshold transition parameters versus the substrate stiffness K^*. For loading or amplitude under the curves in figure 7-4, the wrinkling regime dominates on the system such that the values of N^*,Φ^* and δ^* satisfy the equations (7-24-A,B,C), while for the area on top of the curves the system undergoes folding and relations (7-24-A,B,C) are not satisfied.

The above results for the effective parameters of the transition are in good agreement with the experimental work presented by other researchers. Pocivavsek *et al*. (2008) considered the wrinkling–folding transition experimentally and proposed the parameters for the transition. They considered a polymer thin film on the water under compression which undergoes wrinkling by a wavelength equal to λ=1.6 cm. They compared the amplitude of the adjacent wrinkle flexures and deduced that for a critical amplitude ratio equal to δ/λ=0.06 under compressive strain 0.1 shown in figure 2 of their work, the wrinkling–folding transition starts such that the amplitude of the adjacent wrinkles diverge from each other. According to abovementioned data for polymer film on the water, by using the wavelength of the wrinkles one may find the stiffness modulus of the substrate approximately as $K^*\approx1.5\times10^9$, which corresponds with the threshold amplitude $\frac{\delta^*_{Tr.}}{\lambda^*}$ =0.064 from equation (7-24-A-C) and figure 7-4. This prediction agrees very well with δ/λ=0.06 in the work of Pocivavsek *et al*. (2008).

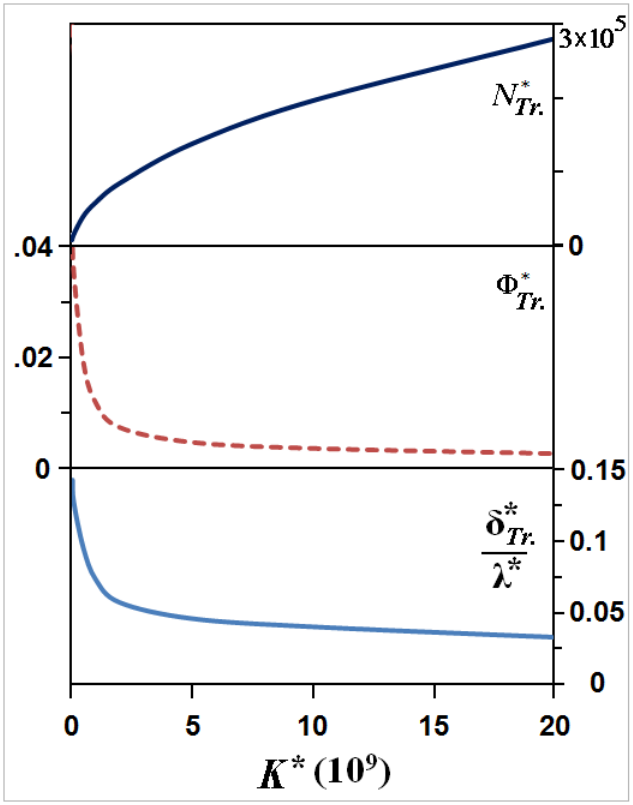

Figure 7-4: Threshold loading and amplitude parameters of wrinkling–folding transition

7.4.4 Wrinkling of a Non–Uniform Beam/Film with Finite Length

When the thickness of the beam/strip is not uniform or the material properties of the system changes along the span like the functionally graded materials (FGM), the bending stiffness modulus of the film varies along the span. Here, the bending stiffness modulus EI^* along the system is assumed as a function in continuity class C^2 along the entire span and the numerical finite difference method is used to find the instability parameters (i.e. load and pattern).

The results of chapter 4 for a FGM film and chapter 5 and 6 for a non–uniform thickness film show that for a film with variable bending stiffness modulus, the wrinkles accumulate around the positions with less bending rigidity, while for a film with uniform bending stiffness, the wrinkles propagate all over the span. The change in the wrinkling pattern effectively changes the wave number and footprint of the wrinkling.

On the other hand, the effect of the wrinkling accumulation on the post–wrinkling behavior is considered for the film with variable thickness in figure 7-5 and load–amplitude relation and wrinkling–folding transition parameters are studied. For this purpose, the results of the linear analysis from chapter 5 are imposed in the finite difference method combined with the successive procedure to find the relation between the wrinkle amplitude and the applied loading on the system.

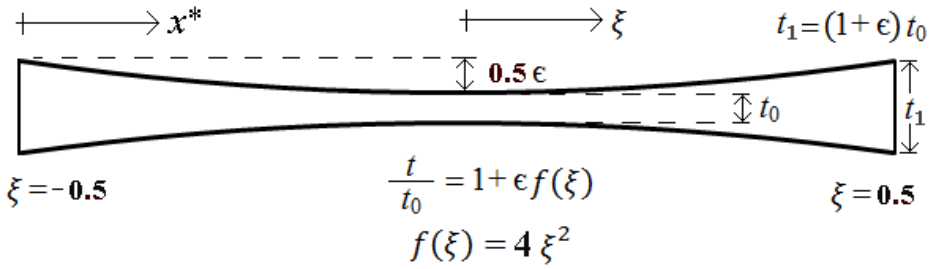

Figure 7-5: Thickness profile of the film

For a variable thickness beam/strip deposited on a substrate in which the wrinkles accumulate around the thinnest location of the film with the lowest bending rigidity, the loading–amplitude relation of the post–wrinkling system follows the same equations (7-21 and 22) shown in figure 7-3 with an ascending quadratic curve followed by a descending curve. However, the post–wrinkling coefficients C_N^* and C_Φ^* are functions

of the substrate stiffness K^* ($K_n^*=10^{-9}\ K^*$) and the thickness amplitude parameter ϵ proposed by

$$C_N^*(K^*,\epsilon) = m_{N,1}\mathrm{EXP}\left(-m_{N,2}\sqrt[3]{\epsilon}\,K_n^{*m_{N,3}}\right) \quad (7\text{-}26\text{-A})$$

$$C_\Phi^*(K^*,\epsilon) = m_{\Phi,1}\mathrm{EXP}\left(-m_{\Phi,2}\sqrt[3]{\epsilon}\,K_n^{*m_{\Phi,3}}\right) \quad (7\text{-}26\text{-B})$$

where m_i's (i=1,2,3 for corresponding subscripts N and Φ) are constants presented in table 7-3 which are obtained from a regression analysis. Obviously, imposing the parameter ϵ =0 into the coefficients C_N^* and C_Φ^* in equations (7-26-A,B) leads to the constant parameters in equation (7-22) for a film with uniform thickness.

Figures 7-6-A and B show the coefficients C_N^* and C_Φ^* in equations (7-26-A,B) versus parameters K^* and ϵ. Obviously, the variation of the parameter C_N^* for various values of K^* and ϵ is small so that it can be approximated by a constant (i.e. $m_{N,1}$ in table 7-3), which has the same value of C_N^* for uniform thickness film in table 7-1. However, the other post–wrinkling coefficient C_Φ^* in equation (7-26-B) drastically changes with the variation of the thickness (i.e. Figure 7-6-B). Once again, the constant coefficient $m_{\Phi,1}$ is very close to the corresponding parameter C_Φ^* in table 7-1 for a film with uniform thickness.

Table 7-3: The parameters of the equation (7-26) for wrinkling load obtained from a regression analysis

Parameter	Estimate	Std. Error	95% Confidence Interval		R^2
			Lower Bound	Upper Bound	
$m_{N,1}$	.220	.002	.216	.225	
$m_{N,2}$	31.89	4.10	22.96	40.82	0.93
$m_{N,3}$	–.258	0.044	–.355	–.162	
$m_{\Phi,1}$	.181	.003	.174	.188	
$m_{\Phi,2}$	.238	.001	.238	.239	0.99
$m_{\Phi,3}$	.092	.050	–.019	.203	

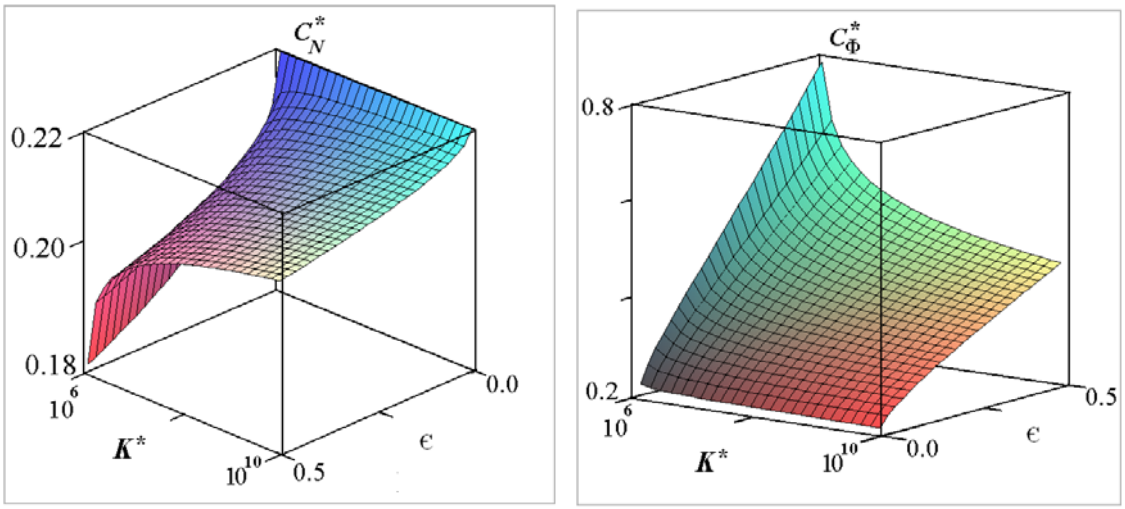

A) Coefficient C_N* B) Coefficient C_Φ*

Figure 7-6: The post–wrinkling coefficients C_N* and C_Φ* versus amplitude parameter ϵ and substrate stiffness K* for variable thickness film deposited on a substrate

By assuming C_N* as a constant parameter (i.e. $m_{N,1}$ in table 7-3), the variation in the applied loading on the system (i.e. P*) versus parameters K* and ϵ is dictated by the variation of C_Φ*. As shown in figure 7-6-B, by increasing the thickness amplitude parameter ϵ, the coefficient C_Φ* increases, while stiffening of the substrate decreases the coefficient C_Φ*.

On the other hand, similar to the case of a uniform thickness film, the transition point is defined at which the mode shape of the system does not resemble the mode shape pattern at the onset of wrinkling and the critical wrinkling load starts to decrease at the end of the quadratic relation region in the load–amplitude curve. The threshold amplitude for various values of the substrate stiffness K* and thickness amplitude parameter ϵ is shown in figure 7-7. The corresponding graphs for parameter $\frac{N_{Tr.}^*}{N_0^*}$ are also shown in figures 7-8-A and B, while Φ* has similar pattern which changes between 0 and 0.08 along the vertical axis. According to these figures, increasing the substrate stiffness leads to the decreasing of the transition load and the transition amplitude similar to the uniform thickness film (ϵ=0). Therefore, for stiffer substrate with finer wrinkling pattern, the threshold amplitude of the wrinkling decreases as well. However, for higher values of the thickness amplitude parameter ϵ which intensifies the accumulating effect, the threshold

amplitude of the wrinkle flexure increases so that the wrinkling pattern holds longer on the film before changing its pattern and transiting to the folding phase.

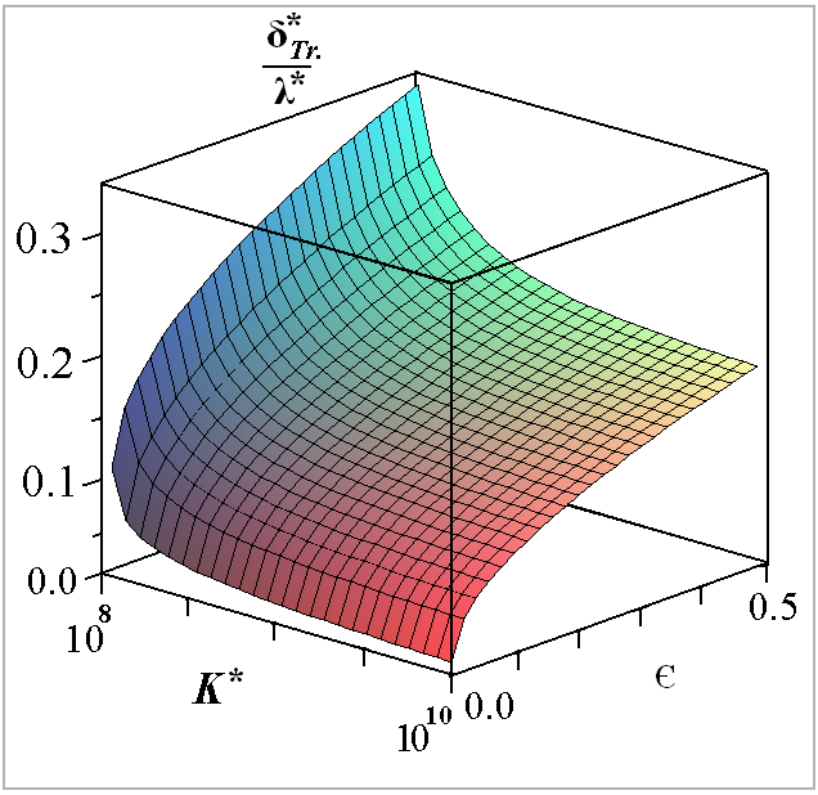

Figure 7-7: The threshold amplitude for various values of substrate stiffness and thickness amplitude parameter

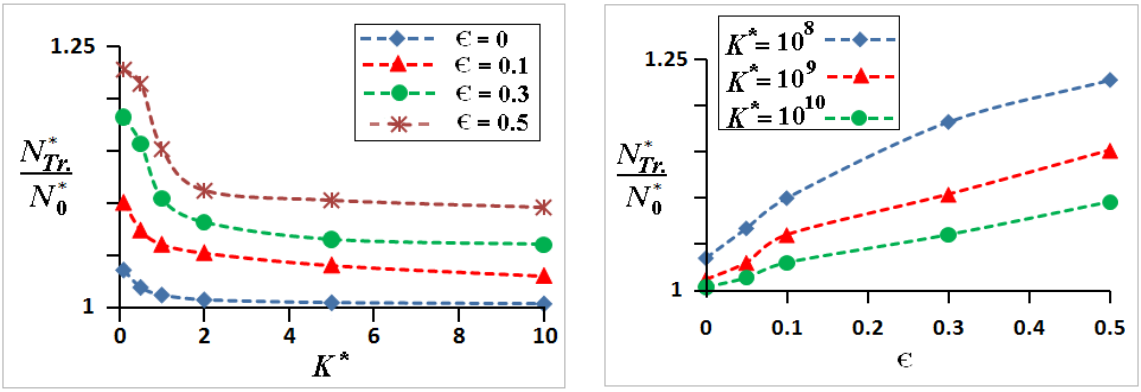

A) Different amplitude parameter B) Different substrate stiffness

Figure 7-8: The normalized transition load $\frac{N^*_{Tr.}}{N^*_0}$ versus (A) substrate stiffness K^* and (B) amplitude parameter ϵ

The relation between the threshold amplitude and the structural parameters K^* and ϵ is given by

$$\frac{\delta^*_{Tr.}}{\lambda^*} = \mathrm{F}_{\epsilon=0}(K^*)\mathrm{G}(K^*,\epsilon) \qquad (7\text{-}27\text{-A})$$

where $\mathrm{F}_{\epsilon=0}(K^*)$ is corresponding with the threshold amplitude of the uniform thickness film presented in (7-24-C) and $\mathrm{G}(K^*,\epsilon)$ is a function of the parameters K^* ($K_n^*=10^{-9}\,K^*$) and ϵ refers to the accumulation effect. The functions $\mathrm{F}_{\epsilon=0}(K^*)$ and $\mathrm{G}(K^*,\epsilon)$ are proposed as

$$\mathrm{F}_{\epsilon=0}(K^*) = C_\delta^{*Tr.}\,\frac{1}{\beta_0^*} \qquad (7\text{-}27\text{-B})$$

$$\mathrm{G}(K^*,\epsilon) = \mathrm{EXP}\left(m_1^\delta \epsilon^{m_2^\delta} {K_n^*}^{m_3^\delta}\right) \qquad (7\text{-}27\text{-C})$$

where m_i^δ's (i=1,2,3) are determined by using a regression analysis presented in table 7-4, while $C_\delta^{*Tr.}$ is obtained similar to the reported value in table 7-2. Obviously, imposing ϵ=0 in equations (7-27-A,C) leads to the same relation for the uniform thickness film in equation (7-24).

Table 7-4: The parameters of the relation (7-24) for wrinkling–folding transition amplitude obtained from a regression analysis

Model Summary		$R^2 = 0.92$		
Parameter	Estimate	Std. Error	95% Confidence Interval	
			Lower Bound	Upper Bound
$C_\delta^{*Tr.}$	12.022	1.190	9.575	14.468
m_1^δ	.228	.016	.196	.260
m_2^δ	.329	.053	.220	.438
m_3^δ	.097	.015	.065	.128

Combining equations (7-27) with (7-22), (7-24) and (7-26) leads to the relations of the threshold loading versus the amplitude and the other parameters of the system (i.e. K^* and ϵ) as

$$\frac{N^*}{N_0^*} \leq \frac{N_{Tr.}^*}{N_0^*} = 1 + C_N^{*Tr.} \frac{1}{N_0^*} \mathrm{EXP}\left(2 m_1^{\delta} \sqrt[3]{\epsilon} K_n^{*0.097}\right) \qquad (7\text{-}28\text{-A})$$

$$\Phi^* \leq \Phi_{\mathrm{Tr.}}^* = C_{\Phi}^{*Tr.} \frac{1}{N_0^*} \mathrm{EXP}\left(m_1^{\delta} \sqrt[3]{\epsilon} K_n^{*0.097}\right) \qquad (7\text{-}28\text{-B})$$

where $C_N^{*Tr.}$, $C_\Phi^{*Tr.}$ and $C_\delta^{*Tr.}$ follow the equation (7-25) and table 7-2. When the equations (7-28) are violated, a folding profile is replaced for the wrinkling pattern on the film. Figures 7-9 and 7-10 show the numerical data of $N^*_{Tr.}$ and $\Phi^*_{Tr.}$ from finite difference method versus the predicted values from equations (7-28-A,B). It is concluded that the loading parameters also change with the thickness amplitude parameter ϵ and substrate stiffness K^* exponentially and with a power law as equations (7-28-A,B) and figures (7-8-A,B) show.

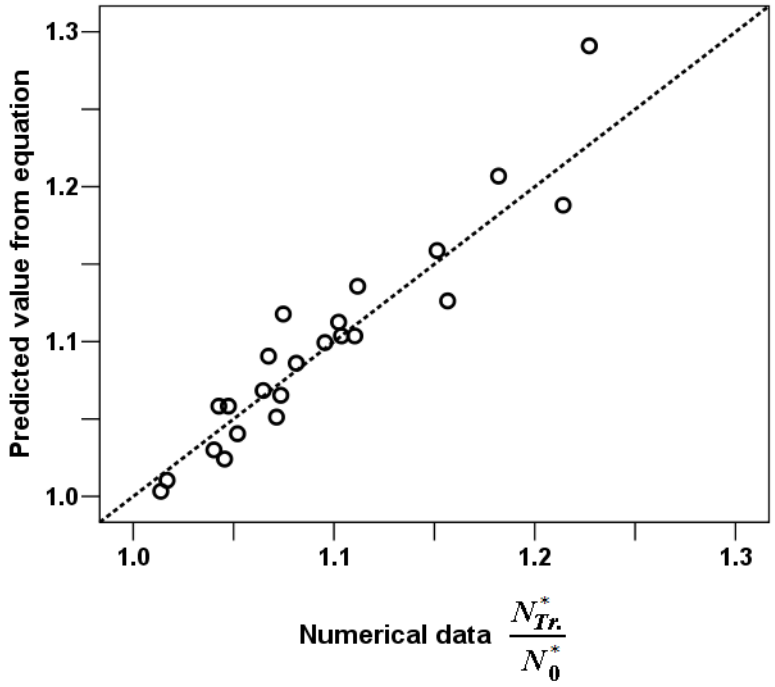

Figure 7-9: Predicted values of parameter $\frac{N_{Tr.}^*}{N_0^*}$ from equation (7-28-A) versus numerical data of the finite difference solution

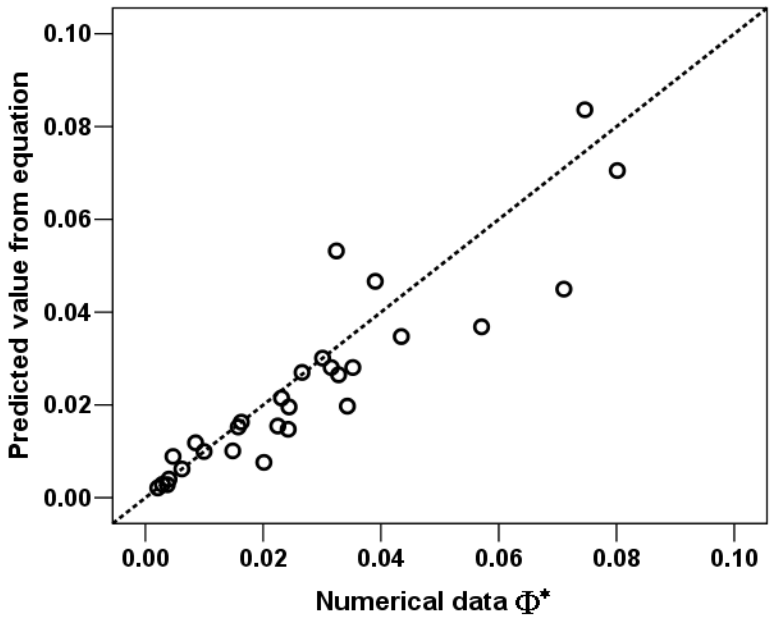

Figure 7-10: Predicted values of parameter $\Phi^*_{Tr.}$ from equation (7-28-B) versus numerical data of the finite difference solution

The above results show that in comparison with the uniform thickness film, the variation of the thickness which leads to the accumulation of the wrinkles around the thinnest location of the system postpones the wrinkling–folding transition by increasing the corresponding threshold parameters. In other words, accumulated wrinkles strengthen the wrinkling pattern against folding in which all the flexures of the wrinkles are vanished and replaced with one fold flexure.

7.5 Summary

The instability problem of a free standing film/deposited film on a Winkler substrate is investigated under uniaxial buckling/wrinkling pattern with large deformation theory and finite difference method. Critical load and pattern versus the structural parameters of the system (i.e. substrate stiffness and film characteristics) are investigated by solving the eigenvalue problem of the differential equation. For the free standing film, the buckling and postbuckling analysis provided the critical load and mode shapes and also load–amplitude relation after buckling. For substrate–bonded film, the wrinkling

parameters such as load and wave number are studied. The post–wrinkling of the system is considered and a quadratic relation for loading–amplitude relation is proposed followed by folding. The parameters of post–wrinkling and folding are studied numerically and the effects of the system characteristics on the wrinkling/post–wrinkling are investigated. It is shown that for wrinkling problem, the wavelength of the wrinkles plays an important role in characterizing the post–instability parameters. On the other hand, unlike the free standing film in which the postbuckling follows by the failure of the system, for substrate–bonded film the post–wrinkling changes to folding pattern on the film and the parameters of the transition are studied and compared with literature.

7.6 References

[1] V. Birman, C.W. Bert, "Wrinkling of composite–facing sandwich panels under biaxial loading", *Journal of Sandwich Structures and Materials*, Vol. 6 (3), 2004, pp. 217–237.

[2] F. Bloom, D. Coffin, *Handbook of Thin Plate Buckling and Postbuckling*, 2001, Chapman & Hall CRC.

[3] D.O. Brush, B.O. Almroth, *Buckling of Bars, Plates and Shells*, 1975, McGraw Hill Inc.

[4] J. Cao, M. C. Boyce, "Wrinkling behavior of rectangular plates under lateral constraint", *International Journal of Solids and Structures*, Vol. 34 (2), 1997, pp. 153–176.

[5] E. Cerda, L. Mahadevan, "Geometry and physics of wrinkling", *Physical Review Letters*, Vol. 90 (7), 2003, pp. 074302/1–4.

[6] W.Fang, J.A.Wickert, "Postbuckling of micromachined beams", *Journal of Micromechanics and Microengineering*, Vol. 4, 1994, pp. 116–122.

[7] D.G. Fertis, *Nonlinear Mechanics*, 2nd. Ed., 1999, CRC Press LLC.

[8] F.B. Hildebrand, *Finite Difference Equations and Simulations*, 1968, Prentice Hall Inc.

[9] X. Chen, J. W. Hutchinson, "A family of herringbone patterns in thin films", *Scripta Materialia*, Vol. 50, 2004, pp. 797–801.

[10] L.H. Kahane, *Regression Basics*, 2nd. Ed., 2008, Sage Publications Inc.

[11] L. Leotoing, S. Drapier, A. Vautrin, "Nonlinear interaction of geometrical and material properties in sandwich beam instabilities", *International Journal of Solids and Structures*, Vol. 39 (13–14), 2002, pp. 3717–3739.

[12] B. Li, S.Q. Huang, X.Q. Feng, "Buckling and postbuckling of a compressed thin film bonded on a soft elastic layer: a three–dimensional analysis", *Archive of Applied Mechanics*, Vol. 80 (2), 2009, pp.175–188.

[13] L. Pocivavsek, R. Dellsy, A. Kern, S. Johnson, B. Lin, K. C. Lee, E. Cerda, "Stress and fold localization in thin elastic membranes", *Science*, Vol. 320 , 2008, pp. 912–916.

[14] M. Sathyamoorthy, *Nonlinear Analysis of Structures*, 1998, CRC Press LLC.

[15] J. Singer, J. Arbocz, T. Weller, *Buckling experiments: Experimental Methods in Buckling of Thin Walled Structures; Basic Concepts, Columns, Beams, and Plates*, 1998, John Wiley and Sons Inc.

[16] B.N. Singh, A. Lal, R. Kumar, "Post buckling response of laminated composite plate on elastic foundation with random system properties", *Communications in Nonlinear Science and Numerical Simulation*, Vol. 14, 2009, pp. 284–300.

[17] S.P. Timoshenko, J.M. Gere, *Theory of Elastic Stability*, 2nd. Ed., 1961, McGraw–Hill Inc.

[18] C. M. Wang, K. Y. Lam, X. Q. He, S. Chucheepsakul, "Large deflections of an end supported beam subjected to a point load", *International Journal of Non–Linear Mechanics*, Vol. 32(1), 1997, pp. 63–72.

[19] Y. Zhang, Y. Wang, Z. Li, "Analytical method of predicating the instabilities of a micro arch–shaped beam under electrostatic loading", *Microsystem Technologies*, Vol. 16 (6), 2010, pp. 909–918.

Chapter 8

8 The Substrate–Film Interaction

In this chapter, the effects of the surface elasticity and residual surface stress on the wrinkling of the film are considered. Also, a non–uniform model for the substrate is proposed and wrinkling of the film on the non–uniform substrate is investigated.

8.1 Introduction

In order to study the effect of a foundation on the beam/plate, various models have been developed by the researchers to analyze the mechanical behavior of the substrate–bonded film for statics, dynamics and stability problems. The models simplify the problem by proposing an equivalent model for the foundation. These equivalent models represent the effect of the substrate on the beam/plate with an external load. Many researchers used the equivalent spring system for the interaction of the beam/plate and the foundation. The spring system is assumed to behave linearly or nonlinearly in a single layer or several layers composition to model various properties of the foundation such as elastic, viscoelastic and plastic foundation [Winkler, 1867; Kerr, 1964; Wang *et al.*, 2005]. A brief review of the elastic foundation models is introduced in chapter 2.

When the characteristic size of the materials and devices approaches microns or nanometers, the aspect ratio of the surface/interface area to volume increases and hence, the surface effects play an important role in the mechanical behavior of the system [Miller and Shenoy, 2000; Huang *et. al*, 2007; Huang, 2008]. The size effect leads the fact that the mechanical properties of the micro/nanosize structures differ from those predicted for their bulk counterparts by conventional continuum mechanics modeling. For example, Fleck *et al.* (1994) observed that the torsional hardening of a micro–wire increases by a factor of three as the wire diameter decreases from 170 to 12 μm. Ma *et al.* (1995) reported that the indentation hardness of the silver single crystal in micro–indentation test increases by a factor of two as the penetration depth of the indenter decreases from 2.0 to 0.1 μm. McFarland *et al.* (2005) observed that the stiffness values of the micro–cantilevers in the micro–bending testing are four times larger than

the stiffness predicted by classical beam theory. Other experiments lead to the similar results on the properties of the systems due to the size effect [Chong and Lam, 1999; Stolken and Evans, 1998]. Many researchers focused on understanding these differences and their effects on the mechanical behavior of the systems to evaluate and improve the performance of the micro/nanoelectromechanical systems [Beskou *et. al*, 2003; Huang *et. al*, 2007]. For example, Kong *et. al* (2008), Wang and Feng (2007 and 2009) considered the influence of surface effects on the dynamic and stability of the micro/nano beams.

The surface effect is a significant issue especially for micro/nano structures when the size of the system is comparable with the characteristic length of the system which can be defined by the ratio of the surface to the volume of the system. In this case, due to the different conditions experienced by the atoms on the surface with respect to the atoms in the bulk of the material, different environmental effects appear on the atoms known as the surface stress on the system. The surface effect of the micro/nano structures was first studied by Lagowski *et al.* in 1975. They considered the influence of the residual surface stress on the vibration of thin crystals modeled with a compressive axial force. However, Gurtin *et al.* (1976) improved the compressive axial force model of Lagowski (1975) by contributing a distributed traction over the surface. Recently, Wang and Feng (2007) considered the effect of the surface elasticity and residual surface stress on the natural frequency of micro–beams. They used the theory of surface elasticity of Gurtin *et. al* (1998) in which the surface has a tiny thickness with a finite surface elastic modulus. Therefore, the effective properties of the system changes according to the surface effect by modifying the parameters such as the bending rigidity of the beam.

On the other hand, the residual surface stress is imposed on the film by different loading patterns such as concentrated or distributed axial force and moment [Zhang *et. al*, 2004; McFarland *et. al*, 2005]. For a bending film, according to the generalized Laplace–Young equation, the stress jump across a surface is related to the curvature of the surface and surface stress. Therefore, by considering the deformation of the system due to bending, the surface effects on the film–substrate system are considered later in this chapter.

8.2 Effect of Surface Elasticity and Residual Surface Stress on the Wrinkling of the Thin Film

The instability of thin film systems especially Micro/Nano structures may be affected by the size effect issues. Hence, the effect of surface stress, including surface elasticity and residual surface stress, on the instability behavior of the system needs to be considered. According to the theory of surface elasticity of Gurtin *et. al* (1998), the surface is assumed with a tiny thickness $h_{Sur.}$ and a finite surface elastic modulus (i.e. $E_S = Eh_{Sur.} = constant$ as thickness $h_{Sur.}$ goes to zero). Therefore, the effective bending stiffness modulus $D_{Eff.}$ of a beam/film with thickness t, width b and bending stiffness modulus of the bulk material D_{Bulk} is defined by [Wang and Feng, 2007]

$$D_{Eff.} = D_{Bulk} + \frac{1}{4}E_S bt^2 \tag{8-6}$$

As a result, the surface elasticity effect contributes in the problem by modifying the bending stiffness modulus of the beam/plate. By introducing the surface elasticity parameter as $\alpha_S = \frac{1}{4}E_S bt^2/D_{Bulk}$, the effective bending modulus is represented as

$$D_{Eff.} = D_{Bulk}\,(1 + \alpha_S) \tag{8-7}$$

In wrinkling problem, the wrinkling parameters such as wave number β and wrinkling load N_W for an infinite long film without the surface effect have been commonly proposed by the researchers in literature as [Cerda and Mahadevan, 2003; Birman and Bert, 2004],

$$N_W = 2\sqrt{b\bar{K}D} \tag{8-8}$$

$$\beta = \sqrt[4]{\frac{b\bar{K}}{D}} \tag{8-9}$$

where $\bar{K}$ is the substrate stiffness. Without considering the residual surface stress, replacing parameter D by the effective bending modulus from equation (8-7), the effective wrinkling load N_S and wave number β_S are modified for the surface elasticity effect as,

$$N_S = N_W\sqrt{1 + \alpha_S} \tag{8-10}$$

$$\beta_S = \frac{\beta}{\sqrt[4]{1+\alpha_S}} \tag{8-11}$$

Also, for the film with non–uniform properties studied in the previous chapters of this thesis, same relations can be derived as equations (8-10) and (8-11). In all of the relations for the non–uniform film, the effect of the surface elasticity influences the bending modulus of the film, and wrinkling load and wave number follow similar relations versus surface elasticity parameter α_S. Figure 8-1 shows the effect of the surface elasticity parameter α_S on the wrinkling load N_S and wave number β_S for a beam with surface elasticity effects, which are normalized by the corresponding wrinkling load and wave number for a beam without the consideration of the surface elasticity effect (i.e. N_W and β in relations 8-8 and 8-9).

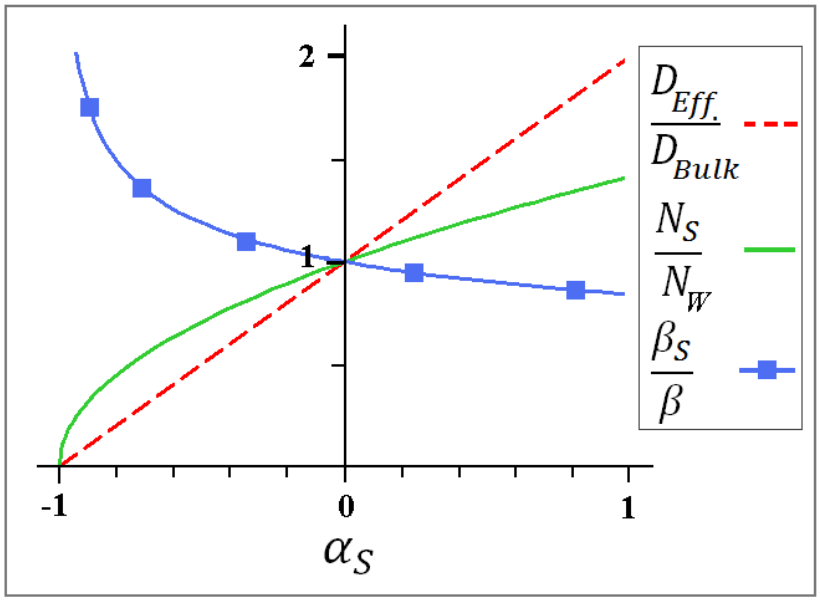

Figure 8-1: The effective bending modulus $D_{Eff.}$ and wrinkling load N_S and wave number β_S versus surface elasticity parameter α_S

On the other hand, in order to consider the residual surface stress in micro/nano structures, different loading patterns are proposed by the researchers. By using concentrated force and moment at the tip of the beam/film or simulating the residual surface stress as distributed transverse loading, researchers studied different mechanical behaviors of the systems from both the static or dynamic perspectives [Zhang *et. al*, 2004; McFarland *et. al*, 2005]. The most commonly used method considering the residual surface stress is to exert a distributed transverse loading across the film surface (i.e. p)

due to the traction jump based on the generalized Laplace–Young equations, which relates the transverse distributed loading to the bending curvature κ of the surface and the total residual surface stress σ_S as,

$$p = 2b\kappa\sigma_S \tag{8-12}$$

where the curvature of the surface is approximated by $\kappa = d^2w/dx^2$ for small deflection w of the beam/film. Hence, the effect of the residual surface stress is contributed in the film problem with an external transverse load applied on the system according to equation (8-12). The modified governing equation of the beam/film with deflection w and the effective bending modulus $D_{Eff.}$ under compressive in–plane load $\bar{N}_x$ on a Winkler substrate with modulus $\bar{K}$ is represented by

$$\frac{d^2}{dx^2}\left[D_{Eff.}\frac{d^2w}{dx^2}\right] + (\bar{N}_x - 2b\sigma_S)\frac{d^2w}{dx^2} + b\bar{K}w = 0 \tag{8-13}$$

which concludes that the residual surface stress directly affects on the axial loading of the film. Mathematically, this model is in analog with the problem of a film deposited on a substrate represented by a two–parameter foundation model, such as Filonenko–Borodich or Pasternak foundation with equivalent parameter $G_f = \sigma_S$ according to equation (8-5). A compressive residual surface stress ($\sigma_S<0$) intensifies the effect of the in–plane loading on the system such that less values of the external compressive load $\bar{N}_x$ is needed for the wrinkling of the film; while for a tensile residual surface stress ($\sigma_S>0$), more external in–plane load is required to achieve a wrinkling state. The external compressive load $\bar{N}_x$ which leads to the wrinkling of the film is given by

$$\bar{N}_x = N_S + 2b\sigma_S \tag{8-14}$$

where N_S is the wrinkling load of the system from equation (8-10).

8.3 Wrinkling of a Film on a Non–uniform Substrate

In this section, the wrinkling of a thin film on a non–uniform substrate with variable stiffness is considered. It is shown that for locally softened/stiffened substrate, the wrinkling pattern is completely different from that of the uniform substrate–film system, i.e., the wrinkles accumulate around the soft locations of the system with less substrate rigidity. The results of this work are promising in characterizing and controlling the wrinkles on thin film structures and corresponding applications.

8.3.1 Formulation of the Problem

For a homogenous isotropic film in figure 8-2 with uniform thickness t, width b, length L and Young's modulus E, deposited on a Winkler foundation with variable modulus $\overline{K}$ under the effect of in–plane compressive load $\overline{N}_x$ and uniaxial deformation with deflection $\overline{w}$, the governing equation is represented by [Timoshenko, 1940]

$$\frac{d^2}{dx^2}\left[D\frac{d^2\overline{w}}{dx^2}\right] + \overline{N}_x\frac{d^2\overline{w}}{dx^2} + b\overline{K}\overline{w} = 0 \tag{8-15}$$

where D refers to the bending rigidity of the film represented by $D = \frac{1}{12}Ebt^3$ which is constant along the span x. Introducing a non–dimensional variable ξ defined as $\xi = x/L – 0.5$ (i.e. $–0.5<\xi<0.5$) and normalized deflection $w = \frac{\overline{w}}{Max\,(\overline{w})}$ lead to the dimensionless form of the equation (8-15) as,

$$\frac{d^4w}{d\xi^4} + N\frac{d^2w}{d\xi^2} + Kw = 0 \tag{8-16}$$

where

$$N = \frac{\overline{N}_x L^2}{D} \tag{8-17-A}$$

and

$$K = \frac{bL^4\overline{K}}{D} \tag{8-17-B}$$

For the classical Winkler substrate, the Winkler modulus K is assumed constant along the span. In this section, the effect of the non–uniform substrate is considered on the film with a variable substrate stiffness $K(\xi)$ along the span. The variation of the substrate stiffness $K(\xi)$ is modeled with a continuous function of class C^0 like a symmetric bell curve similar to a Gaussian function shown in the figure 8-3 [Abramowitz

and Stegun, 1972]. The maximum amplitude of the function, the position of the peak of the function and the parameter of the widening of the function are shown in the figure with ϵ, μ and σ, respectively. Increasing the amplitude of the Gaussian function (i.e. parameter ϵ) raises the magnitude of the variation of the substrate stiffness. Also increasing the smoothness parameter σ increases the width of the bell curve and expands the non–uniform area. Far from the peak position of the Gaussian function, the function goes to zero and the variation of the substrate stiffness is neglected. Here, the peak of the variation of the substrate stiffness $K(\xi)$ is positioned at the middle of the length span (i.e. ξ =0) corresponding with μ=0 in the figure 8-3. The analytical Gaussian function for modeling the stiffening/softening of the substrate by magnitude parameter ϵ and smoothness parameter σ is introduced by

$$K(\xi) = K_0 \left[1 + \epsilon \, \mathrm{EXP}\left(-\frac{\xi^2}{2\sigma^2}\right)\right] \tag{8-18}$$

where K_0 is the characteristic substrate stiffness. And for stiffening and softening substrate, the amplitude parameter ϵ is given by a positive and negative value, respectively. For a uniform film–substrate, the substrate stiffness is constant along the entire span corresponding with the case of ϵ = 0.

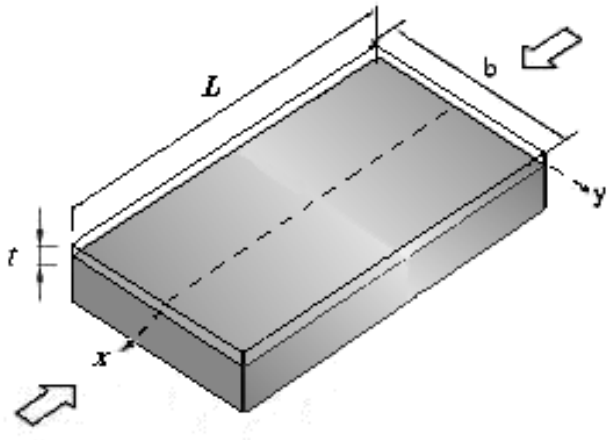

Figure 8-2: Deposited film on the non–uniform substrate

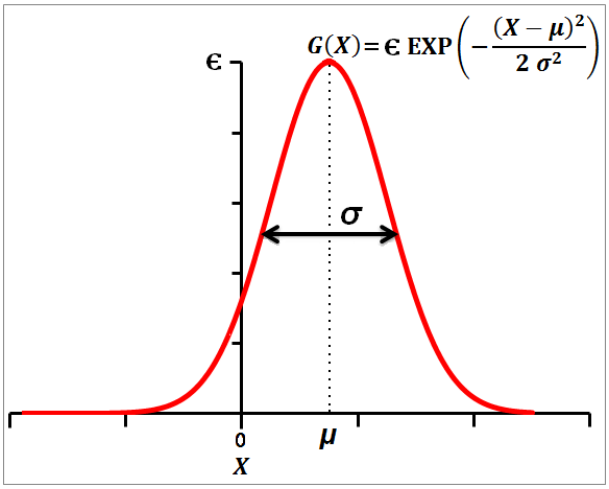

Figure 8-3: Gaussian function of the substrate stiffness

In order to solve the eigenvalue problem of the film–substrate system in equation (8-16) a series solution is constructed as

$$w(\xi) = \sum_{i=0}^{i\to\infty} c_i\, \xi^i \tag{8-19}$$

Also, the Taylor expansion of the function $K(\xi)$ is given by

$$K(\xi) = \sum_{m=0}^{m\to\infty} k_m\, \xi^m \tag{8-20}$$

Plugging $w(\xi)$ and $K(\xi)$ from (8-19) and (8-20) into differential equation (8-16), and using the recurrence relations of the series solution leads to the wrinkling pattern of the film as

$$w(\xi) = \sum_{m=0}^{4} c_m \varphi_m(\epsilon, \sigma, K_0, N, \xi) \tag{8-21}$$

By applying the clamped conditions on both edges of the film and normalizing the deflection of the film, one can find the characteristic equation of the system and determine the wrinkling pattern and the critical load N versus structural parameters of the system K_0, σ and ϵ.

On the other hand, a finite difference method similar to the pervious chapters is used to solve the eigenvalue problem of the wrinkling of the film. Here the central difference approach with 6^{th} order of accuracy is used to solve the problem. Applying the difference formulas into the governing equation of the system in (8-16) discretizes the differential equation and replaces it by a set of algebraic equations as

$$[A]\{w\} + N[B\,]\{w\} = 0 \tag{8-22}$$

in which [A] and [B] are square matrices. This general eigenvalue problem with eigenvector $\{w\}$ and eigenvalue parameter N has a straight forward solution. The eigenvalues of the problem correspond with the wrinkling loads of the system and the eigenvectors represent the wrinkling pattern.

8.3.2 Results and Discussions

The effect of the non–uniform substrate on the instability parameters (load, wrinkling pattern …) is presented and compared with the instability of the film on the uniform substrate by using the finite difference method which leads to similar results of the series solution approach.

For a long film on the uniform substrate (i.e. ϵ =0 and K=K_0), the critical compressive load and wave number of the wrinkling are represented versus non–dimensional substrate stiffness K_0 in the equation (8-17-B) as [Cerda and Mahadevan, 2003; Birman and Bert, 2004]

$$N_0 = 2\sqrt{K_0} \tag{8-23}$$

$$\beta_0 = \sqrt[4]{K_0} \tag{8-24}$$

However, for the film on the non–uniform substrate, the wrinkling load and wave number are affected by the substrate parameters K_0, ϵ and σ.

The wrinkling load N normalized by N_0 in equation (8-23) versus parameters ϵ and K is shown in figure (8-4) for two different values of σ obtained from finite difference method. Clearly, the effect of the parameter K_0 is negligible on the wrinkling load except for very soft substrates, while the magnitude parameter ϵ dominates the normalized load and changes it effectively. For locally softening substrate (ϵ<0), the wrinkling load according to different parameters K and σ follows the same pattern with an exponential relation as

$$\frac{N}{N_0} = 1 + m_1[1 - \mathrm{EXP}(-m_2\epsilon)] \tag{8-25}$$

where the constant parameters m_1 and m_2 are obtained from a regression analysis of the numerical data as m_1= 0.56 ± 0.09 and m_2= 0.81 ± 0.10 with R^2=0.99. Clearly, imposing ϵ=0 in equation (8-25) leads to N = N_0 corresponding to the wrinkling load of the

film–substrate with uniform stiffness. On the other hand, for locally stiffening film with $\epsilon>0$, the wrinkling load increases due to increasing the stiffness of the system as expected. In this case, the wrinkling load follows a relation as (8-25) while parameters m_1 and m_2 are functions of smoothness parameter σ. The solution of finite difference is compared with that of series solution method in figure 8-5. Similar to pervious chapters, the wrinkling load obtained from both methods are similar.

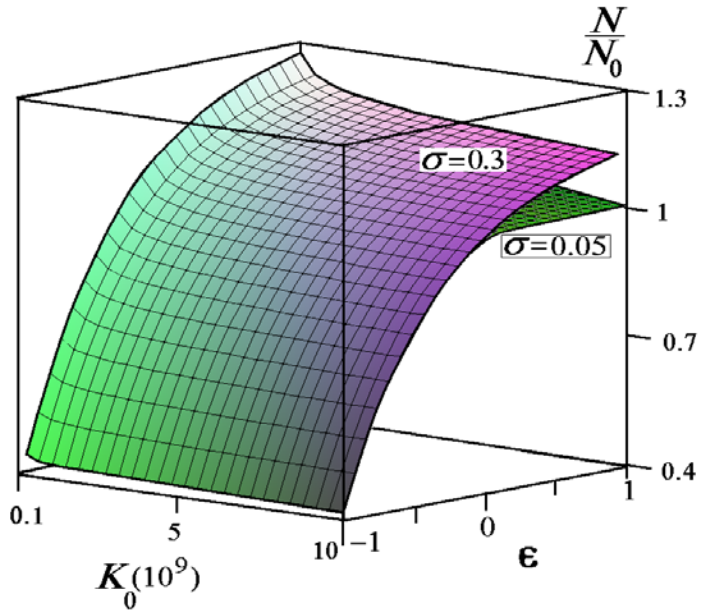

Figure 8-4: Normalized wrinkling load N/N_0 versus parameter ϵ and K_0 for σ=0.05 and 0.3

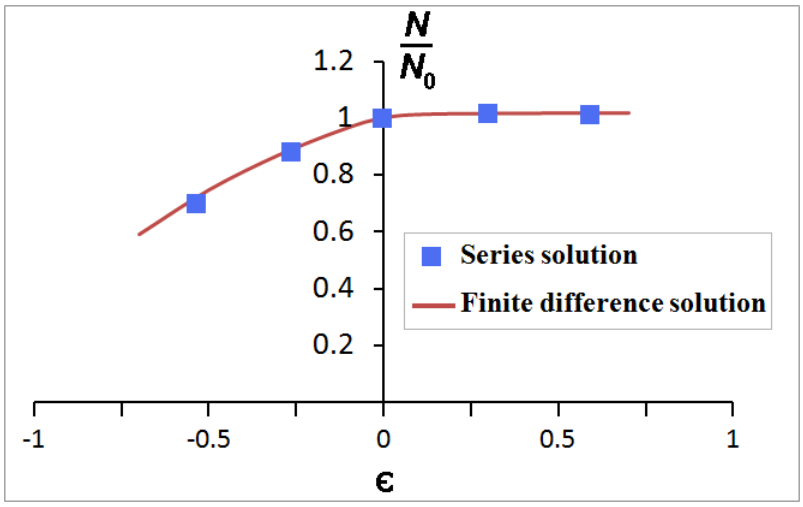

Figure 8-5: Normalized wrinkling load N/N_0 versus parameter ϵ for σ=0.05 and K_0=10^9 obtained from finite difference method and series solution

The non–uniformity of the substrate also changes the wrinkling pattern on the film. For a film–substrate with uniform stiffness (i.e. ϵ=0), whole length span undergoes wrinkling as shown in figure 8-6-A; while for locally softening substrates (ϵ<0), wrinkles accumulate at the position with minimum stiffness (here, at the middle of the length span according to equation 8-18) which is shown in figures 8-6-B and 8-6-C. Increasing the magnitude parameter ϵ compresses the wrinkles even more and decreases their number. On the other hand, for locally stiffening film (ϵ>0), wrinkles propagate on both sides of the location with higher stiffness (here, the middle of the film) as shown in figure 8-6-D. In order to characterize the wrinkling pattern, two parameters are introduced; the wave number of the wrinkling which shows the number of the wrinkles in the affected area and the footprint of the wrinkling that represents the size of the region on the film influenced by the wrinkles which are discussed as follows.

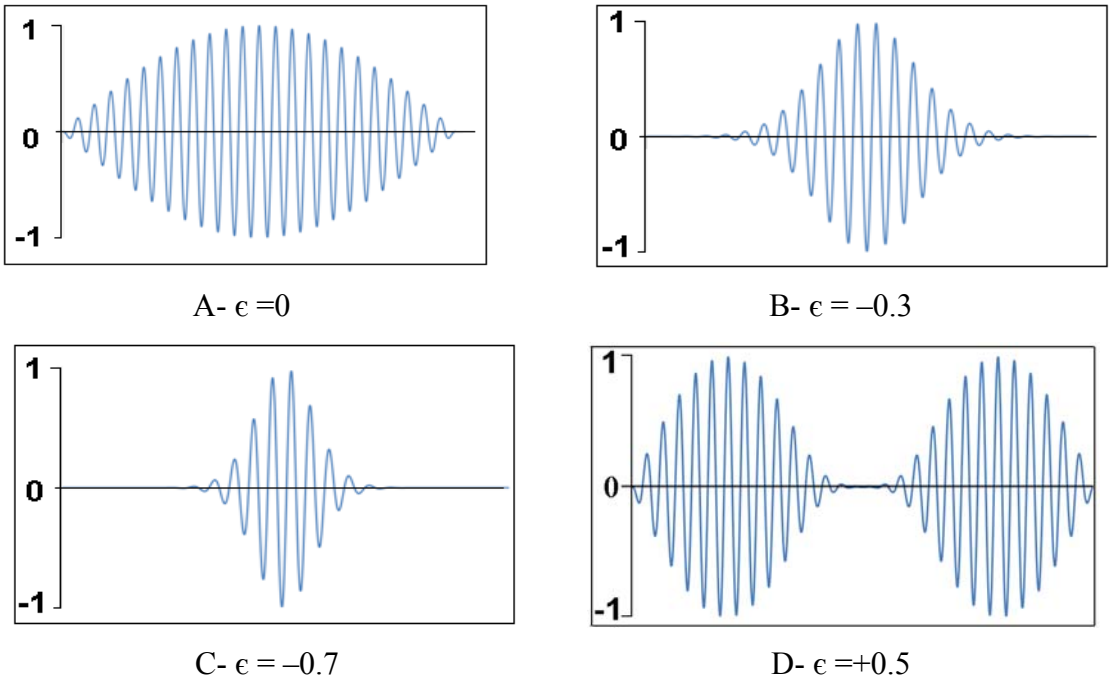

A- ϵ =0 B- ϵ = –0.3

C- ϵ = –0.7 D- ϵ =+0.5

Figure 8-6: Wrinkling of the film on the non–uniform substrate and the effect of the various magnitude parameters ϵ on the wrinkling pattern

Figures 8-7-A and B show the wave number of the wrinkling normalized by β_0 in equation (8-24), for two cases of smoothness parameters σ =0.05 and 0.3. Obviously, the wave number is highly affected by the change of the magnitude parameter ϵ. A regression analysis shows that the normalized wave number follows an exponential relation of

magnitude parameter ϵ as EXP (–m ϵ) where m is a function of parameter σ. By increasing the substrate stiffness K_0, similar to the case of the film on the uniform substrate in equation (8-24), the wave number of the wrinkling increases. However, the increasing rate of the wave number of the film–substrate with uniform stiffness is faster than the corresponding value of the film–substrate with variable stiffness. Therefore, the normalized wave number β/β_0 decreases by increasing K_0 as figures 8-7-A and B show.

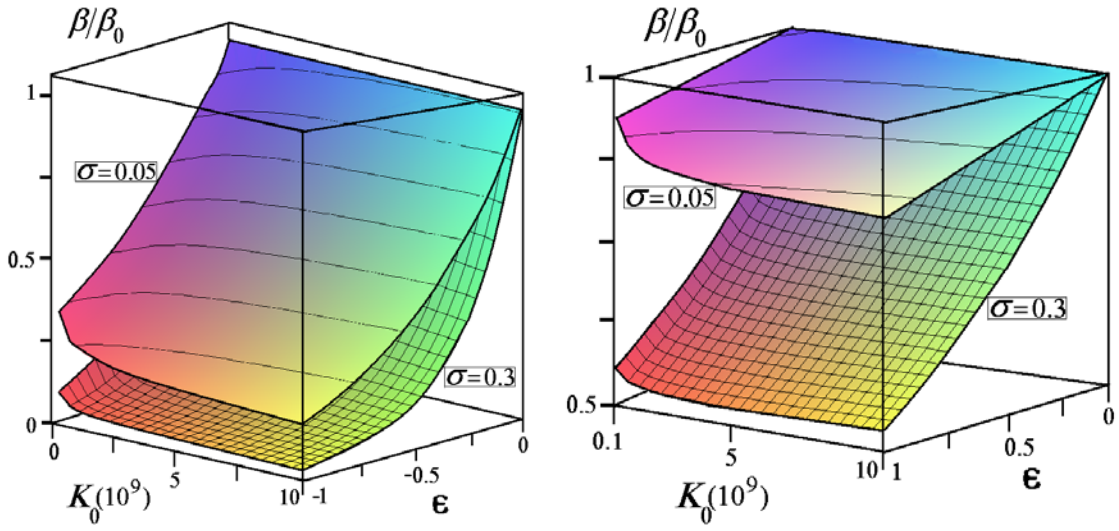

A- Negative magnitude parameter ϵ<0 B- Positive magnitude parameter ϵ>0

Figure 8-7: Normalized wave number β/β_0 versus substrate stiffness K_0 and magnitude parameter ϵ for smoothness parameters σ =0.05 and 0.3

In order to consider the localization of the wrinkles along the length span, a non–dimensional parameter is introduced as the footprint of the wrinkling which represents the effective length of the film span undergoing wrinkling. The footprint changes between zero and one, such that when the footprint is equal to one, the whole length span is affected by the wrinkles corresponding to the case of the wrinkling of the film with uniform substrate (i.e. ϵ=0). A regression analysis between footprint and wave number of the wrinkling shows that these parameters are strongly proportional to each other linearly so that footprint follows the same pattern as normalized wave number discussed above. Figure 8-8 shows the footprint parameter versus corresponding normalized wave number for 60 datapoints around the reference line Y= m_0+ m_1X.

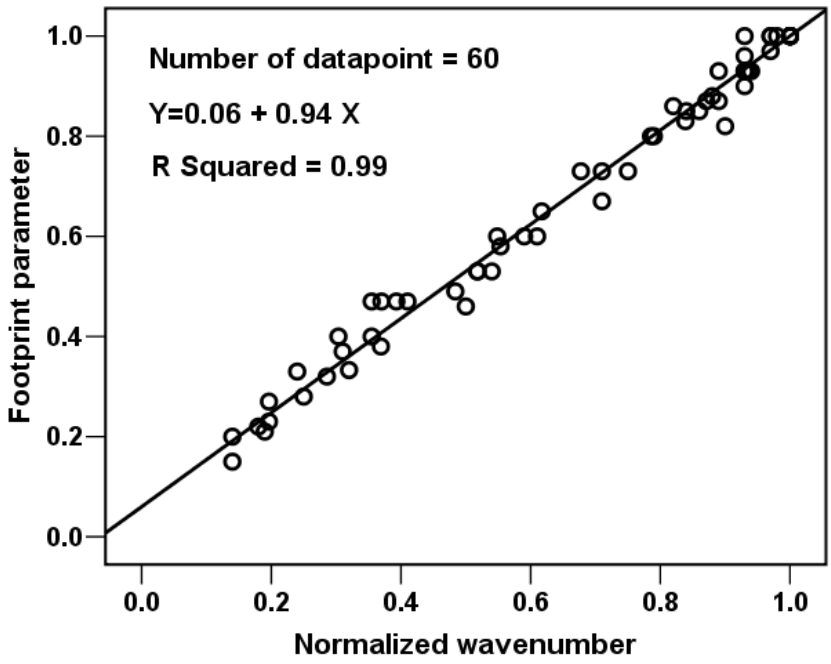

Figure 8-8: The linear relation between footprint and normalized wave number β/β_0 of the wrinkling

High sensitivity of the footprint parameter with respect to the magnitude parameter ϵ of the substrate stiffness as shown in figure 8-9 concludes that even under small disturbances in the uniformity of the substrate, wrinkles accumulate densely at the particular locations of the film. On the other hand, the microstructure of the substrate in thin film technology increases the importance of considering the variation of the substrate stiffness so that it intensifies the abovementioned accumulative effect too. The non–uniformity of the system which accumulates wrinkles around a region leads that the behavior of the wrinkled system to be completely different in a non–uniform system compared to a uniform one.

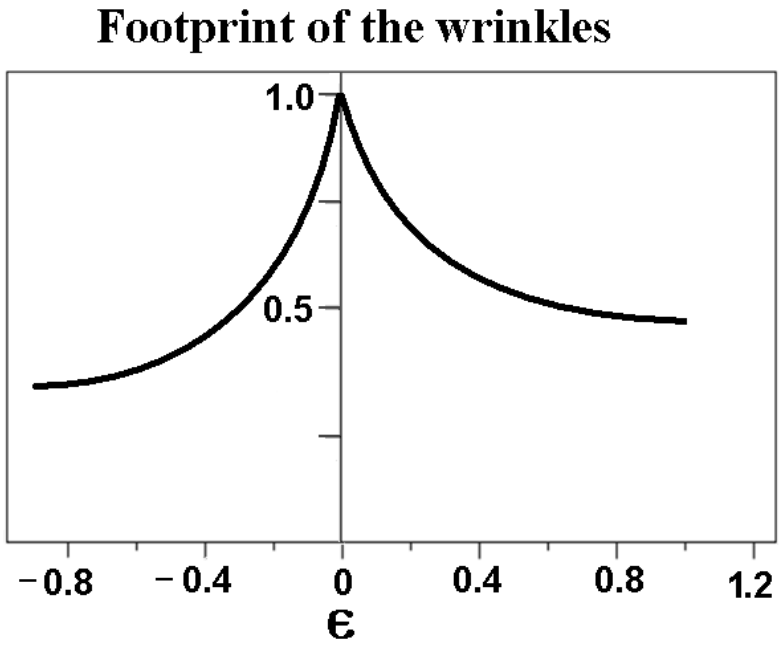

Figure 8-9: Footprint of the wrinkling versus substrate stiffness magnitude parameter ϵ

8.3.3 Conclusion

For deposited film on the substrate, the uniaxial wrinkling problem was investigated and the effect of the variable substrate stiffness on the load and pattern of the wrinkling was studied. Numerical results show that for a film on the uniform substrate, the wrinkles propagate on the entire length span, while for the case of the non–uniform substrate, they accumulate around the soft locations of the system with less substrate stiffness. For locally stiffened films, the wrinkles develop on both sides of the stiffened location such that film undergoes an internal clamped boundary condition at the location of the stiffening. Increasing the variation of the substrate stiffness shrinks wrinkles more on the soft locations of the substrate. On the other hand, the wrinkling load changes for non–uniform substrate such that for softened substrate, the load decreases while for stiffened substrate the wrinkling load increases. The results of this analysis are promising in predicting and controlling the wrinkling pattern in experimental works, MEMS applications and sensor/actuator systems.

8.4 Summary

In this chapter, the effect of the substrate on the wrinkling pattern of the thin solid film was considered. The effects of the surface elasticity and residual surface stress on the wrinkling of the film with micro and nanometer thickness were described. It was shown that the surface elasticity changes the effective bending stiffness of the film, which eventually influences the wrinkling load and pattern. On the other hand, the effect of the residual surface stress was considered in analog with a two–parameter foundation model and it shows how the compressive and tensile residual surface stresses affect on the wrinkling load. In addition, the effect of the non–uniformity of the substrate was investigated on the localization of the wrinkling. The non–uniform substrate accumulates the wrinkles at particular locations of the system (i.e. the soft positions on the substrate) which affects the wrinkling pattern, the wave number and the effective length of the system undergone wrinkling.

8.5 References

[1] M. Abramowitz, I.A. Stegun, *Handbook of Mathematical Functions*, 1972, Dover Publications, New York.

[2] S.P. Beskou, K.G. Tsepoura, D. Polyzos, D.E. Beskos, "Bending and stability analysis of gradient elastic beams", *International Journal of Solids and Structures*, Vol. 40 (2), 2003, pp. 385–400.

[3] V. Birman, C.W. Bert, "Wrinkling of composite–facing sandwich panels under biaxial loading", *Journal of Sandwich Structures and Materials*, Vol. 6 (3), 2004, pp. 217–237.

[4] E. Cerda, L. Mahadevan, "Geometry and physics of wrinkling", *Physical Review Letters*, Vol. 90 (7), 2003, pp. 074302/1–4.

[5] A.C.M. Chong, D.C.C. Lam, "Strain gradient plasticity effect in indentation hardness of polymers", *Journal of Materials Research*, Vol. 14 (10), 1999, pp. 4103–4110.

[6] N.A. Fleck, G.M. Muller, M.F. Ashby, J. W. Hutchinson, "Strain gradient plasticity: theory and experiment", *Acta Metallurgica et Materialia*, Vol. 42 (2), 1994, pp. 475–487.

[7] M. E. Gurtin, X. Markenscoff, R. N. Thurston, "Effect of surface stress on the natural frequency of thin crystals", *Applied Physics Letters*, Vol. 29, 1976, pp. 529– 530.

[8] M.E. Gurtin, J. Weissmuller, F. Larche, "A general theory of curved deformable interfaces in solids at equilibrium", *Philosophical Magazine A: Physics of Condensed Matter, Structure, Defects and Mechanical Properties*, Vol. 78(5), 1998, pp. 1093–1109.

[9] D.W. Huang, "Size–dependent response of ultra–thin films with surface effects", *International Journal of Solids and Structures*, Vol. 45, 2008, pp. 568–579.

[10] R. Huang, C. M. Stafford, B.D. Vogt, "Effect of surface properties on wrinkling of ultrathin films*", Journal of Aerospace Engineering* (*ASCE*), Vol. 20 (1), 2007, pp. 38–44.

[11] A.D. Kerr, "Elastic and viscoelastic foundation models", *Journal of Applied Mechanics* (*ASME*), Vol. 31, 1964, pp. 491–498.

[12] S. Kong, S. Zhou, Z. Nie, K. Wang, "The size–dependent natural frequency of Bernoulli–Euler micro–beams", *International Journal of Engineering Science*, Vol. 46 (5), 2008, pp. 427–437.

[13] J. Lagowski, H. C. Gatos, E. S. Sproles, “Surface stress and the normal mode of vibration of thin crystals: GaAs”, *Applied Physics Letters*, Vol. 26, 1975, pp. 493–496.
[14] Q. Ma, D.R. Clarke, “Size dependent hardness of silver single crystals”, *Journal of Materials Research*, Vol. 10 (4), 1995, pp. 853–863.
[15] A.W. McFarland, J.S. Colton, “Role of material microstructure in plate stiffness with relevance to micro–cantilever sensors”, *Journal of Micromechanics and Microengineering*, Vol. 15 (5), 2005, pp. 1060–1067.
[16] A.W. McFarland, M.A. Poggi, M.J. Doyle, L.A. Bottomley, J.S. Colton, “Influence of surface stress on the resonance behavior of microcantilevers”, *Applied Physics Letters*, Vol. 87, 2005, pp.053505–1/3.
[17] R.E. Miller, V.B. Shenoy, “Size–dependent elastic properties of nanosized structural elements”, *Nanotechnology*, Vol. 11, 2000, pp. 139–147.
[18] J.S. Stolken, A.G. Evans, “Microbend test method for measuring the plasticity length scale”, *Acta Materialia*, Vol. 46 (14), 1998, pp. 5109–5115.
[19] S.P. Timoshenko, *Theory of Plates and Shells*, 1940, McGraw–Hill Book Company, Inc.
[20] Y.H. Wang, L. G. Tham, Y. K. Cheung, “Beams and plates on elastic foundations: A review”, *Progress in Structural Engineering and Materials*, Vol. 7 (4), 2005, pp. 174–182.
[21] G.F. Wang, X.Q. Feng, “Effects of surface elasticity and residual surface tension on the natural frequency of microbeams”, *Applied Physics Letters*, Vol. 90, 2007, pp. 231904/1–3.
[22] G.F. Wang, X.Q. Feng, “Surface effects on buckling of nanowires under uniaxial compression”, *Applied Physics Letters*, Vol. 94, 2009, pp. 141913/1–3.
[23] E. Winkler, *Die Lehre von der Elastizitat und Festigkeit*, 1867, Dominicius, Prague.
[24] Y. Zhang, Q. Ren, Y.P. Zhao, “Modelling analysis of surface stress on rectangular cantilever beam”, *Journal of Physics D: Applied Physics*, Vol. 37, 2004, pp. 2140– 2145.

Chapter 9

9 General Discussion and Conclusions

Besides the conclusion section for each part of the thesis in chapters 3, 4, 5, 6, 7 and 8, the current chapter summarizes all of the results of the different chapters of the dissertation and provides an overall conclusion about the thesis. It also introduces some useful applications of the results of the thesis which provides more understanding about the importance of the project.

9.1 Overview of the Different Chapters

In this thesis, the mechanical instability of thin film structure including buckling and wrinkling is investigated under applied compressive loading on the film. The effects of the loading on the system, the change in material properties of the film and substrate, the geometrical non–uniformity of the system and other similar factors on the wrinkling pattern and its characteristic parameters such as wave number of the wrinkles and length of the wrinkles are considered. A summary of the results of different chapters are concluded in the following.

In chapter 3, the wrinkling of the film around an inclusion is considered. The inclusion is defined as a region on the film which applies compressive eigenstrain on the system locally and wrinkles develop around that region. For the inclusion line on the free standing film and deposited film on the substrate, it is shown that wrinkles develop on the film perpendicular to the inclusion line. The wrinkling parameters such as length and wave number of the wrinkles are derived in terms of loading parameters and material properties of the film/substrate. The results provide physical insight in modeling the suturing of the wound in surgical operations, the effect of the glue or other constraints on thin structures and so on.

Chapters 4, 5 and 6 mainly focus on the non–uniformity of the system with finite length. The non–uniformity arises due to the variation of the material properties as discussed in chapter 4, or the variation of the thickness of the film as presented in chapters 5 and 6. In fact, they show that for a non–uniform film, wrinkles accumulate at

some specific locations while the other regions of the film remain unwrinkled. These specific locations of the film with accumulated wrinkles are the weakest locations of the system with thinner thickness or lower stiffness. Chapter 4 shows that unlike the homogenous films in which the wrinkles propagated along the entire domain, for a functionally graded material (FGM) film where the stiffness of the film changes with a continuous function along the length span of the film, wrinkles accumulate around the softest region of the film. It also provides simple explicit expressions for the wrinkling parameters such as wave number and effective length of the film influenced by the wrinkles. High sensitivity of the wrinkling parameters with the FGM gradient parameter shows the importance of the proposed model in this work. Chapters 5 and 6 represent similar results for wrinkling of a non–uniform film with variable thickness. They show that for different profiles of the film thickness, the wrinkles accumulate at the thinnest position (or positions) of the system. This conclusion becomes more significant for thin film systems where the uniformity of the film cannot be guaranteed due to the tiny thickness of the system. High sensitivity of the wrinkling accumulation around the thin positions of the system intensifies the importance of the analysis.

On the other hand, in contrast with other works in the literature, the effect of finite length of the film has not been considered on the wrinkling pattern based on the best knowledge of the author. In fact, researchers focus on the wrinkling of the film with infinite length while the wrinkles propagate uniformly all over the system. However, the results of this thesis show that for a finite length film, the wrinkles are constrained at the edges of the film and the pattern of the wrinkling drastically changes. The finite length model proposed in this work provides more compatibility with real applications of the wrinkling in thin film technology.

In order to investigate the amplitude of the wrinkling after instability, a nonlinear analysis is presented in chapter 7. The post–wrinkling analysis shows how the amplitude of the wrinkles increases by increasing the applied compressive load on the wrinkled film. Moreover, it illustrates that there is a threshold for amplitude and compressive load on the film such that, beyond the threshold value, the wrinkling is substituted by folding of the film at some special points. The post–wrinkling parameters and the effect of

non–uniformity of the system on accelerating the wrinkling–folding transition phase are investigated.

Chapter 8 considers the effect of the substrate on the wrinkling pattern of the film. The effects of the surface elasticity and residual surface stress are considered on the wrinkling of the film. Also, a non–uniform model for the substrate is proposed and the accumulative effect of the wrinkling on the soft regions of the substrate is considered.

The results of different chapters represent some clear insights in the physics of wrinkling of thin film structures. They consider the effect of the non–uniformity of the system with finite length on the wrinkling parameters by proposing explicit expressions in terms of the loading and structural parameters and show the accumulation of the wrinkles at some special positions. In other words, they provide adequate insight in the physics and mechanics of wrinkling of thin film structures.

9.2 Contribution of the Research

In this work, the instability of thin film structures as buckling and wrinkling are considered and the loading parameters and mode shape of the film at the instability onset and after that are determined. Other works on the wrinkling of the substrate–bonded films mainly use the homogenous assumption for the film material properties with uniform thickness all over the domain and ignore the effect of non–uniformity of the film and substrate and boundary conditions of the system with finite length. However, in this work such issues are focused and their effects on the load and pattern of the instability are studied. In contrast with the other works, the assumption of the uniformity of the periodic pattern of the wrinkled film is neglected and various parameters such as the non–uniformity of the film and substrate including the geometrical and material non–uniformity for films with finite and infinite length under compressive loading are studied on the wrinkling load and pattern. The results of the work show that the non–uniformity of the film–substrate has a significant effect on the wrinkling parameters such that wrinkles accumulate at thinner and softer positions with smaller bending rigidity of the film. In comparison with other works, the wrinkling pattern is not uniform along the span and is affected by the non–uniformity and boundary conditions of the film.

In addition, post–wrinkling of the system which determines the behavior of the wrinkling amplitude is investigated and it is shown that the amplitude of the wrinkles grows by increasing the loading on the system. Consequently, by increasing the amplitude, a wrinkling–folding transition appears such that the wrinkles of the film are substituted by one or few folds on the film. The threshold parameters of wrinkling–folding transition are considered in this work and compared by other experimental works. These results propose new criteria for wrinkling–folding transition in thin film structures. Moreover, considering the effect of the surface elasticity and residual stress on the wrinkling of Micro/Nano–scale thin films provides better understanding in wrinkling of MEMS/NEMS. The results of this research are expected to increase the insight in the physics and mechanics of instability of thin film structures and open new windows in potential applications of thin film technology in various fields.

9.3 Future Research Directions

The thesis was motivated by the idea that non–uniformity in the system induces specific effects on the wrinkling of the thin film structure. It was shown that the wrinkling pattern changes effectively for a non–uniform film when the thickness or the mechanical properties of the system vary such that wrinkles accumulate at some particular locations. Accordingly, the wrinkling load of the system and wave number of the wrinkles also change. This idea was demonstrated for different systems with different sources of non–uniformity in the system for one dimensional model. This non–uniformity issue can also be explored for two dimensional models with different non–uniformity effects on the system in different directions. As expectation, the wrinkles of the film accumulate at some specific locations, and the wavelength of the two dimensional wrinkling in each direction is affected by the non–uniformity of the whole system depending on the modeling assumptions. On the other hand, the extension of the problem for Micro/Nano systems attracts great attention since for those systems the microstructure and thickness of the layers cannot be assumed as uniform. High non–uniformity of such systems violates all the results obtained by the researchers for the wrinkling problem of the ultra–thin layers based on the uniform assumption. These investigations need accurate

experimental works in laboratories which open new insight in physics of the wrinkling of the surfaces. Another important issue is the surface effects on the two–dimensional buckling of thin film/film–substrate structures, which needs further investigation for the full potential applications of nanofilm–based devices in NEMS.

In addition, many applications are introduced based on the results obtained from this thesis for wrinkling of a system. According to the results, the wrinkling load and wrinkling pattern of the film can be controlled by imposing special effects on the system. Doping of the film at some specific positions changes the material properties of the layer so that the stiffness of the film varies consequently. Carving the film at some positions or using special profile for etching of the film during deposition techniques also changes the thickness of the film. Hence, the wrinkles of the film accumulate around some particular positions of the non–uniform film as shown in this work. This technique provides appropriate tools for controlling the wrinkling of the film. Consequently, controlling the wrinkling of the film is a promising tool in developing new tools and techniques in various fields such as sensor and actuators, elastomers in deformable electronics know as stretchable electronics and stretchable interconnectors [Wanger *et al*., 2004; Lacour *et al*., 2003 and 2006; Watanabe *et al*., 2002], semiconductor devices [Yin *et al*., 2002], sandwich panel structures [Birman and Bert, 2004], biological assays [Cerda *et al*., 2002] and cell locomotion [Harris *et al*., 1980; Teixeira *et al*., 2003], microelectromechanical systems (MEMS) and nanoelectromechanical systems (NEMS) [Fu *et al*., 2006], metrology methods [Wilder *et al*., 2006], solar sails and gossamer spacecrafts [Imhof, 1997], micro/nano structures and technologies [Schmid *et al*., 2003], and all the other fields related to physics and mechanics of wrinkling in science and technology.

9.4 References

[1] V. Birman, C.W. Bert, “Wrinkling of composite–facing sandwich panels under biaxial loading”, *Journal of Sandwich Structures and Materials*, Vol. 6 (3), 2004, pp. 217–237.

[2] E. Cerda, K. Ravi–Chandar, L. Mahadevan, “Thin films: Wrinkling of an elastic sheet under tension”, *Nature*, Vol. 419, 2002, pp. 579–580.

[3] Y.Q. Fu, S. Sanjabi, Z.H. Barber, T.W. Clyne, W.M. Huang, M. Cai, , J.K. Luo, , A.J. Flewitt, W.I. Milne, "Evolution of surface morphology in TiNiCu shape memory thin films", *Applied Physics Letters*, Vol. 89 (17), 2006, pp. 171922–1/3.

[4] A.K. Harris, P. Wild, D. Stopak, "Silicone – Rubber substrata – New wrinkle in the study of cell locomotion", *Science*, Vol. 208 (4440), 1980, pp. 177–179.

[5] B. Imhof, "Modern sandwich core materials offer new attractive design possibilities", *Aircraft Engineering and Aerospace Technology*, Vol. 69, 1997, pp. 332–333.

[6] S.P. Lacour, S. Wagner, Z. Huang, Z. Suo, "Stretchable gold conductors on elastomeric substrates", *Applied Physics Letters*, Vol. 82 (15), 2003, pp. 2404–2406.

[7] S.P. Lacour, S. Wagner, R.J. Narayan, T. Li, Z.G. Suo, "Stiff subcircuit islands of diamondlike carbon for stretchable electronics", *Journal of Applied Physics*, Vol. 100 (1), 2006, pp. 014913–1/6.

[8] H. Schmid, H. Wolf, R. Allenspach, H. Riel, S. Karg, B. Michel, E. Delamarche, "Preparation of metallic films on elastomeric stamps and their application for contact processing and contact printing", *Advanced Functional Materials*, Vol. 13 (2), 2003, pp.145–153.

[9] A.I. Teixeira, G.A. Abrams, P.J. Bertics, C.J. Murphy, P.F. Nealey, "Epithelial contact guidance on well–defined micro– and nanostructured substrates", *Journal of Cell Science*, Vol. 116 (10), 2003, pp. 1881–1892.

[10] S. Wagner, S.P. Lacour, J. Jones, P.H.I. Hsu, J.C. Sturm, T. Li, Z.G. Suo, "Electronic skin: architecture and components", *Physica E-Low-Dimensional Systems & Nanostructures*, Vol. 25 (2–3), 2004, pp. 326–334.

[11] M. Watanabe, H. Shirai, T. Hirai, "Wrinkled polypyrrole electrode for electroactive polymer actuators", *Journal of Applied Physics*, Vol. 92 (8), 2002, pp. 4631– 4637.

[12] E.A. Wilder, S. Guo, S. Lin–Gibson, M.J. Fasolka, C.M. Stafford, "Measuring the modulus of soft polymer networks via a buckling–based metrology", *Macromolecules*, Vol. 39 (12), 2006, pp. 4138–4143.

[13] H. Yin, R. Huang, K.D. Hobart, Z. Suo, T.S. Kuan, C.K. Inoki, S.R. Shieh, T.S. Duffy, F.J. Kub, J.C. Sturm, "Strain relaxation of SiGe islands on compliant oxide", *Journal of Applied Physics*, Vol. 91, 2002, pp. 9716–9722.

Curriculum Vitae

Name: Masoud Noroozi

Post-secondary Education and Degrees:

Sharif University of Technology
Tehran, Iran
2001–2005 B.A.

Sharif University of Technology
Tehran, Iran
2005–2007 M.A.

The University of Western Ontario
London, Ontario, Canada
2008–2012 Ph.D.

Honours and Awards: Western Graduate Research Scholarship (WGRS)
2008–2012

Related Work Experience

Teaching Assistant
Sharif University of Technology
2005–2007

Teaching Assistant, Research Assistant
The University of Western Ontario
2008–2012

Publications:

- ✓ M. Noroozi, R. Naghd abadi, A.Irajizad, "The mechanical effects due to various patterns of attachment between thin solid film and substrate", *Proceeding of the 15th Annual International Conference of Mechanical Engineering ISME*, 2007, Tehran, Iran.
- ✓ M. Mofid, M. Noroozi, "A plate on Winkler foundation with variable coefficient", *Scientia Iranica, Transaction A: Civil Engineering*, Vol. 16 (3), 2009, pp. 249–255.
- ✓ M. Noroozi, L.Y. Jiang, "Wrinkling around an inclusion line on thin film structures", *Proceedings of the 23rd Canadian Congress of Applied Mechanics*, Vol. 1, 2011, pp. 674–677.
- ✓ M. Noroozi, L.Y. Jiang, "Buckling and wrinkling of a functionally graded material (FGM) thin film", *International Journal of Applied Mechanics*, D–12–00013R1, Accepted 17 March 2012.